SYNTHESIS AND APPLICATION OF SURFACTANTS CONTAINING POLYMERIZABLE GROUPS

by

Adele Pienaar

Thesis presented on partial fulfillment of the requirements for the Degree of Master of Science in Polymer Science

at the

University of Stellenbosch

Study leaders:

Prof. R.D. Sanderson (Stellenbosch)

Dr. H. Pasch (Germany)

Stellenbosch **December 2002**

Abstract

The surfmers sodium 11-methacryloyloxy undecanyl-1 sulfate (MET) and sodium 11-crotonoyloxy undecanyl-1 sulfate (CRO) were synthesized and purified. Both contain a sulfonate and polymerizable double bond connected by a hydrocarbon chain. Sodium 4-[11-(3-carboxypropionoyloxy)-undecyloxy] benzenesulfonate (PSA-MA) could not be synthesized successfully. MET and CRO were characterized by means of nuclear magnetic resonance spectroscopy (NMR), elemental analysis (EA), thermal gravimetric analysis (TGA), determination of the critical micelle concentration (CMC), differential scanning calorimetry (DSC), and microscopy. MET and CRO displayed a liquid crystalline behavior.

MET and CRO were used in combination with poly(diallyl dimethyl ammonium chloride) to form polyelectrolyte-surfactant complexes by common precipitation in water. These complexes were redissolved in methanol and cast in films. The cast films were investigated by wide angle X-ray scattering (WAXS) and small angle X-ray scattering (SAXS) with regard to ordered mesomorphous phases. Due to the destabilization of the lyotropic phase, little order were observed in the complexes.

MET was co-polymerized with styrene and methyl methacrylate, in different proportions, by means of free radical polymerization. The co-polymers were characterized by NMR and infrared spectroscopy (IR) and analyzed by DSC, TGA and gel permeation chromatography (GPC). All analytical techniques showed that the co-polymers were synthesized successfully. TEM indicated a fine, lamellar micro-structure.

Opsomming

Die polimeriseerbare sepe, natrium-11-metakrieloloksi-undekaniel-1sulfaat (MET) en natrium-11-krotonieloksi-undekaniel-1-sulfaat (CRO) is berei en gesuiwer. Beide bevat 'n sulfonaat en 'n polimeriseerbare dubbelbinding wat deur 'n koolwaterstofketting verbind word. Natrium-4-[11-(3-karboksipropionieloksi)-undekieloksi]-benseensulfaat (PSA-MA) kon nie suksesvol berei word nie. MET en CRO is deur middel van kernmagnetieseresonansspektroskopie (KMR), elementele-analise (EA), termiese-gravimetriese analise (TGA), kritiese miselkonsentrasie (CMC), differensieëlskandeerkalorometrie (DSC) en mikroskopie gekarakteriseer. Beide MET en CRO het 'n vloei-kristalgedrag getoon.

MET en CRO is met poli(diallieldimetielammoniumchloried) gereageer om polyelektroliet-seepkompleks te vorm deur presipitasie uit water. Die komplekse is in metanol opgelos en films daarvan gemaak. Die films is deur wyehoek X-straal diffraksie (WAXS) en kleinhoek X-straaldiffraksie (SAXS) ondersoek om geordende mesomorfiese fases te ondersoek. As gevolg van destabilisasie van die liotropiese fase is min orde in die komplekse gevind.

MET is met stireen en metielmetakrilaat deur middel van vryeradikaalpolymerisasie gekopolimeriseer. Die kopolimere is deur middel van KMR- en infrarooispektroskopie (IR), DSC, TGA en gelpermeasiechromotagrafie (GPC) ondersoek. Al hierdie analitiese metodes het die suksesvolle sintese van die kopolimere bewys. Transmissie-elektronmikroskopie het die teenwoordigheid van 'n fyn, laminêre mikro-struktuur bewys.

Acknowledgements

Prof. R.D. Sanderson, my promoter, for his input and many hours of discussions.

Dr. H. Pasch, my co-promoter, for the opportunity to work at the Deutsches Kunststoff Institut (DKI), Darmstadt, Germany and his help with the analytical work in this work.

Dr. C. Götz, post-doc, for his practical guidance in the lab, hours of editing and most worthwhile discussions.

The staff, students and my co-workers at the Institute of Polymer Science, Stellenbosch, for their friendship and input in the finalization of this work.

The staff at DKI, Germany, for their friendship and assistance with the analytical work and interpretation of the results.

Thank you to Robert and my parent for being there for me and helping to get me through the difficult times.

Table of contents

List of abbreviations v

List of figures viii

List of tables xi

Chapter 1: Introduction 1

1.1 Definition of nanochemistry 1

1.2 Amphiphiles and self-assembly 1

1.3 Motivation 2

1.4 Objectives 3

1.5 Layout of thesis 5

Chapter 2: Theoretical and historical background 6

2.1 Amphiphiles as surfactants 6

2.1.1 Classification 6

2.1.2 Bola-amphiphiles 7

2.1.3 Nature of bola-amphiphiles 7

2.1.4 Behavior in solvents 8

2.1.5 Self-assembly 10

2.1.6 Self-assembly of bola-amphiphiles 13

2.2 Self-assembly into mesomorphic phases 14

2.2.1 Liquid crystals 14

2.2.2 Classification of mesomorphic phases 14

2.3 Polyelectrolyte-surfactant complexes 17

2.3.1 Polyelectrolyte-surfactant complexes in solution 17

2.3.2 Polyelectrolyte-surfactant complexes in solid self-organizing building blocks 22

2.3.3 Polymerization in polyelectrolyte-surfactant complexes 25

2.4 Analytical techniques 25
2.4.1 Introduction 25
2.4.2 Elemental analysis (EA) 26
2.4.3 Differential scanning calorimetry (DSC) 26
2.4.4 Thermal gravimetric analysis (TGA) 28
2.4.5 Polarized light microscopy 28
2.4.6 X-ray diffraction (WAXS and SAXS) 29
2.4.7 Infrared spectroscopy (FTIR) 31
2.4.8 Gel permeation chromatography (GPC) 31

Chapter 3: Synthesis of surfactant monomers 33

3.1 Introduction
3.2 Experimental 33
3.2.1 Materials 33
3.2.2 Instrumental techniques 34
3.2.3 Synthesis of sodium 11-methacryloyloxy undecanyl-1 sulfate (MET) 34
3.2.3.1 Preparation of sodium methacrylate 34
3.2.3.2 Preparation of 11-methacryloyloxy undecanol-1 (MET1) 35
3.2.3.3 Preparation of 11-methacryloyloxy undecanyl-1 sulfate (MET) 36
3.2.4 Synthesis of sodium 11-crotonoyloxy undecanyl-1 sulfate (CRO) 38
3.2.4.1 Preparation of sodium crotonate 38
3.2.4.2 Preparation of 11-crotonoyloxy undecanol-1 (CRO1) 39
3.2.4.3 Preparation of 11-crotonoyloxy undecanol-1 sulfate (CRO) 39
3.3 Results and discussion 41
3.3.1 Synthesis of sodium 11-methacryloyloxy undecanyl-1 sulfate (MET) and sodium 11-crotonoyloxy undecanyl-1 sulfate (CRO) 41
3.3.1.1 Purity and critical micelle concentration of MET and CRO 43
3.3.2 Analysis of sodium 11-methacryloyloxy undecanyl-1 sulfate (MET) and sodium 11-crotonoyloxy undecanyl-1 sulfate (CRO) 44
4.3.2.1 Thermal gravimetric analysis (TGA) 44
4.3.2.2 Differential scanning calorimetry (DSC) 45
4.3.2.3 Polarized light microscopy with heating stage 46

3.4 Synthesis of sodium 4-(15-carboxy-12-oxa-13-oxapentadecyl-14-E-enololoxy) benzene sulfate (PSA-MA) 48
3.4.1 Introduction 48
3.4.2 Preparation of PSA-MA, by synthetic route 1 50
3.4.2.1 Attempt 1 50
3.4.2.2 Attempt 2 51
3.4.3 Preparation of PSA-MA, by synthetic route 2 51
3.4.3.1 Preparation of mono-11-bromoundecyl maleiate (Br-MA) 52
3.4.3.2 Synthesis of PSA-MA based on Br-MA, attempt 1 53
3.4.3.3 Synthesis of PSA-MA based on Br-MA, attempt 2 53
3.4.4 Conclusion 58

Chapter 4: Synthesis of polyelectrolyte-surfactant complexes 59
4.1 Introduction 59
4.2 Experimental 59
4.2.1 Experimental techniques 59
4.2.2 Preparation of polyelectrolyte-surfactant complexes 60
4.3 Results and discussion 60
4.3.1 Complex formation and analysis of MET/pDADMAC and CRO/pDADMAC 60
4.3.1.1 Elemental analysis (EA) 61
4.3.1.2 Polarized light microscopy 61
4.3.1.3 WAXS analysis 61
4.1.3.4 SAXS analysis 63

Chapter 5: Co-polymerization of MET and styrene 67
5.1 Introduction 67
5.2 Experimental 67
5.2.1 Experimental techniques 67
5.2.2 Polymerization of MET 67
5.2.3 Co-polymerization of MET with styrene and methyl methacrylate 68
5.3 Results and discussion 69
5.3.1 Co-polymerization 69
5.3.1.1 Solubility of polymers 72

5.3.2 Analysis of polymers 72
5.3.2.1 Molecular weight determination 72
5.3.2.2 Thermal stability 75
5.3.2.3 Differential scanning Calorimetry (DSC) 76

Chapter 6: Conclusions 79
6.1 Conclusions 79
6.2 Future work and recommendations 80

Chapter 7: References 81

Addendum 87

CMC determinations 88
TGA spectra 89
DSC spectra 90

List of abbreviations

δ	Chemical shift
ΔH	Heat (enthalpy)
2θ	Scattering angle
Å	Ångstrom
a_0	Optimal head group area
AIBN	Azo-*iso*-butyronitrile
ATR	Attenuated total reflection
Br-MA	Succinic acid mono-(11-bromo-undecyl) ester
c	Concentration
CAC	Critical aggregation number
CMC	Critical micelle concentration
C_p	Heat capacity
CRO	Sodium 11-crotonoyloxy undecanyl-1 sulfate
CRO1	11-Crotonoyloxy undecanol-1
d	Spacing between layers
β	Degree of binding
DSC	Differential scanning calorimetry
DMF	N,N-dimethylformamide
dw/dt	Weight loss per time
E	Linear charge density
EA	Elemental analysis
ESR	Electron spin resonance spectroscopy
FTIR	Fourier Transform Infrared spectroscopy
GPC	Gel Permeation Chromatography
HLB	Hydrophilic-lipophilic balance
IR	Infrared spectroscopy
KPS	Potassium persulfate
l_c	Critical hydrocarbon chain length
m	Mass
M	Mean aggregation number

M_n	Number average molecular weight
M_w	Weight average molecular weight
MALDI	Matrix-assisted laser desorption ionization
MET	Sodium 11-methacryloyloxy undecanyl-1 sulfate
MET1	11-Methacryloyloxy undecanol-1
MET-X-YY	Co-polymer of MET and [with X = amount of MET incorporated] either polystyrene (PS) or poly(methyl methacrylate) (PMMA) [YY = PS or PMMA]
n	Integral number of wavelengths
N	Number of monomers
nm	Nanometer
NMR	Nuclear magnetic resonance spectroscopy
opd.	optical path difference
P	Packing parameter
P	Power
pDADMAC	Poly(diallyl dimethyl ammonium chloride)
PE-Surfs	Polyelectrolyte-surfactant complex
PMMA	Poly(methyl methacrylate)
ppm	Parts per million
PS	Polystyrene
PSA	Phenol sulfonic acid, sodium salt dihydrate
PSA-MA	Sodium 4-[11-(3-carboxypropinoyloxy)-undecyloxy] benzenesulfonate
PTC	Phase transfer conditions
R	Radius of a micelle
s	Scattering vector
SANS	Small angle neutron scattering
SAXS	Small angle X-ray scattering
SDS	Sodium dodecyl sulfate
T	Temperature
t	Time
TEM	Transmission electron microscopy
TGA	Thermal gravimetric analysis
THF	Tetrahydrofurane
T_{max}	Maximum temperature of degradation
T_{on}	Onset temperature of degradation

T_P	Temperature of chosen program
T_R	Temperature of reference
T_S	Temperature of sample
v	Hydrocarbon chain volume
λ	Wavelength
WAXS	Wide angle X-ray scattering

List of figures

Chapter 1

1.1 Structures of synthesized surfmers (MET, CRO and PSA-MA).

1.2 Structure of poly(diallyl dimethyl ammonium chloride) (pDADMAC).

Chapter 2

2.1 Formation of supramolecular aggregates in a multi component equilibrium.

2.2 Amphiphiles such as surfactants and lipids can associate into a variety of structures in aqueous solution.

2.3 Association of N monomers into an aggregate (e.g. a micelle).

2.4 Parameters affecting packing: optimal head group area a_0, hydrocarbon chain volume v, critical chain length l_c.

2.5 Schematic representation of the molecular arrangement in the (A) isotropic phase; (B) nematic phase; (C) smetic A phase; (D) smectic C phase.

2.6 Schematic representation of the occurrence of the lyotropic mesophase.

2.7 A micro-zoology of supposed and observed shapes of micelles.

2.8 Conditions in bulk and surface of a solution containing a polyelectrolyte (fixed concentration) and a surfactant (variable concentration).

2.9 Formation of a complex by cooperative zipper mechanism between a polyelectrolyte chain and an oppositely charged surfactant.

2.10 Interaction of polarized light with an anisotropic material.

2.11 Definition of scattering vector s.

Chapter 3

3.1 ^{1}H NMR spectrum of sodium methacrylate.

3.2 ^{1}H NMR spectrum of sodium methacryloyloxy undecanol-1 (MET1).

3.3 ^{1}H NMR spectrum of sodium methacryloyloxy undecanyl-1 sulfate (MET).

3.4 ^{13}C NMR spectrum of sodium methacryloyloxy undecanyl-1 sulfate (MET).

3.5 ^{1}H NMR spectrum of sodium crotonate.

3.6 ^{1}H NMR spectrum of crotonoyloxy undecanol-1 (CRO1).

3.7 ^{1}H NMR spectrum of crotonoyloxy undecanyl-1 sulfate (CRO).

3.8 ^{13}C NMR spectrum of crotonoyloxy undecanyl-1 sulfate (CRO).

3.9 Reaction scheme for attachment of polymerizable group.

3.10 Reaction scheme for sulfonation of MET1 and CRO1.

3.11 ^{1}H NMR spectra of MET1 and MET with shift of $-C\underline{H}_2$-OH ($-OSO_3^-$) to indicate sulfonation.

3.12 ^{1}H NMR spectra of CRO1 and CRO with shift of $-C\underline{H}_2$-OH ($-OSO_3^-$) to indicate sulfonation.

3.13 Different stages during the melting of MET.

3.14 Crystals formed after MET (A) and CRO (B) were cooled to room temperature.

3.15 Possible reaction scheme 1 for synthesis of PSA-MA.

3.16 Possible reaction scheme 2 for synthesis of PSA-MA.

3.17 Reaction scheme for opening of MA and addition to 11-bromoundecanol-1.

3.18 ^{1}H NMR spectra to show differences between PSA and deprotonated PSA.

3.19 Reaction scheme for addition of PSA to Br-MA.

3.20 ^{1}H NMR spectra to show differences between Br-MA and PSA-MA.

Chapter 4

4.1 Schematic representation of 1 : 1 copy of MET/pDADMAC complex.

4.2 WAXS diffractogram of MET surfactant and MET/pDADMAC complex.

4.3 WAXS diffractogram of CRO surfactant and CRO/pDADMAC complex.

4.4 SAXS data for MET/pDADMAC complex.

4.5 SAXS data for CRO/pDADMAC complex.

4.6 Conformation of monomers at micelle-water and water-gas interfaces, showing 'loop' formation.

Chapter 5

5.1 Possible resonance structures for CRO.

5.2 Representative infrared spectrum of MET-styrene co-polymers.

5.3 Representative infrared spectrum of MET-MMA co-polymers.

5.4 Typical molecular weight distribution for MET-10-PS and MET-10-PMMA.

5.5 Overlay of infrared spectra of MET-20-PMMA to determine the chemical composition of fraction 1, 2 and 3.

5.6 TGA thermograms of co-polymers.

5.7 Typical DSC melting curve for MET-10-PMMA and MET-10-PS.

5.8 Formation of intermolecular bridges in the co-polymers.

5.9 TEM photo of MET-20-PS, showing a lamellar micro-structure.

List of tables

Chapter 2

2.1 Some specific examples of components in various amphiphilic classes.
2.2 General classification of uses of surfactants according to their HLB values.
2.3 Mean packing shapes and the structures they form, based on intermolecular and surface forces.

Chapter 3

3.1 Literature and experimental CMC values.
3.2 Thermal degradation of MET and CRO.

Chapter 4

4.1 WAXS peak positions for surfactants MET and CRO.
4.2 Peak position ratios for classical morphologies.

Chapter 5

5.1 Infrared band assignments for co-polymers.
5.2 Values of ratios of integrated areas in FTIR to determine the amount of MET incorporated into co-polymer.
5.3 Molecular weight values of co-polymers.
5.4 Degradation onset temperatures measured by TGA of co-polymers.
5.5 Specific melting and crystallization temperatures.

Chapter 1

Introduction

1.1. Definition of Nano-chemistry

Over the past decade, scientists from different fields have put forward the idea of synthesizing on a scale beyond that of single atoms and small molecules; they have been looking at synthesis on a supramolecular scale. The dimensions of supramolecular chemistry are mesoscopic (1 – 500 nm) and bridge the gap between atoms and solid-state science. Preformed building blocks and their introduction into ordered nano-structures have led to the formation of chemical systems with novel properties and combinations of properties [1]. The dimensions of the resulting chemical systems are one to two orders above that of classical low molecular weight compounds and such systems are known as the structures of "nano-chemistry". Micellization, aggregation, and the rules of stability and solubility that apply to classical colloids are closely related to many of the structural features of supramolecular chemistry. The products of nano-chemistry are novel materials with new and potentially very useful properties, but there is not necessarily a need for new starting materials. Properties of the products of nano-chemistry and potential new applications are a result of tailoring material on a nanometer scale and subsequently arranging the components by means of chemical interactions [1].

1.2. Amphiphiles and self-assembly

The field of colloid and surface science focuses on systems whose behaviour is dominated by the existence of mesoscopic length scales and / or significant interfacial regions.

An amphiphile can be defined as a molecule containing both a hydrophilic (or water loving) and lyophilic (or oil loving) part, which differ greatly in their solubilities. A bola-amphiphile contains two hydrophilic head-groups, linked by a lyophilic hydrocarbon chain.

McBain [2] was the first to suggest that molecules of an amphiphilic nature would self-assemble into aggregates called micelles (from the Latin *micella*, meaning small bit). This suggestion was made after noting a drastic change in the osmotic pressure of an amphiphilic system.

Self-assembly is the spontaneous intermolecular association via non-covalent bonds (such as electrostatic, hydrophilic and hydrogen bonds) that result in thermodynamically stable, well-defined structures. These structures have a complex hierarchical structure and form without external intervention [3].

Self-organized systems and their products have many industrial applications. Potential applications of nano-structured materials include

- nano-powders (catalysts, dielectrics, transducers, optical amplifiers) [4],
- thin films and nano-multilayers (semiconductor devices, flat-panel displays, passivation layers) [5, 6],
- nano-phase coatings (wear-resistant surfaces, thermal barriers) [6],
- nano-phase composites (gas turbine engines, bullet-proof vests) [6].

1.3. Motivation

Faul [7] reported the first successful attempt to create discrete, nano-shaped polymeric structures in a soft, self-assembled organic templating host (a polyelectrolyte-surfactant complex). These structures were a colloidal copy of the deformable host. The motivation for the present study was to create functional, nano-shaped polymeric structures in the same type of host. The surfactants used include three surfmers MET (**1**),

CRO (**2**) and PSA-MA (**3**), (Figure 1.1). All of them contain an anionic and an ester group as hydrophilic heads and a hydrocarbon chain with 11 methylene units as spacer. MET (**1**) and CRO (**2**) are known in literature [8] but have, up to date, only been synthesized in low purity. The polyelectrolyte used is poly(diallyldimethyl ammonium chloride) (pDADMAC) (**4**) (Figure 1.2) for its availability and low cost.

Block co-polymers are regarded as one of the most widely studied cases of self-ordering macromolecules due to their ability to organize spontaneously into a wide range of nano-structural elements in the same manner as low-molar-mass surfactants [9 - 11]. This was used as a motivation to investigate the behavior of a self-assembling monomer in a random co-polymer.

1.4. Objectives

The overall objective of this work was to synthesize three surfactants (MET (**1**), CRO (**2**) and PSA-MA (**3**)) with a polymerizable group, to use them in the formation of polyelectrolyte-surfactant complexes and determine whether the complexes with polyelectrolytes would make suitable hosts for templating. Furthermore, MET (**1**) was to be co-polymerized with styrene and methyl methacrylate to investigate the behavior of MET (**1**).

The specific tasks were therefore to:

- Synthesize, purify and characterize the three surfactants MET (**1**), CRO (**2**) and PSA-MA (**3**).
- Use the surfmers as surfactants to form polyelectrolyte-surfactant complexes. The surfactants were to be complexed with the polyelectrolyte, pDADMAC (**4**).
- Examine the formed complexes by means of small angle X-ray scattering (SAXS) to determine their suitability as hosts for templating.
- Co-polymerize 5, 10 and 20 % of MET (**1**) with styrene and methyl methacrylate and to characterize the formed co-polymers.

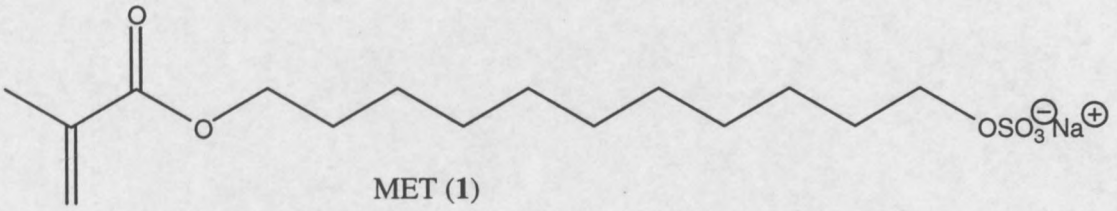

MET (**1**)

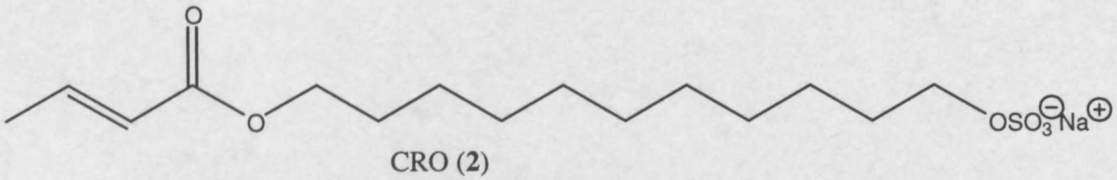

CRO (**2**)

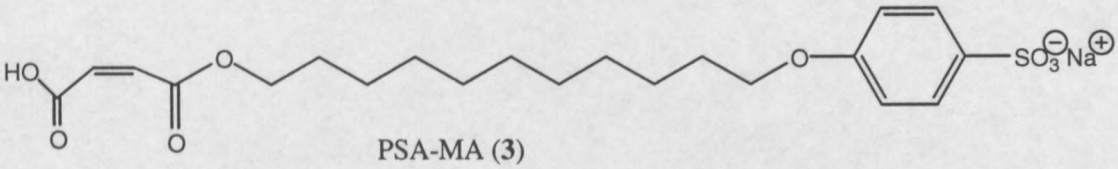

PSA-MA (**3**)

Figure 1.1. Structures of synthesized surfmers MET (1), CRO (2) and PSA-MA (3).

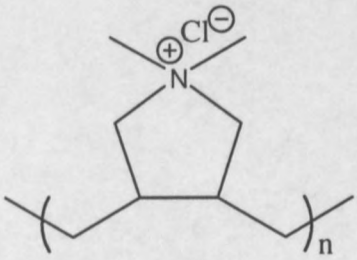

pDADMAC (**4**)

Figure 1.2. Structure of poly(diallyldimethyl ammonium chloride) (pDADMAC) (4).

1.5. Layout of Thesis

Chapter 1 introduces the area of research and includes the motivation for and objectives of the study.

A theoretical and historical background to this research is given in Chapter 2. Self-assembly, polyelectrolyte-surfactant complexes and the analytical methods used to characterize the synthesized materials, are discussed.

In Chapter 3 the synthesis and characterization of the three different surfactants to be used in the making of polyelectrolyte-surfactant complexes are described.

Results of investigations (SAXS) into polyelectrolyte-surfactant complexes (PE-Surfs) of the prepared surfactants and poly(diallyldimethyl ammonium chloride) (**4**) are presented and discussed in Chapter 4. The PE-Surfs are discussed in terms of being structure-directing hosts.

Chapter 5 describes the synthesis of the co-polymers of MET (**1**) and styrene or methyl methacrylate and their characterization.

Chapter 6 contains a summary of the results of this research and conclusions are made. References are given in Chapter 7. Complementary data is included in the addendum.

Chapter 2

Theoretical and Historical Background

2.1. Amphiphiles as Surfactants

2.1.1. Classification

Amphiphilic molecules possess a special molecular structure with both a hydrophilic (i.e. "water loving") and a hydrophobic or lipophilic ("oil loving") component.

They can be described and classified according to the charge carried by the hydrophilic part. A wide range of amphiphiles is available [12]:

- anionic (negatively-charged head-group may comprise of sulfonate, sulfate, carboxylate, phosphate),
- cationic (positively-charged head-group may comprise of ammonium, pyridinium, phosphonium),
- non-ionic (polyethylene oxide hydrophiles, amines, alcohols),
- amphoteric / zwitter-ionic (exhibit anionic properties at high pH and cationic properties at low pH),
- bolaform (hydrophilic group at each end of the hydrophobic chain) and
- higher star amphiphiles.

Some specific examples are given in Table 2.1.

Table 2.1. Some specific examples of components in various amphiphilic classes.

Type of amphiphile	Specific examples
Anionic	Sodium dodecyl sulfate (SDS), sodium palmitate
Cationic	Lauryldimethylbenzylammonium chloride, Cetylpyridinium bromide
Non-ionic	Lauryl alcohol, Cholesterol
Zwitter-ionic	Lecithin, Proteins
Bola-form	Amino acids

Surfactants are characterized by a number of physical parameters including the hydrophilic-lipophilic balance (HLB) and critical micelle concentration (CMC). In 1949 Griffin proposed an empirical scale, the HLB scale [13], to describe the balance between the hydrophilic and

lipophilic portions in molecules. It indicates the polarity of the molecules in an arbitrary range. This has been widely used for the selection of surfactants in emulsifying processes. The HLB number increases with increasing hydrophobicity. A broad classification of applications for surfactants according to their assigned HLB values is given in Table 2.2.

Table 2.2. General classification of uses of surfactants according to their HLB values [14, 15].

Application of surfactant	HLB range	Specific example (HLB value)
Antifoaming agent	--	Ethylene glycol distearate (1,3)
Water-in-oil emulsifier	3 – 6	Propylene glycol monostearate (3,5)
Wetting agent	7 – 9	N,N-Dimethyl stearamide (7)
Oil-in-water emulsifier	8 – 18	4-Cetyl-phenyl sulfonate (~11^{+})
Detergent	13 – 15	*tertiary*-(Poly oxyethylene) amine (~14)
Solubilizer	15 – 20	Potassium oleate (20)

2.1.2. Bola-amphiphiles

Bola-amphiphiles contain two hydrophilic head-groups which are bound by one or two hydrophobic chains. The name 'bola' refers to a weapon used by South American indigenous people, consisting of two balls at the ends of a piece of rope.

These surfactants are typically present in the membranes of Archaebacteria, primordial microorganisms, that live in extreme environments and experience drastic environmental conditions [16].

Bola-form electrolytes (e.g. Me_3N^{+}-$(CH_2)_{12}$-$^{+}NMe_3$) can display physiological activity, bind to polymers, associate in water and form crystalline clathrates [17].

2.1.3. Nature of polymerizable amphiphiles

Some amphiphiles, such as surfactants, have generated much interest due to their dual nature as surface active species and as polymerizable monomers. The more general term 'surfmer' is used; it is derived from the terms SURFactants monoMERs.

Surfactants are surface active because of their ability to be absorbed at various interfaces (e.g. air-water, oil-water, etc.) and alter the properties of the interface. As reactive surfmers, these compounds have been used to synthesize entirely novel materials and to achieve polymerization in structurally-ordered media [18]. They have also been used in heterogeneous polymerizations, e.g. in emulsion polymerizations, replacing conventional surfactants with the aim of improving latex properties [19].

Unlike solid particles or rigid macromolecules such as DNA, amphiphilic molecules are soft and flexible, i.e., fluid-like in aqueous media. The forces that hold them together in micelles and bilayers (see section 2.1.4) are not strong covalent or ionic bonds but are rather van der Waals, hydrophobic, hydrogen-bonding and screened electrostatic interactions [20].

2.1.4. Behavior of surfactants in solvents

The hydrophilic head and hydrophobic tail of amphiphilic molecules in aqueous media behave differently. To minimize unfavorable solvophobic (solvent-hating) interactions, they spontaneously aggregate to form a variety of microstructures. The hydrophobic effect is the driving force behind any form of aggregation. For instance, the formation of ionic micelles is the result of two effects, i.e. of a promotional one involving the repulsion of hydrocarbon chains from water and that of an opposing one due to the mutual repulsion of the ionic head groups. The second effect is reduced by the presence of counterions close to the micellar surface [21].

Changes occurring on a nano-structural level as the concentration of an amphiphile in an aqueous solution increases (Figure 2.1) can be discussed in term of changes in various properties of the solution, e.g. surface tension, conductivity, viscosity, etc. The approach followed, is to explain the changes on molecular level in terms of changes in the surface tension of a model surfactant system. Other experimental techniques used to follow changes occurring on this nano-structural level include conductivity and viscosity measurements, solubilization studies and scattering studies [22].

At low concentrations, surfactant molecules will arrange themselves at the air-water interface, with their hydrocarbon tails away from the water, and the charged headgroups interacting with the water molecules. The presence of the molecules at the interface will lower the

surface tension as an air-water interface has a higher surface tension than an air-hydrocarbon interface, which will decrease further with increasing surfactant concentration. Some of the amphiphilic molecules will be present as free "monomer" in the solution [20, 23].

At a very specific concentration, the so-called critical micelle concentration or CMC, a sudden change will be observed in the surface activity of the solution. After this point, the surface tension will remain constant over a wide concentration range. On a nano-structural level, this sudden change in the observed properties is characterized by a large change in the rearrangement of the amphiphile molecules. The "free monomeric" amphiphiles in solution aggregate, above the CMC, into spherical-like aggregates, termed micelles (Figure 2.1).

As the concentration of the amphiphile is increased, more micelles are formed in the solution, but the concentration of the amphiphilic molecules will remain constant as the surface tension remains constant. The number of molecules combining to form a micelle is called the aggregation number and remains constant as the amphiphilic concentration is increased.

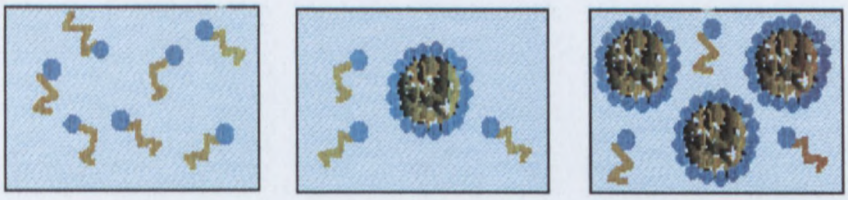

Figure 2.1. Formation of supramolecular aggregates in a multi-component equilibrium. The spots represent the polar head-groups and the lines indicates the hydrophobic tails [16].

The size, shape and structure of micelles have been investigated by various methods, including scattering techniques, electron spin resonance spectroscopy (ESR) and nuclear magnetic resonance spectroscopy (NMR). Using NMR and fluorescence probes it has been established that the core of the micelles is fluid-like, e.g. pure hydrocarbon, with some penetration by the surrounding water molecules into the so-called Stern-layer surrounding the micelle [24].

2.1.5. Self-assembly

Amphiphilic molecules in aqueous solution spontaneously self-organize into a variety of structures such as micelles, bilayers and vesicles (Figure 2.2) which can transform from one to another when the solution conditions, e.g. temperature, concentration or pH, are changed.

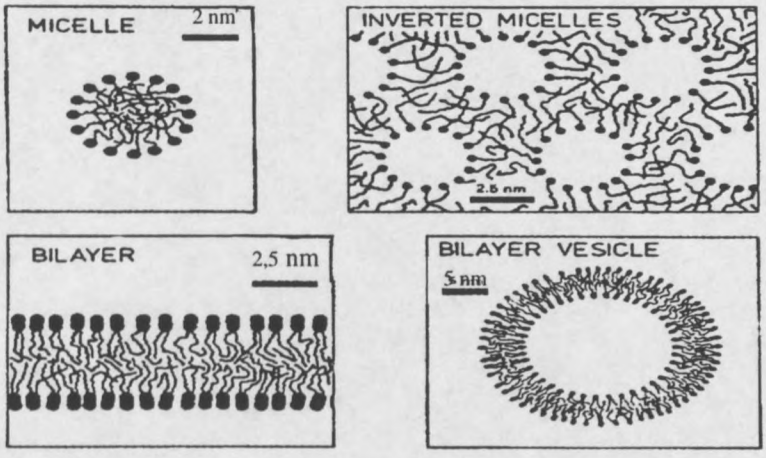

Figure 2.2. Amphiphiles such as surfactants and lipids can associate into a variety of structures in aqueous solutions [20, p344].

Association of amphiphilic molecules into structures is driven by two forces: the thermodynamic force of self-assembly and the intra-aggregate forces. Thermodynamics and intra-aggregate forces, together with the strength of the forces between aggregates in more concentrated systems, determine which equilibrium structures will be formed.

Equilibrium thermodynamics requires for a system, that forms aggregated structures in solution (Figure 2.3), that the chemical potential of all identical molecules in different aggregates be the same. Aggregates will only form when there is a difference in the cohesive energies between the molecules in the aggregated and dispersed states.

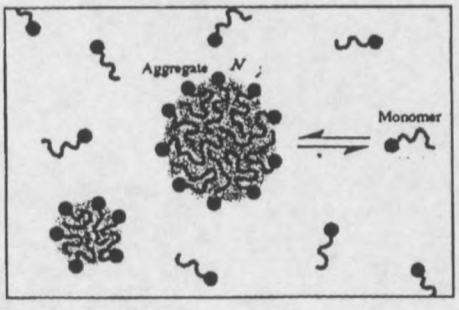

Figure 2.3. Association of N monomers into an aggregate (e.g., a micelle) [20, p346].

At low concentrations most of the molecules in solution will be isolated monomers. At some stage the monomer concentration cannot increase any further and this is the critical aggregation concentration (CAC) which is related to the CMC. This concentration is the critical concentration of all self-assembled structures. Further addition of solute molecules will form more aggregates while leaving the monomer concentration more or less unchanged [20].

The intra-aggregate forces can be discussed by the following parameters (Figure 2.4) and how they affect the packing: the optimum surface area per molecule at the hydrocarbon-water interface a_0 [nm^2], hydrocarbon chain volume v [nm^3] and critical length l_c [nm]. The packing parameter or shape factor

$$P = v/a_0 l_c \qquad (2.1)$$

determines which aggregate will be formed (Table 2.3).

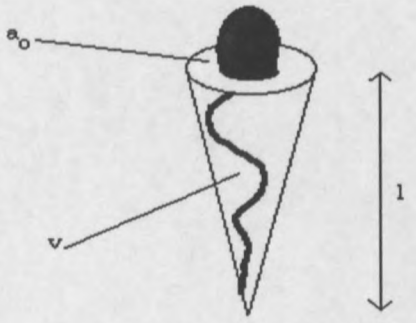

Figure 2.4. Parameters affecting packing: optimal head-group area a_0, hydrocarbon chain volume v, critical length l_c (adapted from [20], p368).

The critical chain length, l_c, sets the limit on how far the chain can extend before it is no longer considered as a fluid. Tanford [25] derived the following equations for determining (1) an extended saturated hydrocarbon chain with n carbon atoms:

$$l_c \leq l_{max} \approx (0{,}154 + 0{,}1265n) \qquad \text{[nm]} \qquad (2.2)$$

where

l_{max} is the maximum length possible for an extended saturated hydrocarbon chain in nanometers and (2) determining the volume (v) of the hydrocarbon chain:

$$v \approx (27{,}4 + 26{,}9n) * 10^{-3} \qquad \text{[nm}^3\text{]} \qquad (2.3)$$

The effective head-group area a (at a minimum energy, $a = a_0$) is determined by the interaction of two opposing forces [25]:

- the hydrophobic attraction at the hydrocarbon-water interface which arises from the hydrophobic or interfacial tension forces, induces the molecules to associate, and
- the hydrophilic, ionic or steric repulsion of the head-groups which induce that they remain in contact with the water. These repulsions are still too complex and difficult to formulate.

With these two opposing forces working on the formation of equilibrium structures, the system will reach a position of an optimal area per head-group a_0 when the total interaction energy per molecule in the aggregate is at a minimum. This optimal area is strongly affected by parameters such as counter-ion concentration and pH.

The effective area a_0 per head-group in a spherical micelle can be calculated by:

$$M = 4\pi R^2 / a_0 \qquad (2.4)$$

where

R – radius of micelle ($4\pi R^2$ - surface of the micelle)

M – mean aggregation number (the number of molecules that form one micelle)

Aggregation numbers can be determined by light scattering, diffusion studies, sedimentation by ultracentrifugation, X-ray and neutron scattering and fluorescence probes.

It has been shown by Isrealachivili [26] that for certain packing parameters P (Equation 2.1), the amphiphilic molecules will have certain packing shapes and micellar aggregates will adopt certain shapes or structures. See Table 2.3.

Table 2.3. Mean packing shapes and the structures they form, based on intermolecular and surface forces [20].

Surfactant	Critical packing parameter	Critical packing shape	Structure formed
Single-chain surfactants with large head-group areas	< 1/3	Cone	Spherical micelles
Single-chain surfactants with small head-group areas	1/3 – ½	Truncated cone	Cylindrical micelles
Double-chain surfactants with large head-group areas, flexible chains	½ - 1	Truncated cone	Flexible bilayers, vesicles
Double-chain surfactants with small head-group areas, fluid chains	~1	Cylinder	Planar bilayers
Single-chain surfactants with small head-group areas, fluid chains	>1	Inverted truncated cone or wedge	Inverted micelles

Factors that cause changes from one micellar structure to another can be summarized as follows:

- Factors affecting head-group area. For anionic head-groups, the salt concentration, or lowering of pH can affect head-group area. This also has the effect of straightening the chains.
- Factors affecting chain packing. Chain branching and unsaturation (particularly of cis double bonds) reduces l_c and thus increases $v/(a_0 l_c)$.
- Change in temperature. Temperature changes can alter both a_0 and l_c.
- Mixtures of surfactants.

2.1.6. Self-assembly of bola-amphiphiles

A special case of self-assembly is associated with bola-amphiphiles. The non-covalent interactions which exist between the hydrophilic / charged groups at the ends of bola-amphiphiles, combined with the hydrophobic interactions of the hydrocarbon spacers, lead to self-assembly into monolayered structures / sheets. These sheets interact to form multilayered helical fibers. Intermolecular hydrogen bonds and hydrophobic interactions also lead to the formation of solid-like supramolecular fibrous and tubular structures of several microns in

length [27]. Other interesting self-assembly phenomena have been observed: during the supramolecular construction of bola-amphiphilic microtubes, vesicles are incorporated into the microtubes [28]. Further manipulation of the self-assembled structures can be performed by structural modifications of the hydrophilic moieties [29].

2.2. Self-Assembly into Mesomorphic Phases

2.2.1. Liquid crystals

Liquid crystals were discovered in 1888 by the Austrian botanist Reinitzer who observed that cholesteryl benzoate exhibits two melting points [30]. Lehmann was the first to describe the properties in 1889 as "flowing crystals," then "crystalline liquid" and finally "liquid crystals" in 1900 [31]. The idea of performing chemical reactions in anisotropic liquids was that of Svedberg who reported his first experimental data in 1916 [32 - 35].

A liquid crystalline or mesomorphic phase or mesophase refers to a state of matter where the degree of order is between that of a solid crystal and that of an isotropic liquid. In solid crystals the degree of long-range order is almost perfect, whereas a liquid or a gas has long-range disorder. In a mesophase there is a certain degree of order but no perfect long-range order. Mesogens give rise to mesophases and can be classified as amphiphilic or non-amphiphilic (usually a rod- or disk-shaped geometry).

2.2.2. Classification of mesomorphic phases

Mesomorphic phases generated by mesogens can be classified into three groups, according to the mechanism of their formation.

- Thermotropic mesophases are induced by a change in temperature.
- Lyotropic mesophases are induced by a solvent (change in concentration).
- Amphotropic mesophases are induced by change in temperature or concentration.

There are many types of liquid crystal states, depending on the amount of order in the material. The nematic phase (Figure 2.5B) has no positional order but tends to point in the same direction. Smectic phases show a degree of translational order but also align themselves in layers or planes. It can be either an untilted layer (smectic A) (Figure 2.5C) or a tilted layer (smectic C) (Figure 2.5D).

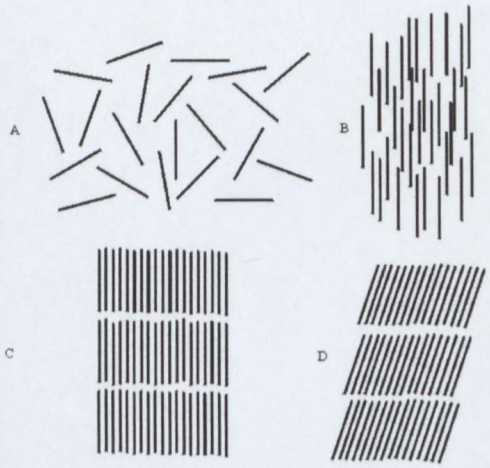

Figure 2.5. Schematic representation of the molecular arrangement in the (A) isotropic phase; (B) nematic phase; (C) smectic A phase; (D) smectic C phase (adapted from [18], p.5).

In the presence of water, amphiphilic molecules tend to form condensed phases. A change in the composition of a water / amphiphile system or a temperature change can generate various mesomorphic phases (Figure 2.6). For many single chain, ionic amphiphiles the most important way to induce a phase change is a variation in concentration / composition.

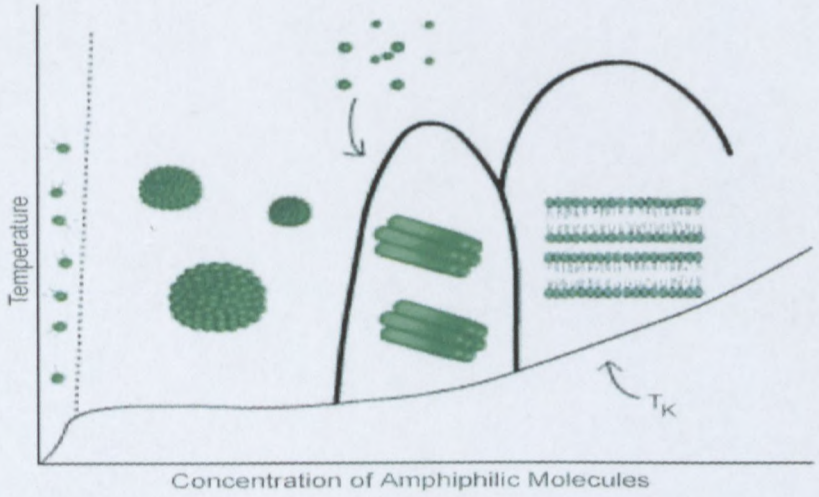

Figure 2.6. Schematic representation of the occurrence of lyotropic mesophases. It shows a phase diagram that indicates the changes in structure dependent on the concentration of the amphiphile and temperature. The CMC is shown with the dotted line. The solid line, T_K, represents a boundary temperature (Krafft temperature). Below the Krafft temperature, some small liquid crystals may be suspended in the solution. The temperature boundary is related to the melting point of the hydrocarbon tails [23].

As the concentration of the amphiphile in the water increases, micelles begin to arrange themselves into loose patterns. These patterns are the actual liquid crystal aspects of the

molecular behavior. Some of the mesophases found (starting from the isotropic and micellar phases) are [36]:

- Cubic phase

  I-phase, consists of micelles in a face-centered or body-centered cubic lattice, occurring between the micellar and hexagonal phases.

- Hexagonal array of rod-like structures (also called the "middle soap" phase)

  H_I-phase, consists of six rod-like structures grouped around a central one to form a hexagonal array.

- Lamellar phase (also known as the "neat soap" phase)

  L_α-phase, consists of surfactant molecules arranged in bilayers separated by water layers.

- Inverse hexagonal array of rod-like structures

  H_{II}-phase, the hydrocarbon chains occupy the spaces between the hexagonally-packed cylinders of water.

Amphiphilic mesogens self-assemble into these structures. The basis of such self-assembly is similar to that of micelle formation. Unfavorable interactions of the amphiphilic groups with the solvent as well as favorable hydrophobic interactions drive the process of mesophase formation [37]. These mesophases are thermodynamically stable and the phase found depends on the amphiphilic / mesogenic component concentration. Generally the order in a mesophase increases with increase in the amphiphilic concentration.

As the mesogenic component concentration is increased, phase transitions will occur. Kekicheff and co-workers [38 - 41] showed that even in the case of a very simple amphiphilic component, such as sodium dodecyl sulfate (SDS), a number of intermediate mesophases exist in the concentration region between the ordered hexagonal and lamellar phases. These structures, which include a tetragonal phase, a cubic phase, a rhombohedral phase and a two-dimensional monoclinic phase, which occur over a very narrow concentration range (< 1%), are suggested to be necessary for the system to change from a system of high curvature (cylinders) to that of zero curvature (bilayers).

The observed transition / intermediate states occur through the deformation of cylinders (the hexagonal phase) into ribbons (two-dimensional monoclinic phase), which merge (side and length wise, rhombohedral phase). Continual deformation leads to a cubic phase, which

finally produces the lamellar phase which still contains some defects. These changes were ascribed to a constant change in the mean curvature of the interfaces.

Certain polymers also exhibit liquid crystalline behavior due to mesogenic groups present in either the main chain of the polymer, the side chain or both. The mesogens can be disc-shaped, rod-like or amphiphilic in nature. Poly(hydroxynaphthoic acid) is a good example of a rigid, rod-like, main chain non-amphiphilic liquid crystalline polymer [42].

Block copolymers phase separate on a mesoscopic length scale due to unfavorable interactions, providing the basis for the formation of mesomorphic phases [43].

2.3. Polyelectrolyte-Surfactant Complexes

2.3.1. Polyelectrolyte-surfactant complexes in solution

The self-assembly of surfactants into micelles is probably one of the best-known and most utilized phenomena. The aggregation of surfactants into micelles is the basis of a variety of technological processes, such as washing and phase-transfer catalysis. In contrast, the beauty and complexity of lyotropic liquid crystalline phases, which are formed in highly concentrated surfactant solutions, is mainly the domain of the specialist. As a result of the underlying energetic rules, these phases show highly symmetric architectures (Figure 2.7).

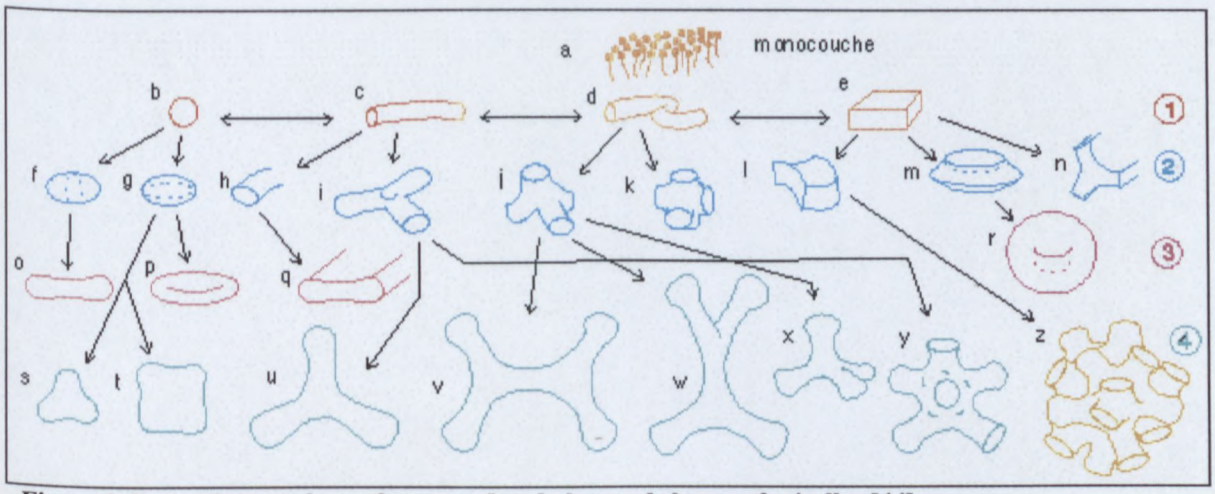

Figure 2.7. A micro-zoology of supposed and observed shapes of micelles [44].

Despite their beauty, it has not been possible to utilize these architectures because of their fragility. Their consistency is best described as oil- or margarine like, which allows their application by virtue of their function, but not by virtue of their structure.

In order to exploit the surfactant phase structures in all their various morphologies, these aggregates have to be nanochemically stabilized by a second component, without compromising their ability to form structures. The function of the second component in this "team" is the introduction of mechanical stability and improvement of handling. This is possible by complexing a polyelectrolyte with oppositely charged surfactants.
The formation of polyelectrolyte-surfactant complexes (PE-Surfs) has been known for some time [45 - 47]. The interactions between proteins and surfactants were one of the first systems to be studied in the 1930's [45]. Since then, research has focused on two broad areas,

- interactions between uncharged polyelectrolytes and charged surfactants and
- interactions between charged polyelectrolytes and surfactants of opposite charge.

Interactions between oppositely charged species will be discussed further.

The combination of oppositely charged polyelectrolytes and surfactants might lead to soluble or insoluble complexes, depending on the charge balance and stoichiometry of the system. The association of surfactants with an oppositely charged polyelectrolyte can be discussed by using the surface tension of such a solution, keeping the polyelectrolyte concentration constant and increasing the surfactant concentration, as shown in Figure 2.8. Surface tension should provide information on the newly formed species in solution, since the surfactant is very active at the air-water interface, and the polyelectrolyte fairly inactive.

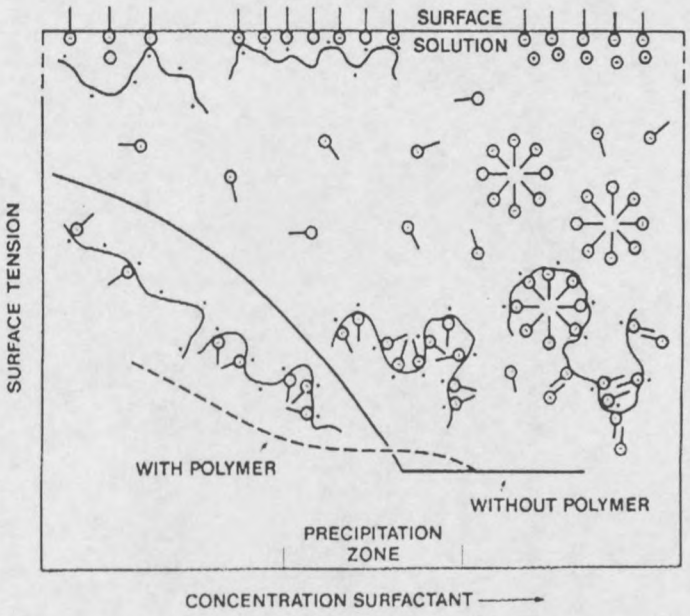

Figure 2.8. Conditions in bulk and surface of a solution containing a polyelectrolyte (fixed concentration) and a surfactant (variable concentration) (taken from [48], p. 175).

The presence of the polyelectrolyte can already be seen at very low surfactant concentrations. The surface tension of the solution is much lower (dashed line in Figure 2.8) than for the surfactant-only (solid line in Figure 2.8) system, indicating the formation of a highly active surface species. This species is shown on the far left top side of Figure 2.8. The polyelectrolyte shows some interaction with the surfactant molecules at the air-water interface. As the surfactant concentration is increased, more interaction is seen between the surfactant and the polyelectrolyte at the air-water interface as well as in the solution. The surface tension is still lower than for the surfactant-only system. As the reaction system approaches 1:1 stoichiometry, the polyelectrolyte-surfactant complex will start to precipitate, first seen as turbidity in the solution. A further lowering of the surface tension is also observed. The surface tension now begins to approach values similar to those found in a surfactant-only system above the CMC. As the surfactant concentration is increased beyond the point of charge neutralisation, the surface tension has the same value as for a surfactant-only system. This indicates that all polyelectrolyte molecules are to be found in the solution in interactions with surfactants, and none at the air-water interface. The excess surfactant can now be found at the air-water interface, behaving as a surfactant in a solution with a concentration higher than that of the CMC. With a further increase in the surfactant concentration, the precipitation zone is crossed, and the polyelectrolyte-surfactant complex

precipitates are re-dissolved (according to the "beads-on-a-string" model as discussed below). The surface tension values now correspond to those of a surfactant-only system.

Investigations into the binding process were performed by Shinoda in the early 1970's [47] followed by a series of studies by Kwak from 1980 to 1983 [49 - 52]. Results showed that the aggregation process is highly cooperative, i.e. the process takes place over a very narrow surfactant concentration range and is driven not only by electrostatic interactions, but also by the interactions of the hydrophobic alkyl tails of the surfactant associating. The degree of binding ß (ß corresponds to the fraction of available charges on the polyelectrolyte neutralised by the binding of surfactant ions) increases very sharply, and levels off at values close to one. Furthermore, it was confirmed that the process commenced at concentrations much lower than the critical micelle concentration (CMC) of the surfactant, at the so-called critical aggregation concentration (CAC). The CAC can be defined as the concentration at which the aggregation of surfactant and polyelectrolyte can first be detected. This concept was initially described by Jones in two papers in the late 1960's [53, 54]. The addition of salt to a reaction system decreases the CAC, indicating higher shielding by the added ions and reduced interaction between the polyelectrolyte and surfactant [55].

Precipitation of the complex is observed at a ß-value of 1, since the binding of the surfactant removes all charges responsible for the stabilisation / solvation of the polyelectrolyte. As the surfactant concentration is increased, the complex is re-solubilized. This takes place at ß-values much higher than unity and probably according to the so-called "beads-on-a-string" model of polyelectrolyte-surfactant interaction. This model for such systems in solution was already proposed in 1974 by Shirahama [56]. Here the excess surfactant will interact with the bound surfactant, forming micelle-like structures in close association with the polyelectrolyte (resembling the beads on a string), causing the total aggregate to be solubilised again. The whole complex is therefore actually converted into a polyelectrolyte of opposite charge (compared to the original polyelectrolyte).

Complex formation is influenced by different properties of polyelectrolytes and surfactants [57].

Polyelectrolyte properties which affect complex formation are:

- linear charge density E (an increase in E causes stronger interactions),
- hydrophobicity of the polymer (interaction enhanced with increasing hydrophobicity),
- flexibility of the polyelectrolyte backbone,
- length of the polyelectrolyte chain.

A study by Shirahama and co-workers [58], focussing on the effect of the size of the polyelectrolyte on the binding process, indicated that both the CAC and the cooperativity of the binding process are influenced by the molecular weight of the polyelectrolyte. The CAC will increase, while the cooperativity will decrease with increasing molecular weight. This was attributed to the effect of a change in the number of binding sites (charges) due to a change in the length of the polyelectrolyte.

Surfactant properties which affect complex formation are:

- geometry of the surfactant,
- alkyl chain length (increased hydrophobicity increases complex formation),
- nature of the counter-ion (strong polyelectrolyte e.g. polystyrenesulfonate (PSS) and weak polyelectrolyte e.g. poly-acrylic acid (PAA)),
- concentration of the surfactant (below the CMC).

Current investigations into polyelectrolyte-surfactant interactions in solution focus on factors such as chemical structures and concentrations of the polyelectrolyte and surfactant, ionic strength and temperature of the reaction solutions. The techniques used to investigate these can be divided into classical physical methods and spectroscopic methods.

- Physical methods include conductance and potentiometry, surface tension, viscometry and calorimetry.

- Spectroscopic methods include techniques such as nuclear magnetic resonance spectroscopy (NMR), electron spin resonance spectroscopy (ESR), infra-red (IR) and Raman spectroscopy, light scattering, UV and fluorescence spectroscopy, microscopy and small angle neutron and small angle X-ray scattering (SANS and SAXS) [57].

Current studies also include investigations of natural polyelectrolyte systems, and the interactions between surfactants and polysaccharides [59], polypeptides [60] and proteins [61]. One variation on the theme, adopted from nature, is the complexation of polyelectrolytes with lipids instead of surfactants [62 - 65].

The combination of polyelectrolytes and surfactants has been extensively used in a wide variety of applications, including the production of photographic film emulsions, cosmetics, pharmaceutical applications, and in paper manufacturing, mining applications, rheology modifiers and various food science applications [66]. Other applications that have been investigated include the utilisation of complexes from lipids and polyelectrolytes as membrane mimicking agents [67]. New trends in similar systems, where electrostatic interactions between oppositely charged polyelectrolytes and other charged components (proteins/enzymes, charged particles) are utilised, are finding application in biochemical and biomedical research and possible drug targeting studies [68].

2.3.2. Polyelectrolyte-Surfactant complexes in solid self-organizing building blocks

The first investigation into the solid-state structure of polyelectrolyte-surfactant complexes (PE-Surfs) was performed by Harada and Nozakura in 1984 [69]. They investigated the structure of dried 1:1 stoichiometry complexes by means of TEM. Ujiie investigated the formation of ion-surfactants and PE-Surf complexes in the early 1990's, tentatively proposing structures for the formed complexes [70]. Ten years after the first investigations, the solid

state structures of these complexes were fully elucidated for the first time by Antonietti and co-workers [71, 72].

The formation of PE-Surfs follows a very simple process of self-assembly: PE-Surfs are "synthesized" by adding an aqueous solution of the polyelectrolyte to an aqueous solution of the surfactant in a 1:1 ratio of charges. The opposite charges on the surfactant molecules and the polymer backbone cause an attractive Coulomb interaction, which - increased by the additional hydrophobic interaction of the alkyl chains – initiates a cooperative aggregation process, resembling of a zipper. Figure 2.9 provides a schematic representation of the initial formation of the complex. As a result, the PE-Surf becomes increasingly less water-soluble and precipitates usually in a strict 1:1 stoichiometry.

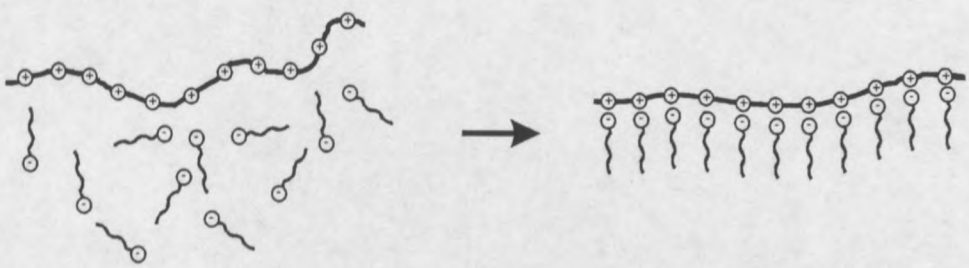

Figure 2.9. Formation of a complex by cooperative zipper mechanism between a polyelectrolyte chain and an oppositely charged surfactant [73].

Once the complex has been synthesized, the system has no well-defined mesomorphic structure. It is only after solvent casting that a mesoscopically ordered structure is obtained. This is due to the very high glass transitions of the ionic layers, which inhibit organization of the structures during the formation of the complex [74]. After casting, the obtained films can be flexible, of high homogeneity, good optical quality and often high mechanical stability.

As the complexes still possess the structural features of the surfactant (a line-up of matching charges on the one hand and the incompatible, wax-like alkyl chains on the other), a micro phase separation occurs in the solid state. Because of the surfactant geometry, the formation of micro phases is limited to approximately twice the length of the surfactant molecule, and formation of an ordered structure is observed. The phase structures formed by such systems

can be extraordinarily manifold and are often highly symmetric (Figure 2.7). The particular morphology depends on a delicate balance of

- charge density of the polyelectrolyte,
- the relative volumes of alkyl and ionic phases,
- the absolute interface energy (determined by the number of surfactant molecules per unit volume),
- the spontaneous curvature of the interface,

as well as many other factors, which are associated with the geometries of the surfactant and the polyelectrolyte component. The characteristic length of the sequence of microphases (or nanophases) depends on the nature of the surfactant and on symmetry, but usually lies between 2 and 8 nm [75].

The polyelectrolyte chains also have to abide by strict geometric rules in the microphase. It can be calculated that the nanocylinder in such a phase offers space for approximately four polyelectrolyte chains.

PE-Surfs have been investigated by various methods, including optical microscopy, thermal analysis [76], mechanical analysis [77], dielectric analyses [78], NMR analysis [75], and X-ray analysis [74] (both wide angle X-ray scattering (WAXS) and small angle X-ray scattering (SAXS)). Investigation by WAXS shows that the complexes are non-crystalline on a local length scale, i.e. the surfactant's side chains exhibit liquid or liquid crystalline type arrangements.

Reported phase structures include

- hexagonally-ordered cylindrical phases, including normal, reverse and undulating cylindrical phases [72],
- cubic,
- normal and perforated (mattress) lamellar,
- egg-carton [75, 79, 80].

PE-Surfs are a typical example of the nanochemical approach and resulting chemical systems: a highly symmetrical, ordered system generated on a nanometer scale by self-assembly and the particular, preserved properties introduced by two incompatible components.

2.3.3. Polymerization in polyelectrolyte-surfactant complexes

Over the last three decades, a variety of experiments have been carried out to perform polymerization reactions in organized media [18]. One aim is to imprint the organized structure onto the polymer to be formed, preserving the shape imprint of the organized state after removal of the surfactant / organized medium / template. Faul [7, 81] set out to create shaped nano-particles as a one to one copy of (or as close as possible to) a template using a PE-Surf of sodium dodecyl sulfate (SDS) and poly(diallyldimethyl ammonium choloride) (pDADMAC). It was found that the high molecular weight polyelectrolyte backbone provided a more stable structure-directing host than a surfactant system alone.

2.4. Analytical Techniques

2.4.1. Introduction

In synthesis, the most important analytical techniques to determine structure and purity, are nuclear magnetic resonance (NMR) and elemental analysis (EA). Liquid crystalline behavior, phase transitions and melting points can be determined by differential scanning calorimetry (DSC) and polarized light microscopy.

X-ray diffraction (small angle X-ray scattering (SAXS), wide angle X-ray scattering (WAXS)) and polarized light microscopy are the analytical techniques generally used to study morphology and characteristics of mesophases and mesostructured systems.

Specific theoretical background to some of the analytical techniques used in this study will be described here. Chapter 4.1.2. gives detailed information on the experimental setup.

2.4.2. Elemental analysis (EA)

EA is used to determine the purity of samples, making use of the ratio of carbon, hydrogen and oxygen present in a sample.

It involves burning an accurately weighed amount of the sample (typically 1-2 mg weighed to +/- 0.1 μg) in oxygen. In this process carbon is fully oxidized to carbon dioxide and hydrogen

is converted to water. The nitrogen initially produces a mixture of oxides of nitrogen which are reduced to nitrogen. The three resultant products are then separated by gas chromatography and quantitatively determined [82].

2.4.3. Differential scanning calorimetry (DSC)

Thermal analysis is defined as a 'term covering a group of techniques in which a physical property of a substance and / or its reaction product(s) is measured as a function of temperature'. DSC curves reflect changes in the energy of a material, that can be chemical or physical in origin. Degradation, polymerization and other chemical reactions and interactions can also be studied.

Two types of DSC instruments are commonly used. A power-compensated DSC consists of two separate furnaces for the sample and the reference sides. The system can be divided into two control loops, the average temperature loop and the differential temperature loop. The average temperature loop heats the sample (T_S) and reference (T_R) sides at the programmed rate (T_p). The differential temperature loop maintains identical temperatures between the reference and sample pans regardless of the different amount of heat (ΔH) needed to enter the sample side. This process ensures that the sample is always kept at the same temperature as that of the reference, regardless of any changes that occur within the sample. When an endothermic process occurs, such as softening or melting, more heat is added to the sample side relative to the reference to make up for a difference in temperature. With an exothermic process less heat is added to the sample relative to the reference side.

The power (P) or heat per time ($\delta H/\delta t$) is described by the following equation

$$P = [\delta H/\delta t]/m = c_p . \delta H/\delta t \qquad (2.5)$$

with

H = heat (or enthalpy) [J],

t = time [s],

m = mass [g],

c_p = capacity of heat [J/(gs)],

T = temperature [K].

To obtain the enthalpy, the equation becomes

$$\delta H/m = c_p.\delta T \text{ [J/g]} \quad (2.6)$$

Power (P) in watts delivered to the sample and reference pans is dependent on the fluctuation of the individual temperatures from that of the programmed rate (T_p), as would be the case for an endothermic process:

$$\text{Power } P_s \text{ delivered to the sample} = c_{P,S}(T_s - T_p)/dt \text{ [W/g]} \quad (2.7)$$

$$\text{Power } P_r \text{ delivered to the reference} = c_{P,R}(T_r - T_p)/dt \text{ [W/g]} \quad (2.8)$$

The differential power requirement (ΔP) can be written as follows:

$$\Delta P = [c_{P,S}\,(T_s - T_p) - c_{P,R}\,(T_r - T_p)] \text{ [W/g]} \quad (2.9)$$

and is the quantity that is plotted and represented as a function of T_p, T_r or T_s.

A heat-flux DSC consists of one furnace with two thermocouples below the surface sensing the temperature on the reference and the sample side. The instrument measures ΔT between the sample and the reference side and converts it to power. The final result is power (heatflow) per mass (W/g).

In order to assess the thermal properties of a material, the heating and cooling rates are of the utmost importance for the investigation. With too high a rate, a thermal lag will exist, where as with too low a rate, possible degradation of the specimen may take place [83 - 86].

2.4.4. Thermal gravimetric analysis (TGA)

A TGA measures the weight loss of a sample as a function of temperature. It is done by placing a sample onto a sample holder that hangs from a micro-gram balance during the entire experiment. The balance mechanism consists of a sample pan holder suspended by a long hang down wire. The hang down wire is connected to the balance lever by a small quartz link to prevent static build up. The weight of the sample holder configuration is electromagnetically balanced on the other side so that the balance can be tiered before each run [86].

2.4.5. Polarized light microscopy

All non-opaque substances can be divided into two groups according to their behavior when examined between cross polars, namely isotropic and anisotropic materials. Isotropic materials have optical properties that are the same in all directions, and allow light to travel through them with the same velocity in all directions. Anisotropic materials, such as non-cubic crystals, liquid crystals, certain drawn polymers and natural fibers, have optical properties that are a function of direction. These materials are birefringent, i.e. they interact with the incident light by altering its plane of polarization and can be investigated and characterized by polarized light microscopy.

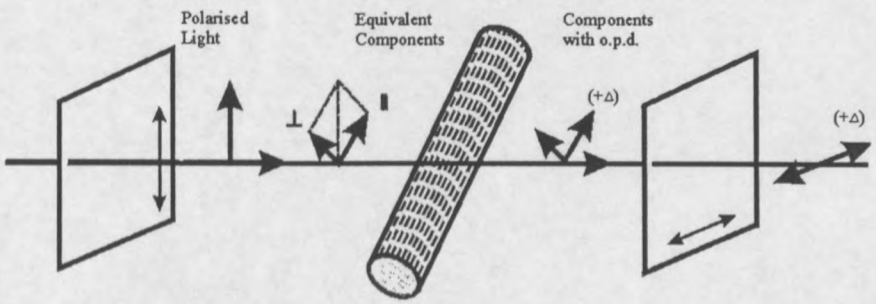

Figure 2.10. Interaction of polarized light with an anisotropic material (from [Spe-82]).

The interaction of polarized light with an optically anisotropic material can be described as shown in Figure 2.10. When polarized light interacts with an anisotropic-oriented sample, it can be considered as broken into two wave components: one polarized parallel to the long axis of an oriented material (∥) and the other polarized parallel to the short axis (⊥). Both travel through the material at different velocities and exhibit different refractive indices ($n_{\parallel}$ and $n_{\perp}$, birefringence). The wave components emerge from the material with an optical path difference (opd). When these components enter a second polarizing filter that is perpendicular to the first, only the fractions vibrating in the vibrating axis of this second filter will be allowed to pass.

Unless the opd = 0 some light will pass and the anisotropic material will appear bright against a dark background.

If one of the two axes of the investigated material lies parallel to the first polarizing filter, one of the component vectors will have zero amplitude. The remaining component will be blocked by the second filter, providing one of four positions of extinction with well organized materials.

Anisotropic materials will exhibit different textures due to the presence of different phases in the material. Through the use of polarized light microscopy it is possible to identify various phases of orientation. H_1 phases generally show a fan-like structure under cross polars and L_α a streaky texture [87 - 89].

2.4.6. X-ray diffraction (WAXS and SAXS)

In order to investigate morphologies and gain structural information of an ordered system by means of a scattering technique, it is imperative that the wavelength of the waves being scattered be of about the same length as the distance between the scattering centers. X-rays have wavelengths of the order of a few angstroms, the same as typical inter-atomic distances in crystalline solids and liquid crystalline mesophases.

The scattering of X-rays occurs as a result of interaction with electrons in the material. The X-rays scattered from different electrons interfere with each other and produce a diffraction pattern that varies with scattering angle. The variation of the diffraction intensity with the angle provides information on the electron density distribution and hence the atomic positions within the material.

Coherent scattering (where all scattered rays have the same wavelength as the original incoming X-ray) is the most important.

The scattered coherent material will interfere either destructively or constructively (giving rise to a scattered beam). When scattering takes place from a three-dimensional array of atoms / scattering centers, characteristic scattering images will result from the constructive and destructive interference of the scattered beams.

This forms the basis of scattering experiments, where the variation of the intensity of the scattered beam is measured in dependence of the scattering angle, 2θ.

Wide angle X-ray scattering (WAXS) can be used to resolve structure (spacing between scattering layers) at inter-atomic level (1nm and smaller). These distances are present in crystalline samples. Here the scattering intensity is measured between $5° < 2\theta < 180°$ (see Figure 2.11). Bragg's Law is used to describe conditions where constructive interference will take place, and can be described by Equation 2.10.

$$n\lambda = 2d \sin\theta \qquad [Å] \qquad (2.10)$$

where

n = integral number of wavelengths

λ = wavelength in Å (wavelength used for these studies: λ = 1,54Å, see chapter 4.1.2.)

d = spacing between layers of scattering centers

θ = half the scattering angle.

In the case of non-crystalline, mesostructured / colloidal systems, structural elements are usually in the range of 2 to 200 nm. The characterization of such systems can be achieved by small angle X-ray scattering (SAXS), with angles of measurement of the scattered intensity between $0° < 2\theta < 5°$.

Normally the sample is irradiated with a collimated beam of X-rays and the intensity of the scattered X-rays is measured as a function of scattering direction. The scattering angle (the direction of the scattered beam in relation to the incident beam) is denoted by 2θ (Figure 2.11). If s_0 is defined as the unit vector in the incident beam and s' as the unit vector in the scattered beam direction, the relation between the incident and scattered beams can be described from Bragg's law by means of the scattering vector s:

$$1/d = 2(\sin\theta) / \lambda \equiv |s| \ [nm^{-1}] \qquad (2.11)$$

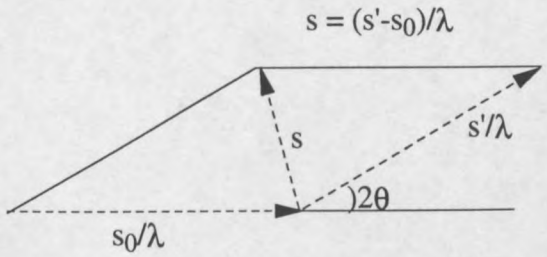

Figure 2.11. Definition of scattering vector s, where s_0 and s' are the unit vectors in the direction of the incident and scattered beams and λ is the wavelength of the x-rays. The length of the vector s is related to the scattering angle 2θ by $|s| = 2(\sin\theta) / \lambda$.

The magnitude of the scattering vector, which is proportional to sinθ as shown in Equation (2.11), is inversely related to distance in real space. The Bragg relation, Equation (2.10), written as

$$d = \lambda/(2\sin\theta) \qquad (2.12)$$

can be used as a good rule of thumb to estimate the size scale *d* of the structure that gives rise to the scattered intensity at 2θ [84, 90].

2.4.7. Infrared spectroscopy (FTIR)

Molecular vibrations and – rotations are created by the absorption of infrared (IR) light. Most functional groups of organic molecules have characteristic vibrations that yield a defined absorption band in IR-spectroscopy by which they can be identified.

With Fourier-Transform infrared (FTIR) an overall infrared spectrum over an interferogram is collected. Through a Fourier-Transform-operation the interferograms are fragmented in the frequency of the vibrations and the infrared spectrum is obtained. On the basis of the fragmentation of the overall wavelengths, FTIR excels by its rapidness, superior sensitivity and wave number precision.

2.4.8. Gel permeation chromatography (GPC)

In GPC polymers are separated by a porous gel according to their hydrodynamic volume. Big coils or molecules will elute first, while small coils or molecules, which can penetrate all the pores, so seeing a larger volume of the eluent, will elute later. In the ideal case there are no adsorptive interactions between the column material and the polymer so that the separation takes place exclusively according to eluted volume and therefore to size. GPC is thus a size

exclusion chromatography where it separates to size. The refractive index or the change in UV-adsorption generally used in detection and then related to the elution's volume. With a range of polymer standards a calibration curve is constructed from which one can read the molecular weight of the samples according to the elution's volume.

Chapter 3

Synthesis of Surfactant Monomers (Surfmers)

3.1. Introduction

Surfactants used for polyelectrolyte-surfactant complexes have to be of high purity. Properties of surfactants that affect the complex formation include: the geometry, length of the alkyl chain, the nature of the counterion and the concentration.

The idea at the onset of this project was to first synthesize two surfmers with a polymerizable double bond known in literature [8]. Until now these known surfmers / surfactants were synthesized in low purity. The aim of this section of the work was the synthesis and purification of these surfmers and to use them then to form either polyelectrolyte surfactant complexes or use them in copolymers.

Second, a new surfmer / surfactant with an aromatic functional and succinic ester group was chosen to be synthesized to add variety to surfactants and polyelectrolyte-surfactant complexes.

The synthesis and characterization of sodium 11-methacryloyloxy undecanyl-1 sulfate (MET) (**1**), sodium 11-crotonoyloxy undecanyl-1 sulfate (CRO) (**2**) and sodium 4-[11-(3-carboxypropinoyloxy)-undecyloxy] benzenesulfonate (PSA-MA) (**3**) are now discussed.

3.2. Experimental

3.2.1. Materials

11-Bromo-1-undecanol (98%, Aldrich); methacrylic acid (Plascon Research); 2,6-di-*tert*-butyl-4-methylphenol (99%, Acros); *n*-tetrabutylammonium bromide (Acros); crotonic acid (Acros); chlorosulfonic acid; (>98% Aldrich), maleic anhydride (Merck); styrene (Sigma Aldrich), phenol

sulfonic acid sodium salt dehydrate (Aldrich); high molecular weight poly(diallyldimethyl ammonium chloride) (pDADMAC) (20 wt% in water, M_w = 375 000 – 500 000 g/mol) (Aldrich); magnesium sulfate (SAARCHEM); sodium hydrogen sulfate (R&S Scientific) and sodium hydroxide (Associated Chemical Enterprises) were all used as received. Deionized water was obtained from a Millipore Q system. Methanol, diethyl ether, chloroform, ethyl acetate, hexane, isopropanol, petroleum ether and dichloromethane were used as received.

3.2.2. Instrumental techniques

Nuclear Magnetic Resonance (NMR) spectra were obtained on a Varian VXR-Unity 600 MHz instrument, University of Stellenbosch, South Africa.

Elemental analysis (CHN) was performed on a Fisons elemental analyzer, model 1108, by using combustion analysis, at the University of Cape Town, South Africa.

Surface tension measurements were done on a White tensiometer at 20 °C, University of Stellenbosch, South Africa.

Differential Scanning Calorimetry (DSC) was done on a DSC22C (Seiko II) at a heating rate of 10°C / min, at the Deutsches Kunststoff-Institut, Darmstadt, Germany.

Degradation studies were carried out with a Thermal Gravimetric Analyzer (TGA50) (Shimadzu instruments), at the Deutsches Kunststoff-Institut, Darmstadt, Germany.

MALDI spectra were obtained on a Kratos Analytical Kompact MALDI, at the Deutsches Kunststoff-Institut, Darmstadt, Germany.

3.2.3. Synthesis of sodium 11-methacryloyloxy undecanyl-1 sulfate (MET) (1)

*3.2.3.1. Preparation of sodium methacrylate (**6a**)*

7,23 g (0,18 mol) sodium hydroxide dissolved in 25 ml deionized water was cooled to 0 °C for 10 minutes. 15,54 g (0,18 mol) methacrylic acid was added drop-wise over 15 minutes. After 30 minutes, the reaction was freeze-dried. The dry product was dissolved in 170 ml methanol and

precipitated with 700 ml diethyl ether. After filtering and drying under vacuum, 17,44 g (0,16 mol) of sodium methacrylate was obtained as a white powder in 90,5 % yield.

^{1}H NMR (20°C, D_2O) δ = 1,9 (s, 3H, C<u>H</u>$_3$-); 5,3 (m, 1H, -C<u>H</u>$_{trans}$=); 5,7 (m, 1H, -C<u>H</u>$_{cis}$=) (Figure 3.1).

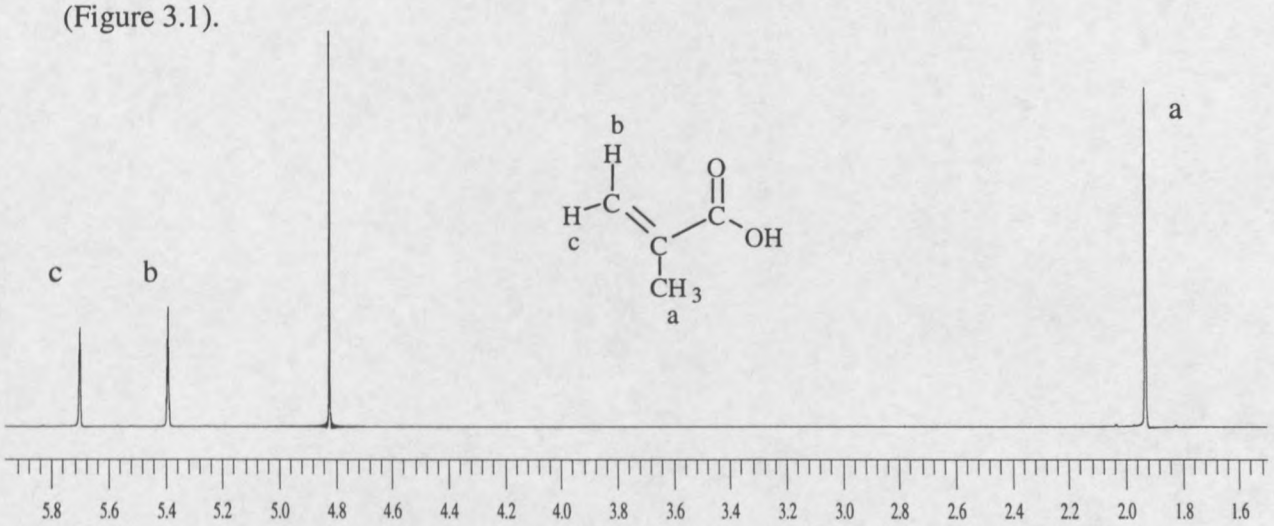

Figure 3.1. ^{1}H NMR spectrum of sodium methacrylate (6a).

3.2.3.2. Preparation of 11-methacryloyloxy undecanol-1 (MET1) (8a)

17,08 g (0,16 mol) sodium methacrylate, 10,21 g (0,04 mol) 11-bromoundecanol-1, 3,74 g (0,010 mol) *n*-tetrabutylammonium bromide and 54 mg (0,24 mmol) 2,6-di-*t*-butyl-4-methyl phenol were dissolved in a mixture of 40 ml deionized water and 20 ml chloroform. The reaction mixture was stirred vigorous at 100 °C for three days. The chloroform layer was washed 4 times with 50 ml of a 2 % aqueous sodium hydroxide solution and once with 50 ml distilled water. After drying the organic layer over magnesium sulfate and removing the solvent under vacuum a viscous yellowish liquid was obtained. 5,17 g (0,020 mol) of 11-methacryloyloxy undecanol-1 was obtained as a viscous clear liquid in 49,3 % yield from the bulb-to-bulb distillation at 5 mbar and 240 °C.

^{1}H NMR: (20°C, $CDCl_3$) δ = 1,27 (m, 14H, -CH_2-); 1,54 (m, 2H, -C<u>H</u>$_2$-CH_2-OH); 1,67 (m, 2H, -C<u>H</u>$_2$-CH_2-O-); 1,93 (s, 3H, C<u>H</u>$_3$-); 3,62 (t, 2H, -C<u>H</u>$_2$-OH); 4,11 (t, 2H, -COOC<u>H</u>$_2$); 5,53 (s, 1H, -C<u>H</u>$_{trans}$=); 6,08 (m, 1H, C<u>H</u>$_{cis}$=) (Figure 3.2).

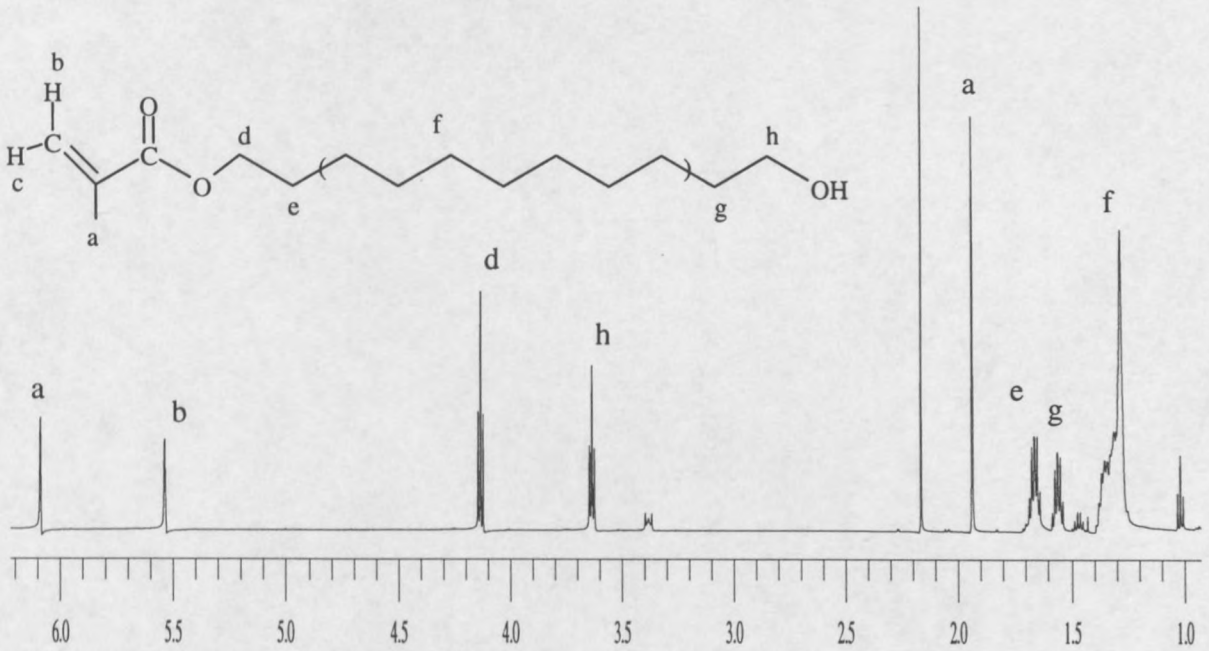

Figure 3.2. ^{1}H NMR spectrum of sodium methacryloyloxy undecanol-1 (MET1) (8a).

3.2.3.3. Preparation of sodium 11-methacryloyloxy undecanyl-1 sulfate (MET) (1)

2,36 g (0,02 mol) chlorosulfonic acid was placed in a two-neck round-bottom flask fitted with a mechanical stirrer, dropping funnel, and a nitrogen inlet. 5,17 g (0,02 mol) 11-methacryloyloxy undecan-1-ol (MET1) was added drop-wise over one hour with vigorous stirring. The reaction mixture was flushed with nitrogen for three hours while stirring vigorously. The resultant viscous brown liquid was added drop-wise to 10 ml of a saturated sodium hydrogen carbonate solution at 0 °C. During the addition the mixture was kept at pH9 by adding excess sodium hydrogen carbonate. After adding a mixture of 40 ml isopropanol and 50 ml water, a fine white precipitate appeared. The precipitate was filtered off and the filtrate washed twice with 50 ml petroleum ether at 40 – 60 °C. After freeze-drying 16,91 g (0,019 mol) of a light-yellow solid was obtained in 95,8 % yield. The crude product was dissolved in chloroform and 1,75 g (25,3 % yield) of a white precipitate filtered off. The filtrate was dried under vacuum and 4,86 g (68,3 %) of sodium 11-methacryloyloxy undecanyl-1 sulfate was obtained. The surfmer was determined to be >95 % pure by ^{1}H NMR.

^{1}H NMR: (20°C, D_2O) δ = 1,35 (m, 14H, -CH_2-); 1,43 (m, 2H, -C<u>H</u>$_2$-CH_2-OH); 1,72 (m, 2H, -C<u>H</u>$_2$-CH_2-O-); 1,96 (s, 3H, C<u>H</u>$_3$-); 4,06 (t, 2H, -C<u>H</u>$_2$-OSO_3^-); 4,18 (t, 2H, -COOC<u>H</u>$_2$); 5,63 (s, 1H, -C<u>H</u>$_{trans}$=); 6,12 (m, 1H, C<u>H</u>$_{cis}$=) (Figure 3.3).

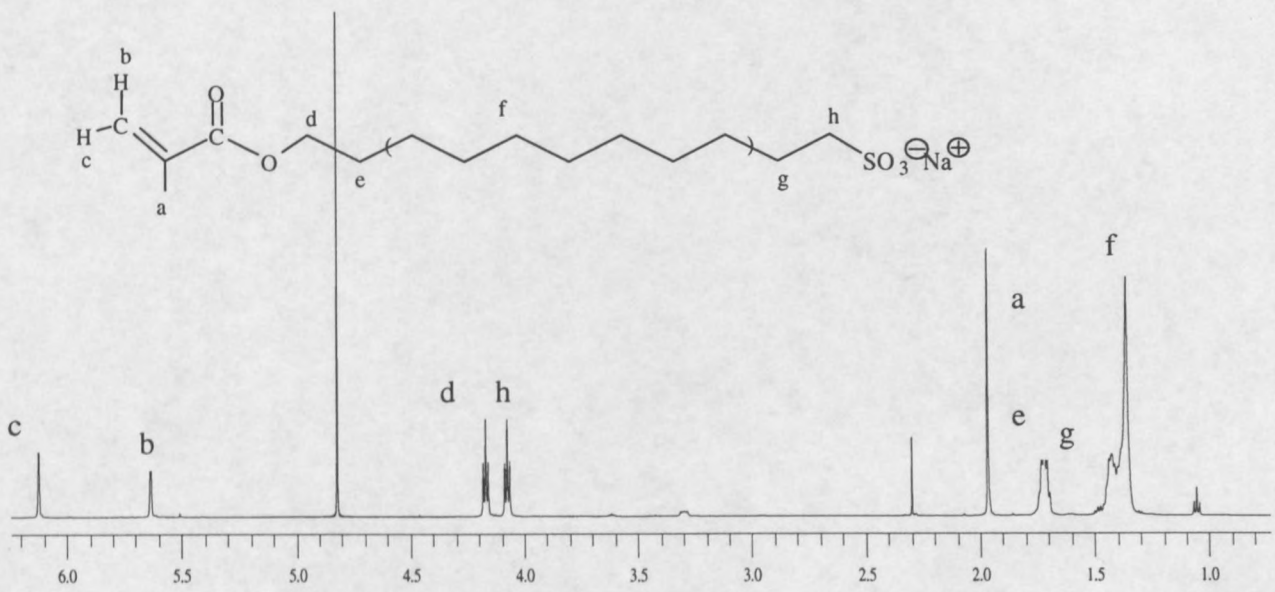

Figure 3.3. ^{1}H NMR spectrum of sodium methacryloyloxy undecanyl-1 sulfate (MET) (1).

^{13}C NMR: (20°C, D_2O) δ = 22,6 (<u>C</u>H$_3$-); 30,4 (-<u>C</u>H$_2$-CH_2-CH_2-O-CO); 30,7 (-<u>C</u>H$_2$-CH_2-CH_2-O-SO_3^-); 33,3 (-<u>C</u>H$_2$-CH_2-O-SO_3 -); 34,2 (-CH_2-), 69,8 (-COO<u>C</u>H$_2$); 74,0 (-<u>C</u>H$_2$-OSO_3^-); 130,5 (-<u>C</u>H$_2$=CH-); 141,5 (CH_2=<u>C</u>H-); 172,8 (-<u>C</u>O) (Figure 3.4).

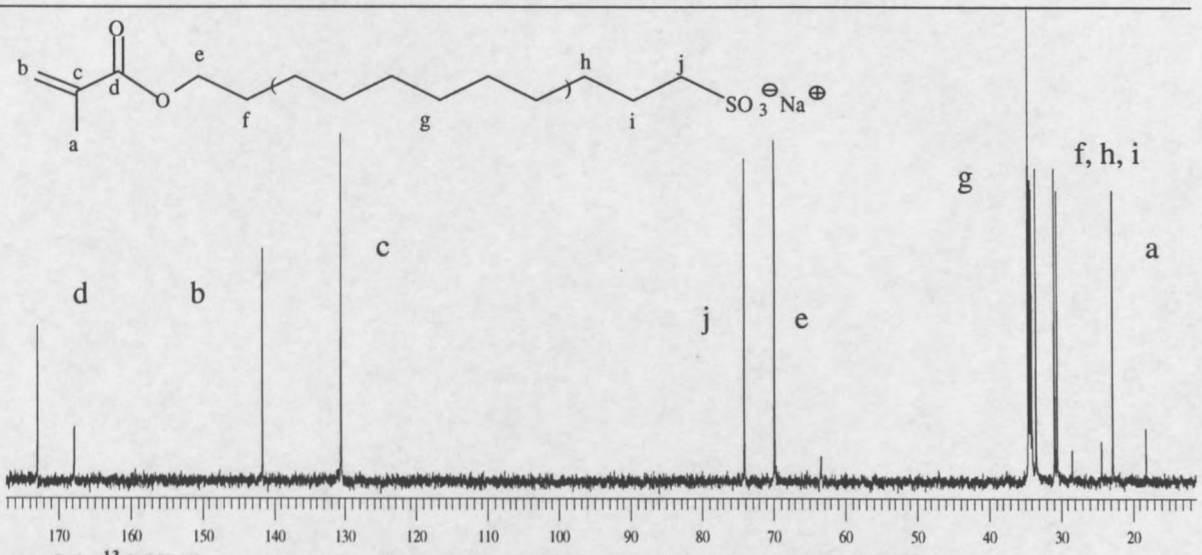

Figure 3.4. ^{13}C NMR spectrum of sodium methacryloyloxy undecanyl-1 sulfate (MET) (1).

Micro analytical data: calculated (found) % = C: 50,2 (49,6); H: 7,2 (8,8); S: 8,9 (6,8).

Melting points: 53,9 °C and 151,8 °C.

CMC: 0,0373 M (See Addendum, Figure 1).

3.2.4. Synthesis of sodium 11-crotonoyloxy undecanyl-1 sulfate (CRO) (2)

*3.2.4.1. Preparation of sodium crotonate (**6b**)*

6b was synthesized according to the procedure in section 3.2.3.1, using crotonic acid as starting material with a yield of 87 %.

^1H NMR: (20°C, D_2O) δ = 1,7 (d, 3H, $C\underline{H}_3$-); 5,78 (d, 1H, =$C\underline{H}$-CO_2); 6,6 (m, 1H, $C(CH_3)\underline{H}$=CH-) (Figure 3.5).

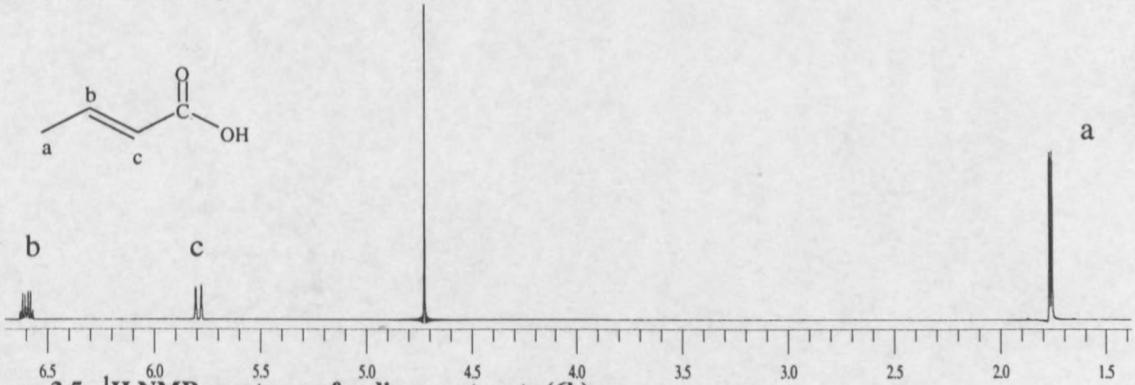

Figure 3.5. ^1H NMR spectrum of sodium crotonate (6b).

3.2.4.2. Preparation of 11-crotonoyloxy undecanol-1 (CRO1) (8b)

CRO1 (**8b**) was prepared according to section 3.2.3.2, using sodium crotonate (**6b**) as starting material with a yield of 80,6 %.

^{1}H NMR: (20°C, $CDCl_3$) δ= 1,27 (m, 14H, -CH_2-); 1,56 (m, 2H, -C$\underline{H}_2$-CH_2-OH); 1,67 (m, 2H, -C$\underline{H}_2$-CH_2-O); 1,87 (d, 3H, C$\underline{H}_3$-); 3,63 (t, 2H, -C$\underline{H}_2$-OH); 4,10 (t, 2H, -COOC$\underline{H}_2$); 5,83 (d, 1H,CH=C$\underline{H}CO_2$); 6,96 (m, 1H, C(CH_3)$\underline{H}$=CH) (Figure 3.6).

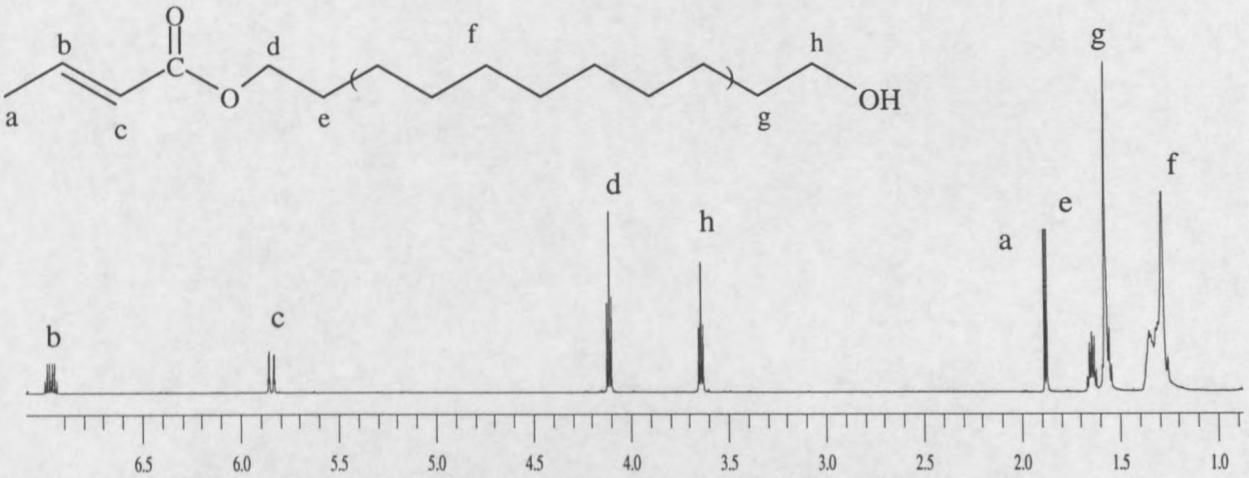

Figure 3.6. ^{1}H NMR spectrum of sodium crotonoyloxy undecanol-1 (CRO1) (8b).

3.2.4.3. Preparation of sodium 11-crotonoyloxy undecanyl-1 sulfate (CRO) (2)

CRO (**2**) was synthesized according to section 4.2.3.3, using 11-crotonoyloxy undecanol-1 (CRO1) (**8b**) as starting material with a yield of 112,8 %.

^{1}H NMR: (20°C, D_2O) δ = 1,34 (m, 14H, -CH_2-); 1,42 (m, 2H, -C$\underline{H}_2$-CH_2-OH); 1,71 (m, 2H, -C$\underline{H}_2$-CH_2-O); 1,95 (d, 3H, C$\underline{H}_3$-); 4,07 (t, 2H, -C$\underline{H}_2$-OSO_3^-); 4,16 (t, 2H, -COOC$\underline{H}_2$); 5,92 (d, 1H,CH=C$\underline{H}CO_2$); 7,04 (m, 1H, C(CH_3)$\underline{H}$=CH) (Figure 3.7).

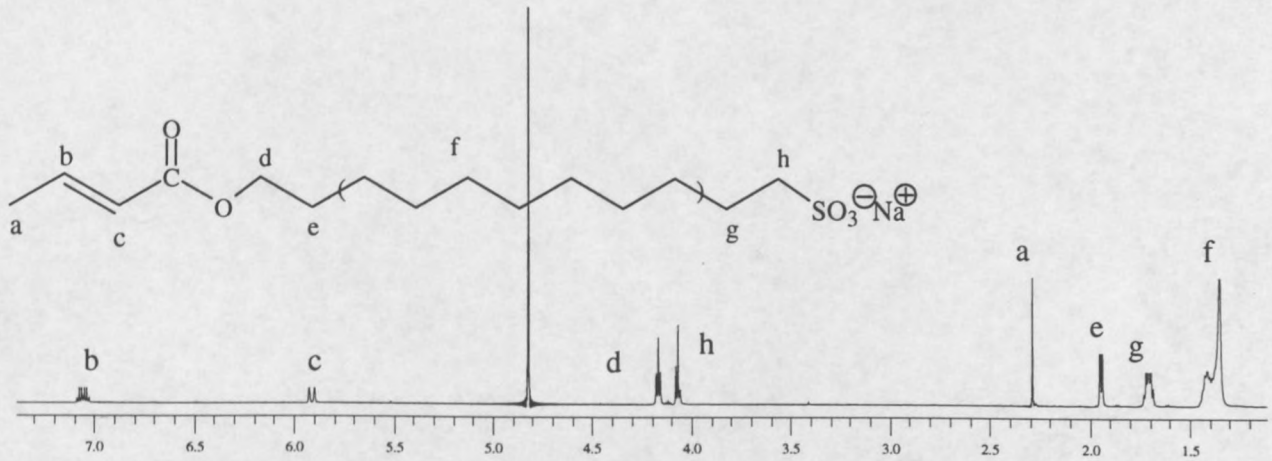

Figure 3.7. ^{1}H NMR spectrum of sodium crotonoyloxy undecanyl-1 sulfate (CRO) (2).

^{13}C NMR: (20°C, D_2O) δ = 22,4 (-$\underline{C}H_3$-); 30,3 (-$\underline{C}H_2$-CH_2-CH_2-O-CO); 30,7 (-$\underline{C}H_2$-CH_2-CH_2-O-SO_3 -); 33,3 (-$\underline{C}H_2$-CH_2-O-SO_3 -); 34,1 (-CH_2-), 69,5 (-COO$\underline{C}H_2$); 74,1(-$\underline{C}H_2$-OSO_3^-); 127,3 (CO-$\underline{C}$H=CH-); 151,1 (-CH=$\underline{C}$H-CH_3); 172,6 (-$\underline{C}$O) (Figure 3.8).

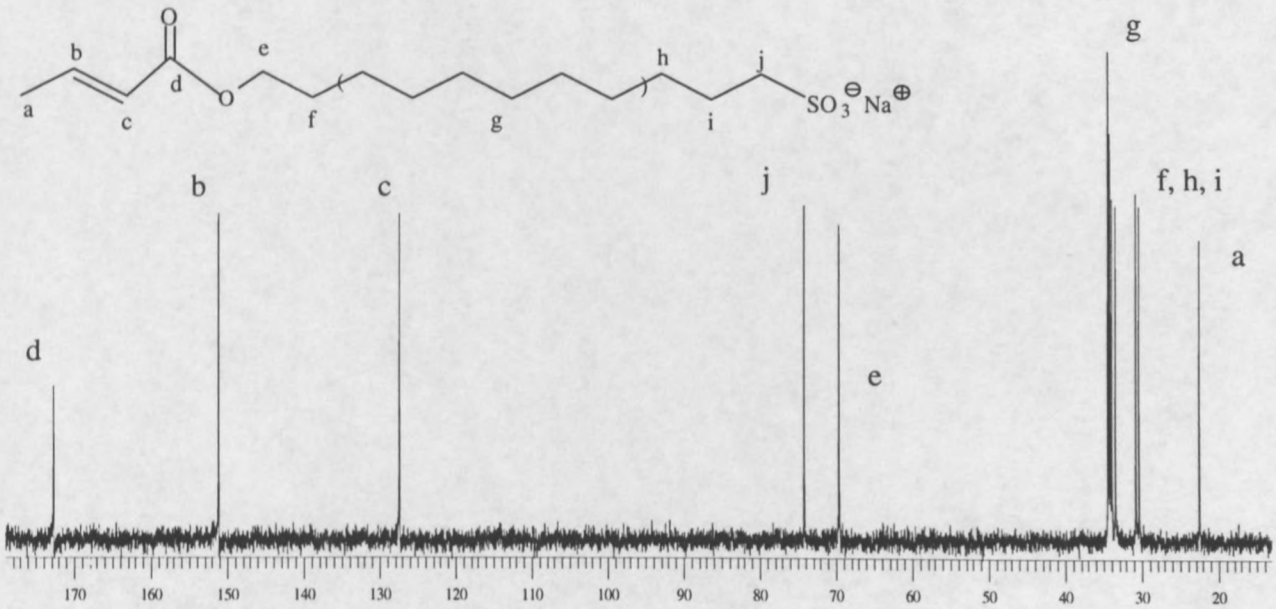

Figure 3.8. ^{13}C NMR spectrum of sodium crotonoyloxy undecanyl-1 sulfate (CRO) (2).

Micro analytical data: calculated (found) % = C: 50,2 (49,3); H: 7,2(8,2); S: 8,9 (6,1).

Melting point: 175 °C.

CMC: 0,0375 M (See Addendum, Figure 2).

3.3. Results and Discussion

3.3.1. Synthesis of sodium 11-methacryloyloxy undecanyl-1 sulfate (MET) (1) and sodium 11-crotonoyloxy undecanyl-1 sulfate (CRO) (2)

The anionic surfmers differ in the nature of the polymerizable group. MET (**1**) is an ester of methacrylic acid and the CRO (**2**) is an ester of crotonic acid. The methacrylic derivative is an example of a very reactive, polymerizable surfmer and the crotonic derivative is an example of a generally non-homopolymerizable surfmer.

A convenient approach to the synthesis of a polymerizable surface-active molecule is to attach the polymerizable group to the hydrophobic tail in a first step, leaving the insertion of the head group to the end of the reaction sequence. This is described in literature [8]. In this manner, working with surface-active intermediates is avoided and problems with isolation and purification are minimized. Another important consideration in the design of the synthesis of a surfmer is the requirement for mild reaction conditions in the various steps, in order to avoid spontaneous polymerization.

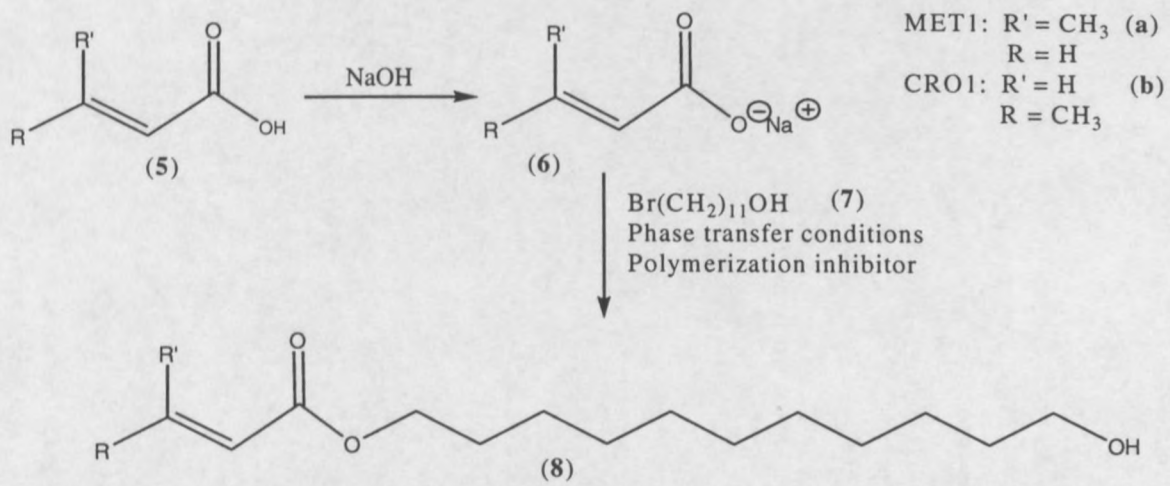

Figure 3.9. Reaction scheme for the attachment of the polymerizable group.

The hydrophobic tail and the polymerizable function were attached via a phase-transfer-catalyzed reaction (Figure 3.9). The sodium salt of the corresponding carboxylic acid (**6a** or **6b**) was used to substitute the bromide ion from 11-bromoundecanol-1 (**7**) to yield the methacryloyl or crotonoyl alkyl alcohol (**8a**, MET1; **8b**, CRO1). A polymerization inhibitor was added in order to avoid polymerization during this step and was removed in the work-up. Alkyl alcohol monomers (**8**) that were obtained showed, by means of NMR analysis, that no impurities were present after vacuum distillation.

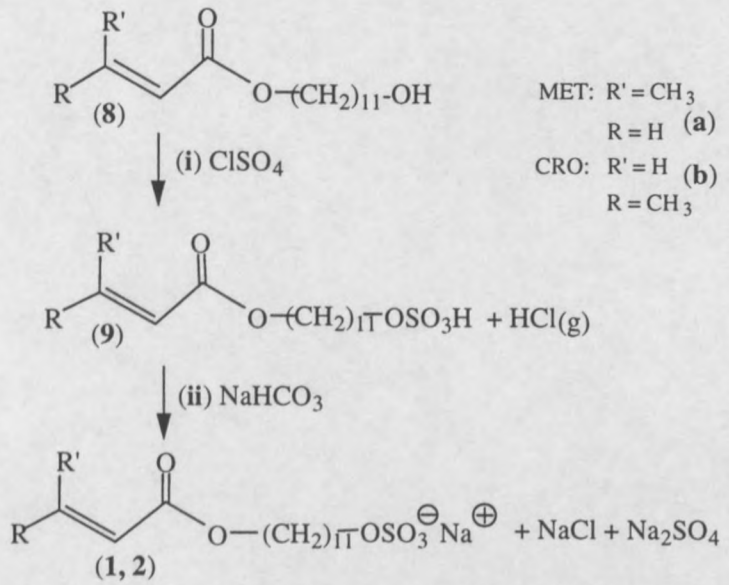

Figure 3.10. Reaction scheme for sulfonation of MET1 (8a) and CRO1 (8b).

The sulfonation reaction (Figure 3.10) is the crucial step in the synthesis. Chlorosulfonic acid (**i**) is used to sulfonate these reactive alcohols **8**. The methacrylic **8a** or crotonic **8b** alkyl alcohol was added in excess chlorosulfonic acid (**i**). The temperature was kept below 5 °C. The addition of alcohol (**8**) was carried out under vigorous stirring to disperse the hydrochloric acid formed because the reaction mixture inevitably became highly viscous. The reaction was quenched with sodium carbonate (**ii**) in order to obtain the desired sodium salt (MET (**1**), CRO (**2**)). Additional inorganic salts were formed from the neutralization of hydrochloric acid and excess chlorosulfonic acid. These impurities are indicated by the high crude yields. The crude product (MET **1**, CRO **2**) was purified by dissolving it in chloroform and filtering the solution. 25 – 27 wt% impurities, mainly inorganic salts [8] were removed.

The ^{1}H NMR spectra of the products **1** and **2** (Figures 3.11 and 3.12) confirmed that the monomers were successfully sulfonated. Most characteristic was the shift of the resonance of the methylene group next to the alcohol function. After sulfonation, the triplet related to this methylene group was shifted from $\delta = 3{,}62$ to lower field ($\delta = 4{,}08$) by $\Delta\delta$ 0,44 ppm.

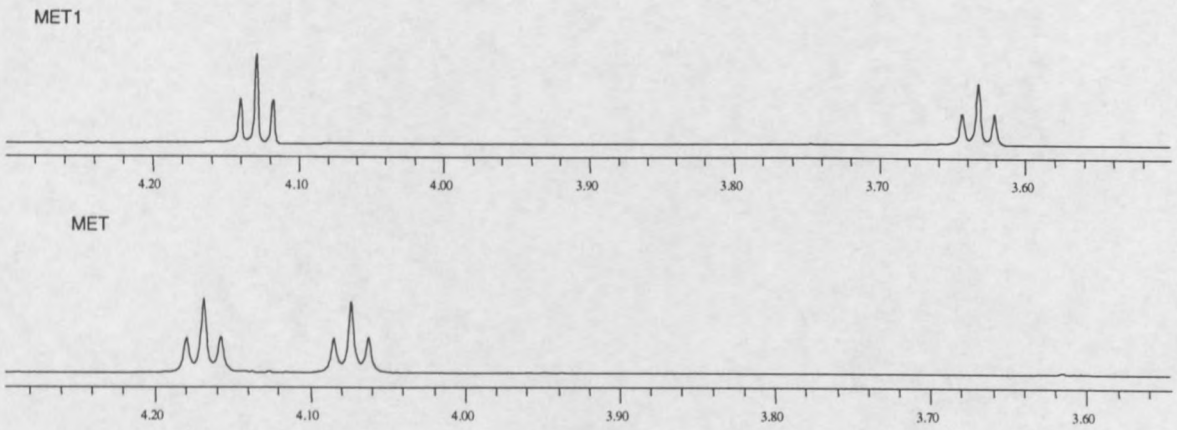

Figure 3.11. ^{1}H NMR spectra of MET1 (8a) and MET (1) with shift of –C$\underline{H}_2$-OH (-OSO_3^-) to indicate sulfonation.

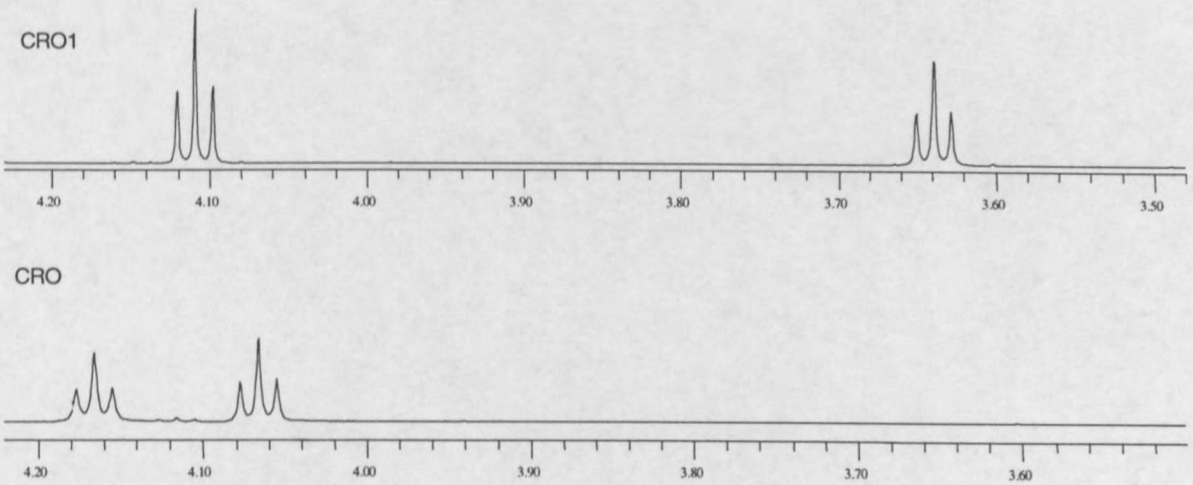

Figure 3.12. ^{1}H NMR spectra of CRO1 (8b) and CRO (2) with shift of –C$\underline{H}_2$-OH (-OSO_3^-) to indicate sulfonation.

3.3.1.1. Purity and CMC of MET (1) and CRO (2)

The purity of the surfmers MET (**1**) and CRO (**2**) was determined from ^{1}H NMR spectra and the elemental analysis. Both techniques indicate surfmers of high purity (>95 %). The impurities that

may remain in the sample include sodium chloride and undecylenic alcohol [8] and may affect the surface properties of PE-Surfs.

At the CMC, several properties of the aqueous surfactant show a discontinuity, e.g. surface tension, conductivity and density. The CMC was determined by monitoring the surface tension as a function of surfactant concentration. All measurements were carried out at 20 °C.

Table 3.1. Literature [8] and experimental CMC values of surfactants MET (1) and CRO (2).

Surfactant	Literature value (mol/L)	Experimental value (mol/L)
MET	0,00698	0,00462
CRO	0,01370	0,00495

At low surfactant concentration, the surface tension decreases with increasing concentration. The break in the curve is indicative of the CMC. Above this concentration the surface tension increases, which is indicative of small amounts of impurities (e.g. undecylenic acid) still present in the sample [22]. The addition of salts decreases the CMC [8] by one order of magnitude. The higher purity of synthesized surfactants (compared to those found in literature) explains the higher experimental CMC values found (Table 3.1).

3.3.2. Analysis of sodium 11-methacryloyloxy undecanyl-1 sulfate (MET) (1) and sodium 11-crotonoyloxy undecanyl-1 sulfate (CRO) (2)

3.3.2.1. Thermal Gravimetric Analysis (TGA)

In TGA, the onset of degradation is governed by the weakest link in a structure or polymer, whereas the most frequent chain of the given groups is responsible for overall stability of the structure or polymer.

The weight loss of a sample during TGA analysis is given by the change in weight per given time (dW/dt). There are two distinct stages of degradation for MET (**1**) and one for CRO (**2**). The onset and maximum temperatures of the first step, T_{1on} and T_{1max}, and the second step, T_{2on} and T_{2max} illustrate the two qualitative degradation steps (Table 3.2). This process ends with the loss of all volatile fractions and a char mass that does not change much after 500 °C. The char mass is due to the presence of sodium and sulfur (Addendum, Figure 3 and 4).

Table 3.2. Thermal degradation of MET (1) and CRO (2).

Component	T_{1on} (°C)	T_{1max} (°C)	T_{2on} (°C)	T_{2max} (°C)	dw/dt at T_{max} (g/min)
MET	219,2	250,2	322,2	411,0	0,89
CRO	225,8	266,1	-	-	1,09

From these results it can be seen that CRO (**2**) is thermally a more stable material as it only starts to degrade at 266,1 °C while MET (**1**) has two degradation steps, at 250,2 °C and at 411,0 °C. The higher dw/dt for CRO (**2**) indicates that once degradation starts it is completed faster than the degradation of MET (**1**).

3.4.2.2. Differential Scanning Calorimetry (DSC)

Results of DSC for MET (**1**) (Addendum, Figure 5, 6 and 7) show two distinct transitions on the first heating cycle at 57,1 °C and at 85,5 °C. The crystal to liquid crystal or melting point transition (refer to section 2.2.2) is seen at 57,1 °C, followed by the clearing point transition at 85,5 °C [23]. The cooling cycle shows a crystallization transition at 74,7 °C. The crystallization transition cannot be assigned to a specific phase transition due to supercooling and partially to hysteresis attributable to the temperature scan rate. The second heating cycle shows melting transitions at 53,6 °C and 84,1 °C, with much smaller melting energies (5,6 mJ/mg to 42,6 mJ/mg and 1,1 mJ/mg to 3,3 mJ/mg) than for the first heating cycle. This indicates a loss of crystalline order in the sample due to the heating process eliminating thermal history.

The DSC results for CRO (**2**) (Addendum, Figure 8, 9 and 10) show two transition peaks, at 67,8 °C and 154,7 °C. These transitions indicate a melting transition and a clearing point transition for the first heating. The cooling cycle shows two crystallization transitions at 47,2 °C and 147,7 °C. The difference in shifts of the melting and crystallization peaks are due to supercooling. The second heating cycle shows a melting transition and a clearing point transition at 56 °C and 154 °C.

The DSC curves confirm the TGA results, namely that CRO (**2**) has a higher melting temperature and can be heated to higher temperatures.

3.4.2.2. Polarized light microscopy with heating stage

MET (**1**) and CRO (**2**) behave differently under polarized light while being heated and cooled. At room temperature MET (**1**) has orange and dark brown colored parts in the sample due to birefringence (chapter 2.5.5). At 53,9 °C the sample becomes lighter in colour with some yellow areas and at 88 °C it is yellow. Part of the sample becomes transparent at 107,1 °C and it is a round droplet (yellow in colour) at 151,8 °C when it is melted (Figure 3.13, A – E). The sample was cooled to room temperature. A few fan-shaped crystals were visible at 110 °C and became more prominent as the temperature was lowered to room temperature (Figure 3.14 A).

CRO (**2**) showed less birefringence than MET (**1**) at room temperature and very little change during heating. At 162 °C more bright colours appear in the sample and at 164,8 °C parts of the sample starts to flow into each other. At 175 °C the material forms a droplet as it melts. The sample was cooled to room temperature (Figure 3.14 B). Fewer crystals were formed during the cooling process and at a much later stage than for MET.

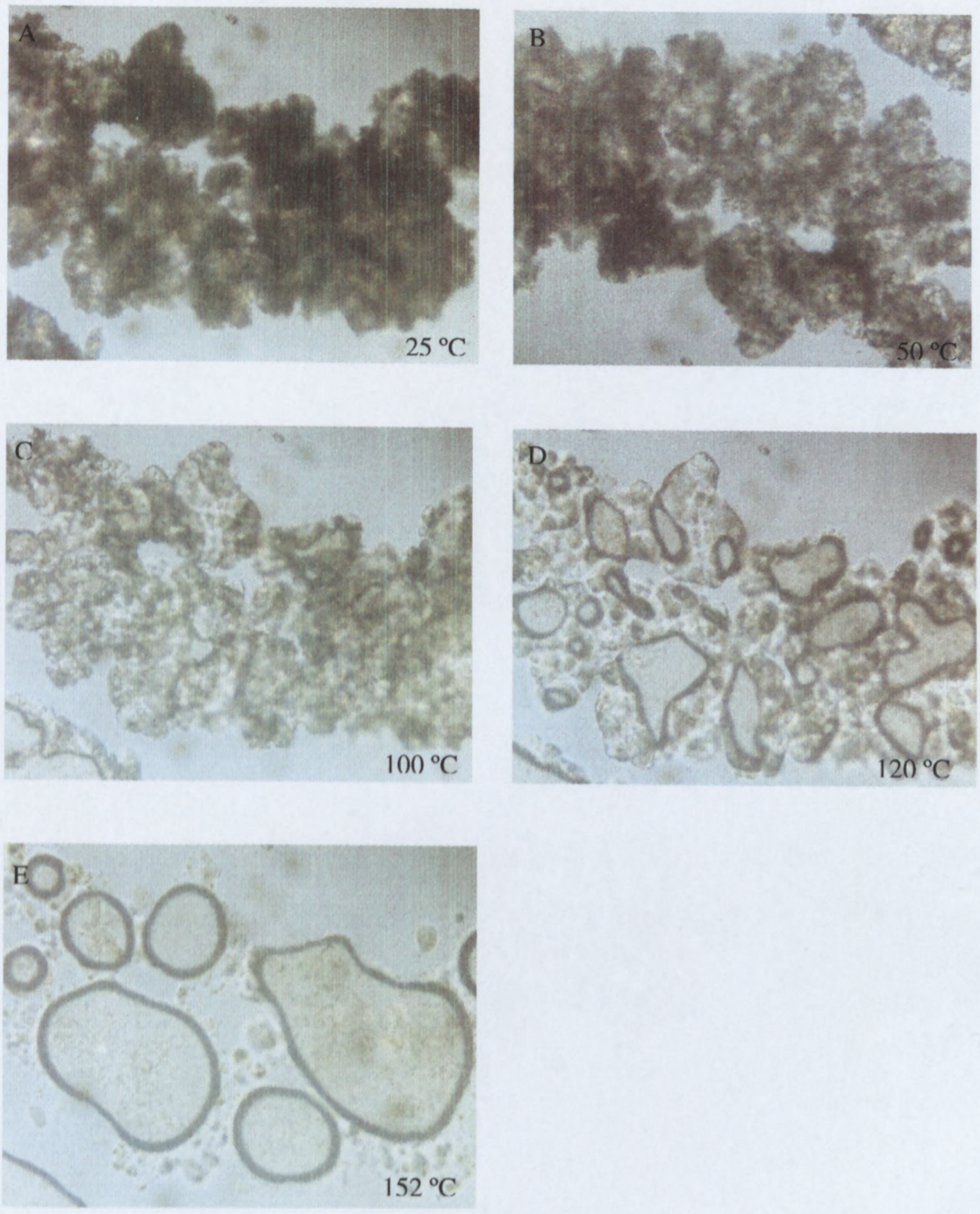

Figure 3.13. Different stages during the melting of MET (1).

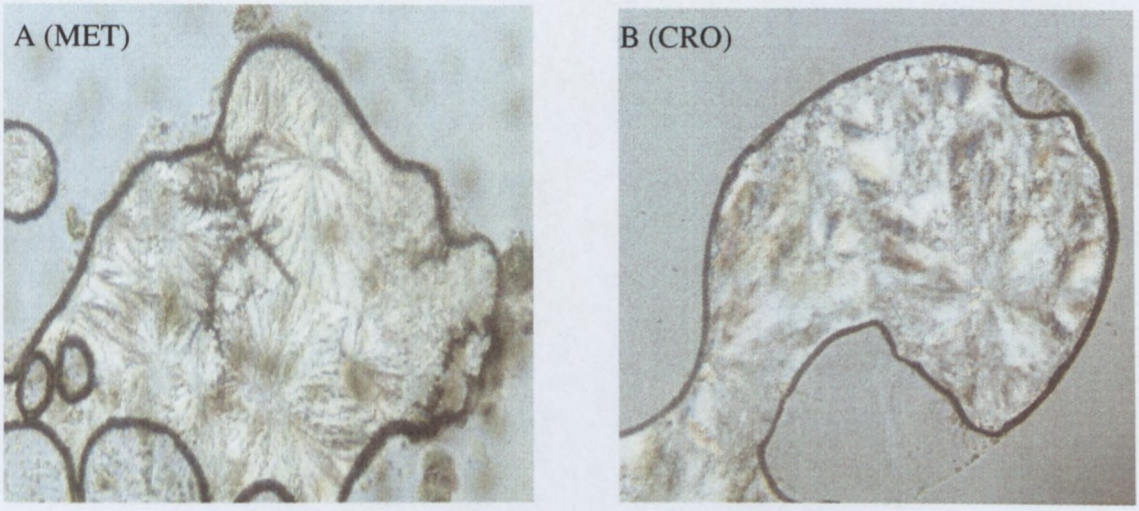

Figure 3.14. Crystal formed after MET (1) (A) and CRO (2) (B) were cooled to room temperature.

These figures show the liquid crystalline behavior of MET (**1**) and CRO (**2**) and confirm the DSC results that there are two melting transitions.

3.4 Sodium 4-[11-(3-carboxypropinoyloxy)-undecyloxy] benzenesulfonate (PSA-MA) (3)

3.4.1. Introduction

PSA-MA (**3**) was chosen to be synthesized to add a spacer, a bulky and rigid benzene ring, to the molecule in order to increase geometry and order in the PE-Surfs. This concept has been proven successful for some polymeric liquid crystals [91]. Maleic anhydride (**12**) was chosen to introduce a non-homopolymerizable function to the molecule that is able to form a cross-linked system with other monomers in the polyelectrolyte-surfactant complex.

Two different reaction routes are possible to synthesize PSA-MA (**3**). The starting material is 11-bromoundecanol-1 (**7**) (Figure 3.15 and 3.16).

The first route is based on the nucleophilic substitution of the bromide of 11-bromoundecanol-1 (**7**) and the subsequent esterification of the intermediate alcohol **11** with maleic anhydride (**12**) (Figure 3.15).

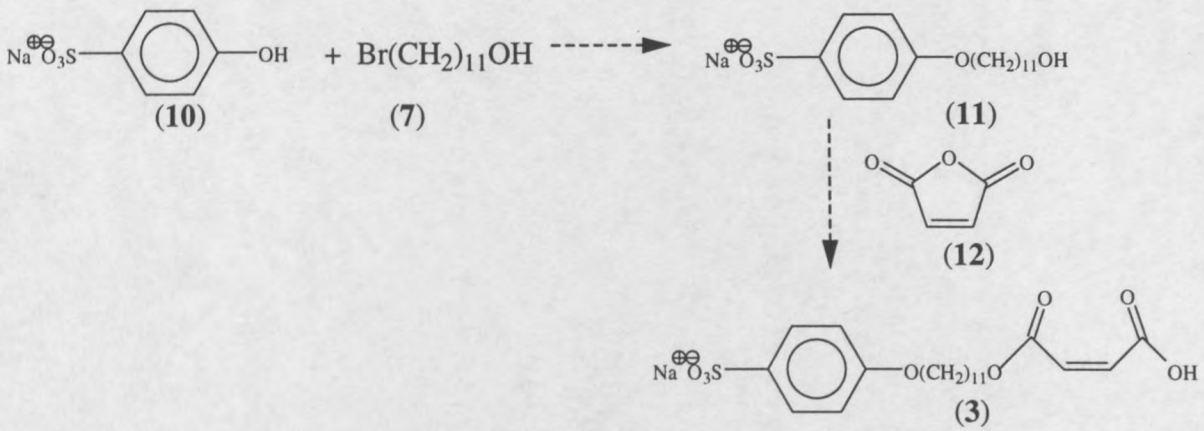

Figure 3.15. Possible reaction scheme 1 for the synthesis of PSA-MA (3).

The alternative synthetic route is the esterification of 11-bromoundecanol-1 (**7**) with maleic anhydride (**12**) followed by the nucleophilic substitution of the bromide **13** (Figure 3.16). A similar reaction is described in literature for the synthesis of dialkyl maleate cationic surfmers [19].

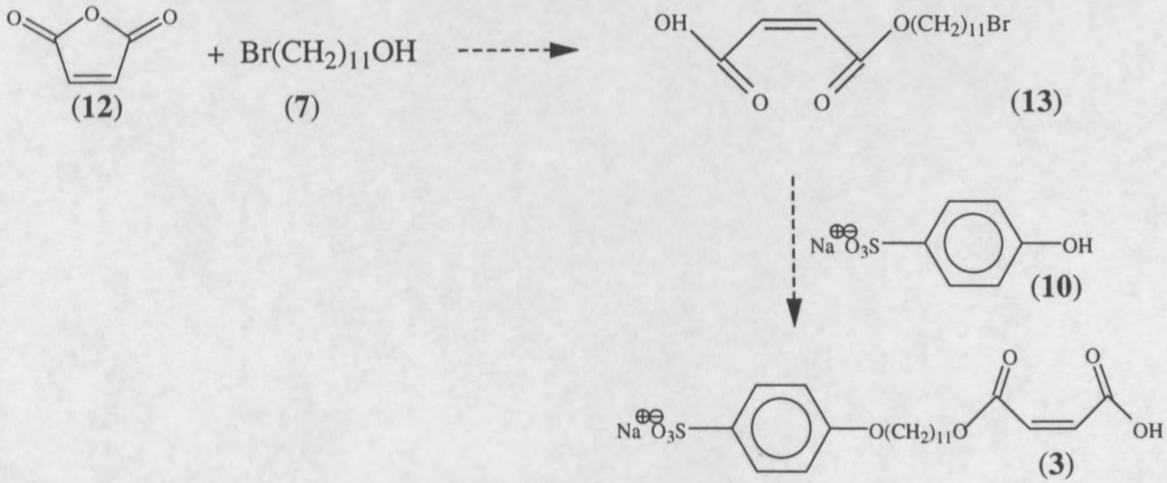

Figure 3.16. Possible reaction scheme 2 for synthesis of PSA-MA (3).

In the attempt to synthesize PSA-MA (**3**), both of the synthetic routes have been used with different experimental conditions. The results will be described in the following sections.

3.4.2. Preparation of PSA-MA, synthetic route 1

(See Figure 3.15)

3.4.2.2. Attempt 1

6,54 g Phenol sulfonic acid (28,0 mmol) were dissolved in 50 ml methanol and added to 0,97 g (42,0 mmol) sodium metal dissolved in 100 ml methanol. 7,06 g (28,0 mmol) 11-bromoundecanol-1, dissolved in 50 ml methanol, were slowly added and the reaction mixture was refluxed at 80 °C for 7 h. A white precipitate was filtered off and recrystallized from ethanol. 1,94 g (5,3 mmol) of sodium 4-(11hydroxy-undecyloxy)-benzene sulfonate were obtained as white crystals, in 18,9 % yield.

^{1}H NMR: (20 °C, D_2O) δ= 1,30 – 1,58 (m, 14H, -C$\underline{H}_2$-); 1,80 (q, 2H, -C$\underline{H}_2$-CH_2-OC_6H_4-); 3,61 (t, 2H, -C$\underline{H}_2$-OH); 4,17 (t, 2H, -C$\underline{H}_2$-OC_6H_4-); 7,13 (d, 2H, *m*-Ar$\underline{H}$); 7,81 (d, 2H, *o*-Ar$\underline{H}$).

1,03 g (2,8 mmol) sodium 4-(11-hydroxy-undecyloxy)-benzene sulfonate and 0,28 g (2,8 mmol) maleic anhydride dissolved in 30 ml pyridine were refluxed at 135 °C for 12 h. The reaction mixture was quenched with 120 ml of an iced, aqueous 0,1 % hydrochloric acid solution. The mixture was washed once with 100 ml dichloromethane. After the organic layer was washed 5 times with 250 ml 0,1 % of hydrochloric acid solution and 3 times with 100 ml water, it was dried over $MgSO_4$, filtered and the solvent removed under vacuum. 0,12 g of a dark yellow oil was obtained.

In the first attempt, sodium metal was used to deprotonate 11-bromoundecanol-1 (**7**) [92]. Sodium 4-(11-hydroxy-undecyloxy)-benzene sulfonate (**11**) was obtained as product with low purity indicated by the ^{1}H NMR spectrum. In the second step, sodium 4-(5-oxa-16-undecanol)benzene sulfonate (**11**) was reacted with maleic anhydride (**12**) to add the polymerizable function. Pyridine was used as solvent and to bind the formed acid. The alcoholate anion should react with maleic anhydride (**12**). ^{1}H NMR data for the final product of the second step show the presence of pyridine and the absence of PSA-MA. None of the desired resonances were present.

3.4.2.2. Attempt 2

1,00 g (0,40 mmol) 11-bromoundecanol-1 dissolved in 10 ml water and 30 ml methanol was added to 0,19 g (0,46 mmol) sodium hydroxide and a solution of 1,12 g (0,48 mmol) phenol sulfonic acid, in 15 ml water and refluxed at 65 °C for 36 h. After precipitation of the reaction mixture into 100 ml chloroform and filtration, the product was dried under vacuum, 0,80 g (0,21 mmol) sodium 4-(11-hydroxy-undecyloxy)-benzene sulfonate were obtained as white crystals in 53 % yield.

^{1}H NMR: (20 °C, D_2O) δ= 1,11 – 1,35 (m, 14H, -C$\underline{H}_2$-); 1,51 (q, 2H, -C$\underline{H}_2$-CH_2-OH); 1,61 (q, 2H, -C$\underline{H}_2$-CH_2-OC_6H_4-); 3,41 (t, 2H, -C$\underline{H}_2$-OH); 3,96 (t, 2H, -C$\underline{H}_2$-OC_6H_4-); 6,91 (d, 2H, *m*-Ar$\underline{H}$); 7,56 (d, 2H, *o*-Ar$\underline{H}$).

0,78 g (0,21 mmol) sodium 4-(11-hydroxy-undecyloxy)-benzene sulfonate and 0,21 g (0,21 mmol) maleic anhydride were dissolved in 30 ml chloroform and refluxed at 65 °C for 6 h. After removal of solvent under vacuum 0,81 g of a white powder was obtained.

In the second attempt, 11-bromoundecanol-1 (**7**) was deprotonated by sodium hydroxide which is a weaker base than sodium metal and not a reducing agent. The ^{1}H NMR analysis for the second attempt had better results than the first. The product had a higher purity. In the second step the intermediate was reacted with maleic anhydride in chloroform to prevent contamination with pyridine. The reaction was not successful as the resonances for maleic anhydride were not present in the spectrum. The required esterification did not take place.

3.4.3. Preparation of PSA-MA (3), synthetic route 2 (see Figure 4.16)

Due to the low purity of the intermediate, (sodium 4-(11-hydroxy-undecyloxy)-benzene sulfonate) (11), the problems with purifying the component and the lack of esterification, a new synthetic route had to be found. Montoya-Goni [19] managed to synthesize a dialkyl maleate cationic surfmer from 11-bromoundecanol-1 (**7**) and maleic anhydride (**12**). The intermediate

was esterified with a bromoalkylalcohol. Instead of the esterification, a Williamson Ether synthesis with a phenol was attempted.

In the first attempt, phenolsulfonic acid (PSA) (**10**) was deprotonated in the presence of Br-MA (**13**). Mild conditions (low temperature and pH8) were used to prevent saponification. In the second attempt, to ensure deprotonation took place, PSA (**10**) was deprotonated in a separate reaction and then reacted with **13**.

*3.4.3.1. Preparation of succinic acid mono-(11-bromo-undecyl) ester (Br-MA) (**13**)*

3,38 g (14,0 mmol) 11-bromoundecanol-1 and 1,38 g (14,0 mmol) maleic anhydride were reacted under reflux at 80 ^{0}C for 20 h. A white solid was obtained and recrystallized from n-hexane. After filtration and drying 3,74 g (11,0 mol) of succinic acid mono-(11-bromo-undecyl) ester was obtained as a white powder in 79,6 % yield.

^{1}H NMR: (20 °C, $CDCl_3$) δ = 1,29 – 1,45 (m, 14H, -C$\underline{H}_2$-); 1,72 (q, 2H, -C$\underline{H}_2$-CH_2-Br); 1,85 (q, 2H, -C$\underline{H}_2$-CH_2-O-); 3,41 (t, 2H, -C$\underline{H}_2$-Br); 4,29 (t, 2H, -C$\underline{H}_2$-O-); 6,37 (d, 1H, -CH=C$\underline{H}CO_2$-); 6,48 (d, 1H, HOOC-C$\underline{H}$=CH-).

^{13}C NMR: (20°C, $CDCl_3$) δ = 25,8 – 34,2 (-$\underline{C}H_2$-); 65,8 (-$\underline{C}H_2$-O-CO); 67,4 (Br-$\underline{C}H_2$-); 129,6 (HO-CO-$\underline{C}$H=CH-CO); 136,4 (HO-CO-CH=$\underline{C}$H-CO); 164,9 (HO-$\underline{C}$O-CH=CH-); 167,9 (-O-$\underline{C}$O-CH=CH-).

Microanalytical data: calculated (found) % = C: 51,6 (51,5); H: 7,2 (7,3).

According to the general rules of synthesizing surfmers (Chapter 3.2.1.), the synthetic route started with the addition of the polymerizable group first. No special precautions (like adding a polymerization inhibitor) were taken to prevent homopolymerization since maleic anhydride (**12**) can not homopolymerize in the aqueous phase, a feature all maleic diesters share [93]. The hydrophobic tail and the polymerizable function were attached via the opening of the maleic anhydride ring (**12**) with 11-bromoundecanol-1 (**7**) (Figure 3.17) to give maleic acid *n*-undecyl monester (**13**). The bromo alkyl monomer **13** was obtained as a solid and purified by

recrystallization from hexane in 80 % yield [19]. Elemental analysis and NMR indicate that this compound (**13**) was 99 % pure.

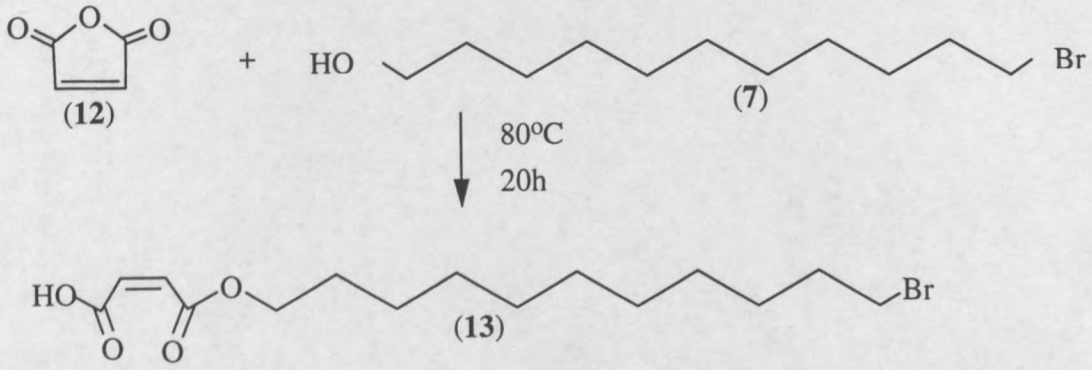

Figure 3.17. Reaction scheme for opening of maleic anhydride (12) and addition to $Br(CH_2)_{11}OH$ (7).

3.4.3.2. Synthesis of PSA-MA (3) based on Br-MA (13), attempt 1

3,0 g (0,86 mmol) Br-MA, dissolved in 30 ml dichloromethane and 3,46 g (1,5 mmol) phenol sulfonic acid and 1,91 g (2,3 mmol) sodium hydrogen carbonate, dissolved in 40 ml water were refluxed at 55 °C for 12 h. After freeze drying, 5,20 g of a white product was obtained.

Milder conditions (low temperature and pH) were used in this attempt to prevent saponification of Br-MA (**13**). The ^1H NMR spectra of the product showed a number of impurities. An assignment of all resonances was possible but it was not possible to conclude whether the aromatic protons are from impure PSA-MA (**3**) or unreacted PSA (**10**). Due to mild conditions PSA (**10**) might not have been deprotonated. Purification of the sample proved to be difficult.

3.4.3.3. Synthesis of PSA-MA (3) based on Br-MA (13), attempt 2

To ensure a phenolate anion was obtained as intermediate, phenol sulfonic acid (**10**) was deprotonated in a separate reaction.

*3.4.3.3.1. Preparation of deprotonated phenol sulfonic acid (**14**)*

1,42 g (35,0 mmol) sodium hydroxide, dissolved in 10 ml deionized water was added drop-wise to 7,82 g (35,0 mmol) phenol sulfonic acid, sodium salt hydrate, dissolved in 40 ml deionized water and reacted for 1 h at 40 °C. The reaction mixture was freeze-dried and 8,44 g (45,0 mol) of deprotonated phenol sulfonic acid was obtained as a white powder in 128 % yield.

^{1}H NMR (PSA): (20°C, D_2O) δ = 6,93 (d, *o*-Ar); 7,65 (d, *m*-Ar).

^{13}C NMR: (20°C, D_2O) δ = 118,94 (*m*-Ar); 126,74 (*o*-Ar); 126,84 (Ar-SO_3); 161,85 (Ar-OH).

^{1}H NMR (deprot. PSA): (20°C, D_2O) δ = 6,60 (d, *o*-Ar); 7,48 (d, *m*-Ar).

^{13}C NMR: (20°C, D_2O) δ = 115,22 (*m*-Ar); 127,32 (*o*-Ar); 133,99 (Ar-SO_3); 158,09 (Ar-OH).

The phenolate **10** was prepared by the reaction of 4-hydroxy benzene sulfonate (sodium salt dihydrate) with sodium hydroxide. The success of the deprotonation can be seen in the shift of the resonances of the aromatic protons to a higher field (Figure 3.18).

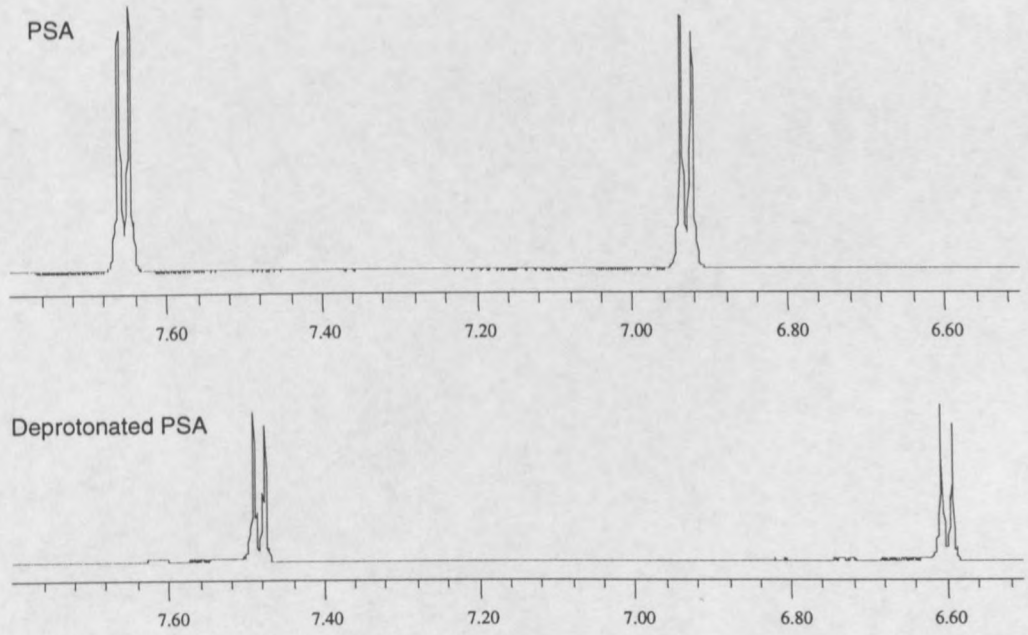

Figure 3.18. ^{1}H NMR to show differences between PSA (10) and deprotonated PSA (14).

3.4.3.3.2. Preparation of Sodium 4-[11-(3-carboxypropinoyloxy)-undecyloxy] benzenesulfonate (PSA-MA) (3)

8,44 g (45,0 mmol) deprotonated phenol sulfonic acid was dissolved in 20 ml deionized water and 11,31 g (33,0 mmol) of MA-Br dissolved in 40 ml dichloromethane was added drop-wise and refluxed at 55 °C for 12 h. After freeze-drying 18,51 g (40,0 mmol) of a white powder was obtained. The powder was dissolved in water and precipitated in n-hexane. The product formed a suspension in the organic layer and was separated. After removal of solvent and drying, 3,62 g (7,8 mol) of a white powder was obtained.

^{1}H NMR: (20 °C, D_2O) δ= 1,30 – 1,43 (m, 14H, -C$\underline{H}_2$-); 1,62 (q, 2H, -C$\underline{H}_2$-CH_2-OCO); 1,85 (q, 2H, -C$\underline{H}_2$-CH_2-O-); 3,43 (t, 2H, -C$\underline{H}_2$-O-); 4,07 (t, 2H, -C$\underline{H}_2$-O-CO-); 5,74 (d, 1H, -CH=C$\underline{H}CO_2$-); 6,53 (d, 1H, HOOC-C$\underline{H}$=CH-); 6,62 (d, 2H, *m*-Ar$\underline{H}$); 7,48 (d, 2H, *o*-Ar$\underline{H}$).

^{13}C NMR: (20°C, D_2O) δ = 28,6 – 36,8 (-$\underline{C}H_2$-); 64,4 (-$\underline{C}H_2$-O-CO); 67,8 (-C_6H_4-O-$\underline{C}H_2$-); 118,5 (Ar); 120,9 (Ar); 130,1 (Ar); 135,7 (HO-CO-$\underline{C}$H=CH-CO); 144,5 (HO-CO-CH=$\underline{C}$H-CO-); 162,7(HO-$\underline{C}$O-CH=CH-); 169,8 (-O-$\underline{C}$O-CH=CH-).

Microanalytical data: calculated (found) = C: 54,31 (41,37); H: 6,25 (5,64).

The incorporation of the benzene sulfonate group is based on the nucleophilic substitution of the bromide by the phenolate via the Williamson Ether synthesis (Figure 3.19).

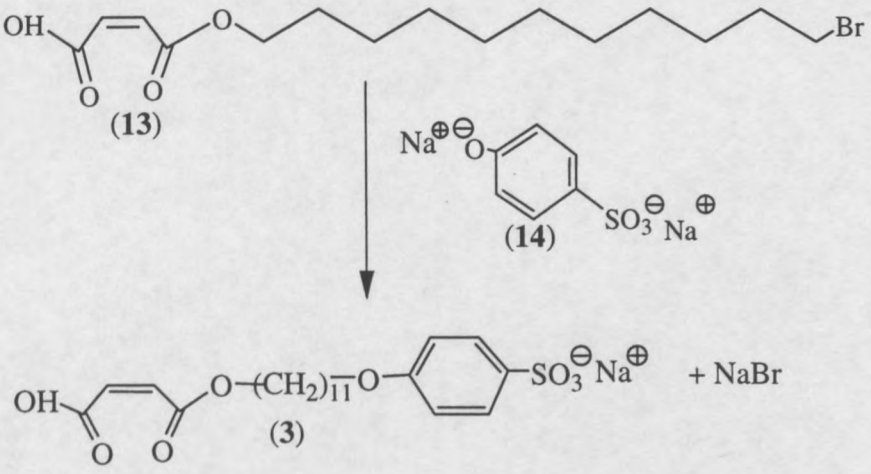

Figure 3.19. Reaction scheme for addition of PSA (14) to Br-MA (11).

Very mild conditions (low temperatures) were used to prevent saponification and hydrolysis of the double bond and the alkyl bromide **11**. Inorganic salts (e.g. sodium bromide) were formed as side products from the reaction. Impurities were indicated by the high yield. Purification was done by precipitation from hexane. The precipitate accumulated at the interface in the organic layer during the extraction procedure. The aqueous phase was removed and the precipitate in the organic phase was dried under vacuum. Cleaning of the product (**3**) was troublesome with no success and gave very low yields.

Figure 3.20 shows the ^{1}H NMR spectra of Br-MA (**13**) (top) and PSA-MA (**3**) (bottom). The methyl protons (7) of Br-MA next to -Br appear at δ = 3,41. The presence of the aromatic protons after the reaction with deprotonated PSA (**14**) can be seen at δ = 6,93 and δ = 7,65 (Figure 4.20., bottom (8 and 9)). These protons have the same shift as PSA (**10**) (Figure 3.19). The ratio of the integrals of the aromatic resonances (8 and 9) and of the resonances of the maleic anhydride (1 and 2) does not indicate that the product PSA-MA (**3**) was formed. These resonances are therefore no evidence for a successful reaction of deprotonated PSA (**14**) with Br-MA (**13**).

It can be seen from the ^{1}H NMR (Figure 3.20) that the maleic anhydride (**12**) was deprotonated (reflected in the shift of the methylene protons (1 and 2)). The small peaks visible in both spectra are due to the formation of fumaric acid that has been splitted off by the phenolate.

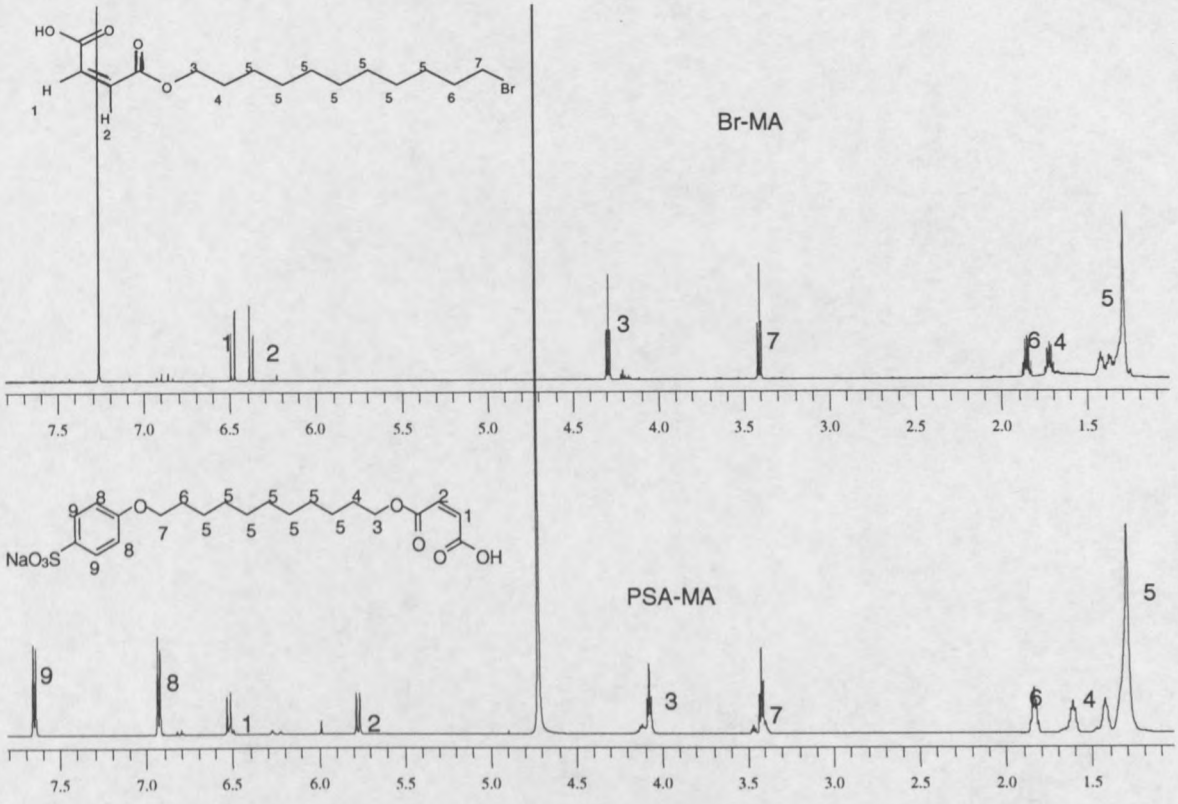

Figure 3.20. ^{1}H NMR spectra to show difference between Br-MA (13) and PSA-MA (3).

The results of elemental analysis indicated a low purity or a mixture of more than one component.

To evaluate if PSA-MA (**3**) was existent in the product mixture a matrix-assisted laser desorption/ionization (MALDI) was done.

In MALDI the sample is mixed with a matrix and this mixture is impinged by a UV laser. Ions are formed in this process that are accelerated to a mass detector.

MALDI results for the obtained product showed mass peaks at 373 and 396 that correlated to Br-MA with one and two sodium ions attached to it respectively. The mass peak corresponding to PSA-MA (487) was not present in the spectrum.

3.4.4. Conclusions

All the synthetic routes yielded the desired intermediate products. The second reaction step was not successful. There was no evidence from analytical results that PSA-MA (**3**) was obtained. No further synthetic attempts were made.

Chapter 4

Polyelectrolyte-Surfactant Complexes

4.1. Introduction

It is well known that ionic surfactants and oppositely charged polyelectrolytes spontaneously form addition complexes which precipitate from aqueous solution. Complexes made out of MET/pDADMAC (**15**) and CRO/pDADMAC (**16**) were formed and analyzed to investigate structure-property relationships (section 4.2.2 and 4.3).

4.2. Experimental

4.2.1. Experimental techniques

Wide angle X-ray Scattering (WAXS) analyses were performed on a Bruker Advance D8 X-ray diffractometer (operating conditions: 40 kV, 40 mA, λ = 0,154 nm), National Accelerator Center, Faure, South Africa.

High resolution SAXS diffractograms were obtained with a camera constructed at the Max-Planck-Institute of Colloids and Interfaces, Golm, Germany. Cu KαX-rays were generated by a rotating anode (Nonius, FR591, P = 4 kW, λ = 0,154 nm). Small angle scattering measurements were carried out with a Nonius rotating anode (FR 591) using image plates as detector. With the image plates placed at a distance of 40cm from the sample, a scattering vector range from s = 0,07 to 1,6 nm^{-1} was available (s = [2/λ*sin (θ)]). 2D diffraction patterns were transformed into a 1D radial average. The data noise was calculated according to Poisson-statistics which are valid for scattering experiments.

4.2.2. Preparation of polyelectrolyte-surfactant complexes 15 and 16

Film preparation followed a standard procedure described in literature [81]. One example of a preparation is given.

For complex formation 1,31 g (3,7 mmol) of MET (**1**) were dissolved in 65 ml distilled water at room temperature and slowly added to a mixture of 0,58 g (3,6 mmol) of a 20 wt % solution of pDADMAC (**4**) (equimolar in terms of repeat units) and 5,8 ml distilled water under slow stirring.

Micro analytical data (MET-pDADMAC complex (**15**)): Calculated (Found) C: 59,9 (57,6); H: 10,6 (10,5); N: 3,0 (3,0).
Micro analytical data (CRO-pDADMAC complex (**16**)): Calculated (Found) C: 59,9 (57,9); H: 10,6 (10,5); N: 3,0 (2,9).

4.3. Results and Discussion

4.3.1. Complex formation and analysis of MET/pDADMAC (15) and CRO/pDADMAC (16)

Only small amounts of complex were formed in both cases. The yields were 15,3 % for MET/pDADMAC (**15**) and 27,4 % for CRO/pDADMAC (**16**) after drying. During complex formation the aqueous phase stayed cloudy even after centrifuging. The low yields can be due to weak electrostatic interactions and steric hindrance (see section 2.3.1). pH also plays an important role in complex formation and influences the yield. An optimal pH is between 8 and 9 [94]. This pH was used for the surfactant solutions. Films were cast and after solvent evaporation and drying, clear and transparent films that are soft and flexible were obtained.

4.3.1.1. Elemental analysis

Elemental analysis indicated the formation of a 1 : 1 complex between the polyelectrolyte (**4**) and the surfactant (**1**) (Figure 4.1).

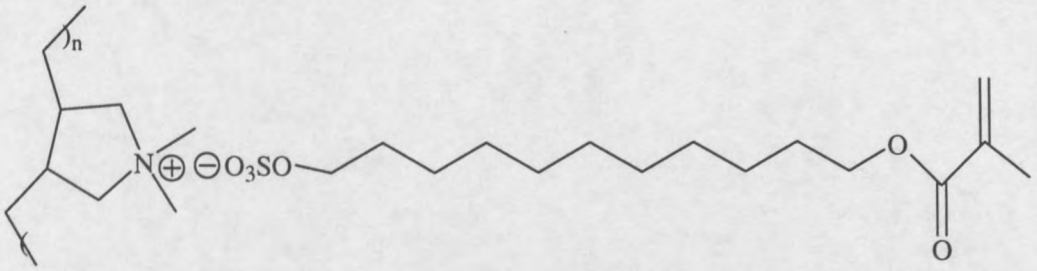

Figure 4.1. Schematic representation of one unit of a 1 : 1 MET /pDADMAC (15) complex.

Microanalytical data were obtained theoretically by using the combined molar masses of MET (**1**) (M_r = 335 g/mol) and pDADMAC (**4**) (M_r = 126,18 g/mol) as it will form one repeat unit and calculating the mass percentage of carbon, nitrogen and hydrogen present in the sample. It was calculated that 3 % nitrogen must be present in the sample where a 1 : 1 complex is formed.

4.3.1.2. Polarized light microscopy

The films were investigated by polarized light microscope. The investigation indicated birefringence (Chapter 2.4.5) in the films. That was the first indication of some structural order.

4.3.1.3. WAXS analysis

WAXS analysis was used to indicate the absence of crystallinity in the complex. Figure 4.2 shows WAXS diffractograms of MET surfactant (**1**) and MET/pDADMAC (**15**) complex and Figure 4.3 that of CRO surfactant (**2**) and CRO/pDADMAC (**16**) complex reflecting the packing on angstrom scale.

Rather broad scattering peaks, typical for ordered, but liquid alkyl phases were observed for the complexes and sharp scattering peaks, that indicate some crystalliny, were observed for the surfactants

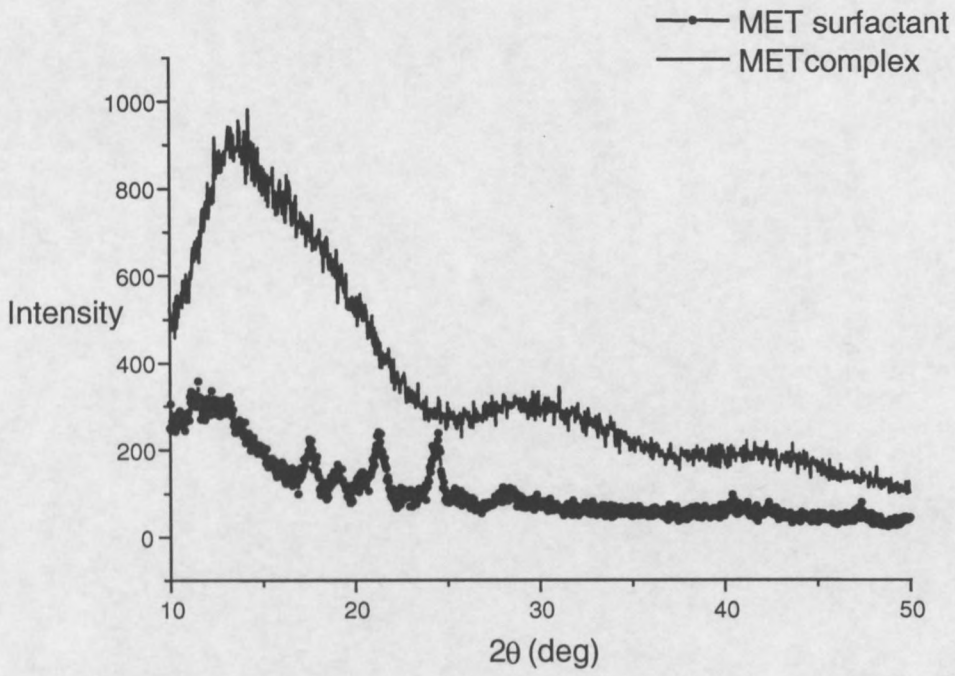

Figure 4.2. WAXS diffractogram of MET (1) surfactant and MET/DADMAC (15) complex.

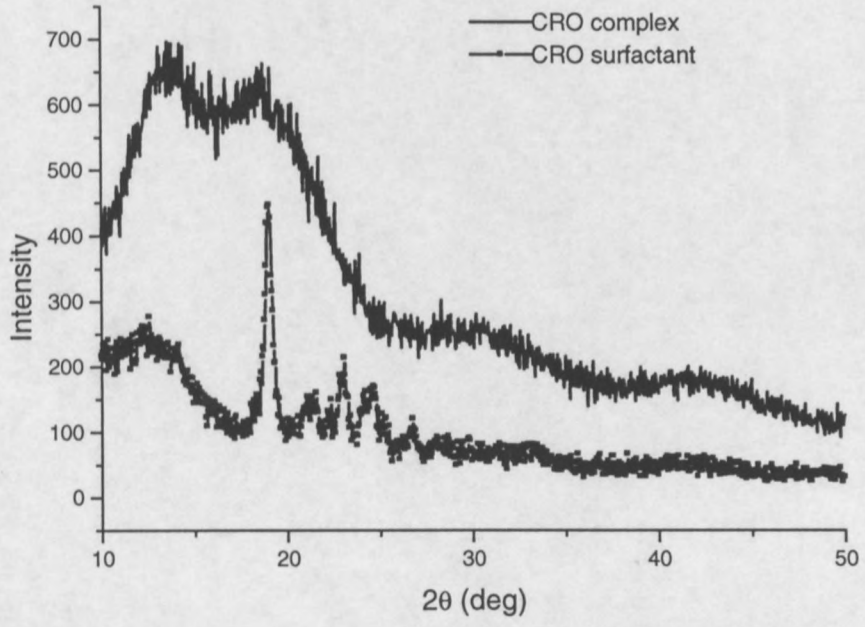

Figure 4.3. WAXS diffractogram of CRO (2) surfactant and CRO/DADMAC (16) complex.

Both surfactants show crystalline peaks in the region of 18° to 25° (Table 4.1). These peaks indicate that the surfactants are crystalline as was also found in the DSC analysis (section 3.3.2.2).

Table 4.1. WAXS peak positions for surfactants 1 and 2.

Surfactant	Peak positions 2θ (°)				
MET (**1**)	17,5	19,2	21,4	24,4	-
CRO (**2**)	19,1	21,4	23,1	24,7	26,7

WAXS analysis of the complexes **15** and **16** showed a non-crystalline structure, i.e. the surfactant side chains exhibit a liquid or liquid crystalline type arrangement. The crystallinity observed in the surfactants are no longer present in the complexes due to liquid crystalline arrangement of the side chains.

A single broad peak at 2θ = 15° is visible for MET/pDADMAC (**15**) (Figure 4.2) while CRO/pDADMAC (**16**) (Figure 4.3) shows a split peak at 2θ = 14° and 19°. In both samples, two broad, less pronounced peaks can be identified at 2θ = 30° and 41°. Since the peak at 2θ = 15° is rather broad, the order within the alkyl chain domain is supposed to be quite low [95].

4.3.1.4. SAXS analysis

Figure 4.4 shows the SAXS scattering peaks for MET/pDADMAC (**15**) and Figure 4.5 that of CRO/pDADMAC (**16**).

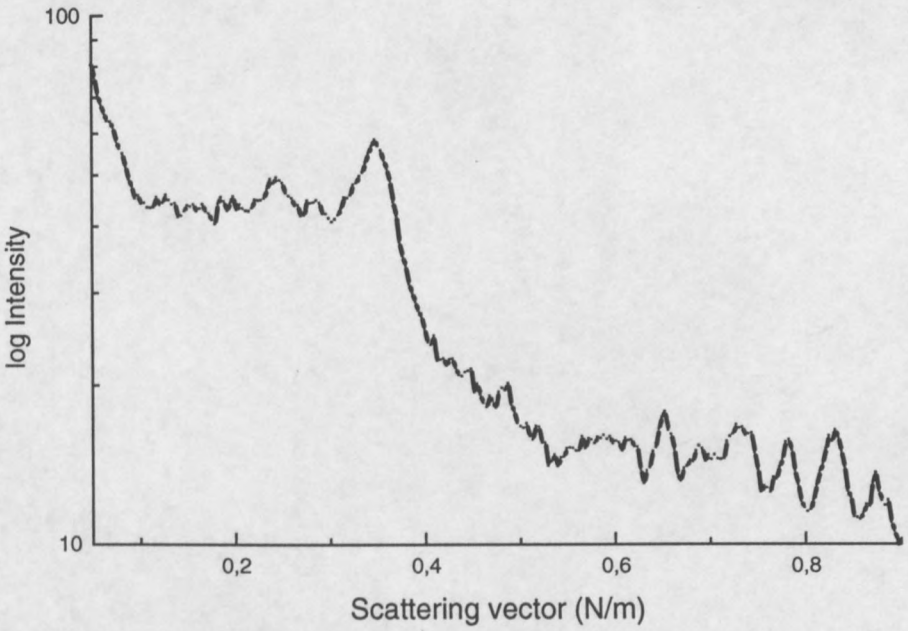

Figure 4.4. SAXS data for MET/pDADMAC (15) complex.

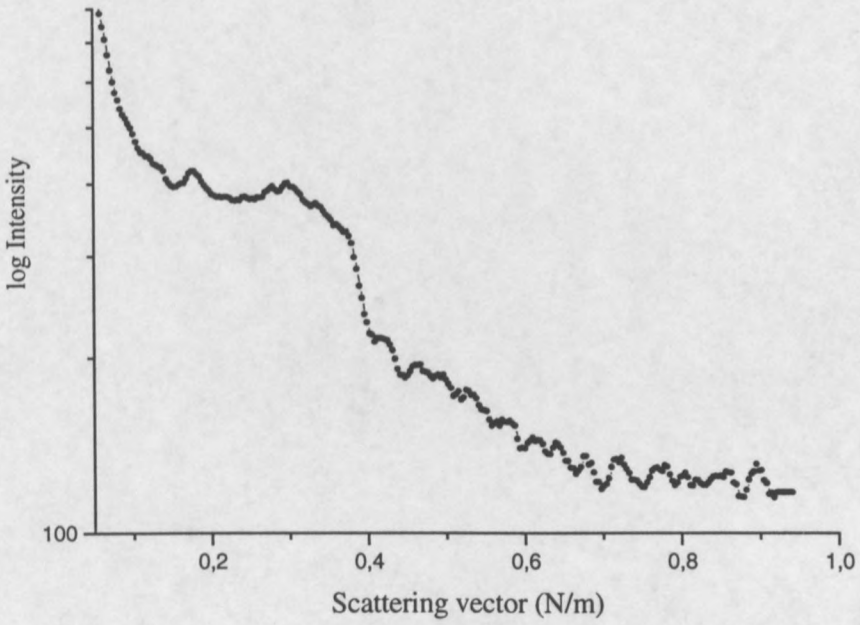

Figure 4.5. SAXS data for CRO/pDADMAC (16) complex.

The MET/pDADMAC complex (**15**) (Figure 4.4) displays scattering peaks at s = 0,24 nm^{-1} and s = 0,35 nm^{-1} and a range of peaks in the region of s = 0,48 nm^{-1} to 0,9 nm^{-1} of low intensity.

Peak ratios of 1 : 2 at s = 0,24 nm^{-1} and s = 0,48 nm^{-1} can be assigned to the lamellar phase (Table 4.2). s = 0,24 nm^{-1} indicates a d spacing of 4,1 nm. Theoretically **1** has a length of 3,8 nm and the difference of the length between the theoretical and experimental values can be due to interdigitation of the alkyl chains and the fact that the polar methacrylic ester group can possibly fold back onto the ionic layer.

The primary peak at s = 0,35 nm^{-1} belongs to no known mesophase and the peaks in the region of s = 0,55 nm^{-1} to 0,9 nm^{-1} can not be assigned to any specific mesophase. These data indicate the possible coexistence of a mixture of different known and unknown mesophases.

Table 4.2. Peak position ratios for classical morphologies [96, 97].

Classical morphology	Peak position ratios
Lamellar	1 : 2 : 3
Hexagonally packed cylinders	1 : $\sqrt{3}$: 2 : $\sqrt{7}$
Body-centred cubic	1 : $\sqrt{2}$: $\sqrt{3}$
Gyroid	1: $\sqrt{4/3}$: $\sqrt{7/3}$: 2

The CRO/pDADMAC complex (**16**) (Figure 4.5) shows a small scattering peak at s = 0,17 nm^{-1} and a broad scattering peak at s = 0,28 nm^{-1}. This can not be assigned to any known mesophase. s = 0,17 nm^{-1} indicate a d-spacing of 6,25 nm and might hint to the presence of a superstructure. A range of peaks is observed between s = 0,5 nm^{-1} and 0,9 nm^{-1} and can not be assigned to any specific known mesophase. These results indicate the coexistence of different mesophases and low order in the complex.

Two possible explanations can be given for the low order observed in the complexes:

- Presence of the acrylate group and
- Formation of a 'loop' structure.

The presence of polymerizable groups such as acrylates, methacrylates, terminal olefins, and diene esters has been used to generate polymerizable surfactants. It has been found that properties such as the hydrophobicity, bulk, and reactivity of these polymerizable groups have a profound effect on the chemical affinity and organizational ability of the surfactant molecules. Polar groups such as acrylates generally tend to destabilize thermotropic liquid crystalline phases, and are detrimental to surfactant phase separation behavior [98].

The formation of a 'loop' or 'wicket-like' structure has been reported at the micelle-water and water-gas interfaces (Figure 4.6). This 'loop' structure may be the source of the steric hindrance and destabilization of the mesophase. It may cause disruption of the alignment of the hydrophobic tails and influence the self assembly mechanism.

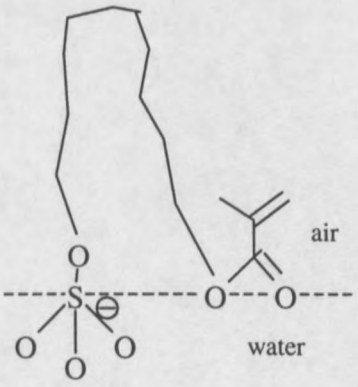

Figure 4.6. Conformation of monomers at micelle-water and water-gas interfaces showing 'loop' formation (adapted from [21, 17]).

Chapter 5
Co-polymerization of MET

5.1. Introduction

The sodium salts of methacrylic acids polymerize quite readily in aqueous isotropic solutions [99]. Amphiphiles self-assemble to form micelles in aqueous solutions (section 2.1.4). This knowledge of self-assembly was used to investigate how MET (**1**), that homo-polymerizes easily, will behave in a polystyrene or poly-(methyl methacrylate) matrix when it is co-polymerized.

5.2. Experimental

5.2.1. Experimental techniques

Gel Permeation Chromatography (GPC) was done on a Waters 150C GPC. A PL-ELSD 1000 (light scattering) detector and a PLgel Mixed A column were used. Sample concentrations of 1 g/ml and a flow rate of 1 ml/min were used. All measurements were carried out at 50 °C in DMF.

Differential Scanning Calorimetry (DSC) was done on a DSC22C (Seiko II) using a heating rate of 10 °C / min. The first heating cycle was used as the sample degraded thereafter.

Fourier Transform Infrared Spectroscopy (FTIR) was done on a Nexus FT-IR.

Degradation studies were carried out with a Thermal Gravimetric Analyzer (TGA50) (Shimadzu instruments). All these were carried out at the Deutsches Kunststoff-Institut, Darmstadt, Germany, unless otherwise stated.

Nuclear magnetic resonance spectroscopy (NMR) was performed on a Bruker AC300 MHz instrument at the Technische Universität Darmstadt, Germany.

5.2.2. Polymerization of MET (1)

MET (**1**) was homo-polymerized by dissolving 0,931 g (0,002 mol) MET in distilled water and slowly adding it to 0,018 g (2 wt%) potassium persulfate (KPS). The reaction mixture was boiled under reflux for 90 minutes at 80 °C. After this time the reaction mixture was freeze-dried, yielding 0,915 g of a light yellow, sponge-like material (98 % yield).

^{1}H NMR: (20°C, 10% $CDCl_3$, DMF) δ = 1,28 – 1,41 (m, 18H, -CH_2-); 1,49 (s, 3H, CH_3-); 4,45 (t, 2H, -CH_2-OSO_3^-); 4,57 (t, 2H, -COO-CH_2-).

^{13}C NMR: (20°C, 10% $CDCl_3$, DMF) δ = 20,1 (CH_3-); 30,1 – 36,8 (-CH_2-), 69,5 (-COOCH_2); 78,9 (-CH_2-OSO_3^-); 130,5 (-CH_2=CH-); 141,5 (CH_2=CH-); 175,9 (-CO).

5.2.3. Co-polymerization of MET (1) with styrene and methyl methacrylate

Styrene and methyl methacrylate were also co-polymerized with 5 %, 10 % and 20 % MET (**1**) (w/w) respectively. The reaction of styrene with 10% MET (**1**) is given as a typical example of the co-polymerizations:

2,0 g (0,019 mol) styrene and 0,20 g (0,055 mmol) MET, dissolved in 20 ml chloroform, were added drop-wise over 10 min to 0,022 g AIBN dissolved in 10 ml chloroform. The reaction mixture was boiled under reflux for 4 hours and precipitated in methanol. After evaporation of the solvent and drying of the sample, 0,37 g of an amber, glass-like material was obtained (16,7 wt% yield).

^{1}H and ^{13}C NMR spectra of MET-PMMA-copolymers:

^{1}H NMR: (20°C, 10% $CDCl_3$, DMF) δ = 1,51 – 1,91 (m, 28 H, -CH_2- and CH_3-C-); 3,63 (s, 3H, CH_3-COO-); 3,90 (t, 2H, -CH_2-OSO_3^-); 4,12 (t, 2H, -COOCH_2).

^{13}C NMR: (20°C, 10% $CDCl_3$, DMF) δ = 19,2 – 19,9 (CH_3-C); 29,9 – 31,7 (-CH_2-); 52,0 (CH_3-COO); 54,7 (-COOCH_2); 69,4 (-CH_2-OSO_3^-); 177,0 and 177,9 (-CO).

^{1}H and ^{13}C NMR spectra of MET-PS-copolymers:

^{1}H NMR: (20°C, 10% $CDCl_3$, DMF) δ = 128 – 1,71 (m, 23 H, -CH_2- and CH_3-C-); 1,91 (s, 1H, -CH_2-CH-C_6H_5-); 3,46 (s, 3H, CH_3-COO-); 3,90 (t, 2H, -CH_2-OSO_3^-); 4,12 (t, 2H, -COOCH_2), 7,06 – 7,12 (5H, C_6H_5-).

^{13}C NMR: (20°C, 10% $CDCl_3$, DMF) δ = 24,1 (CH_3-C); 29,9 – 35,7 (-CH_2-); 44,5 (CH-C_6H_5); 64,9 (-COOCH_2); 66,9 (-CH_2-OSO_3^-); 125,4 – 129,0 (aromatic carbons); 159,4 and 164,7 (-CO).

The co-polymers were named in the following manner: MET-X-YY. X indicates the percentage of MET (**1**) (5, 10 or 20) that was used as co-monomer and YY indicates whether styrene (PS) or methyl methacrylate (PMMA) was the other co-monomer.

5.3. Results and discussion

MET (**1**) is a very reactive monomer which homo-polymerizes readily and in high yields. CRO (**2**) on the other hand, is a very unreactive monomer that does not homo-polymerize under free-radical conditions [8]. It rather forms a number of stable resonance structures as shown in Figure 5.1. For this reason only co-polymerizations were performed with MET (**1**).

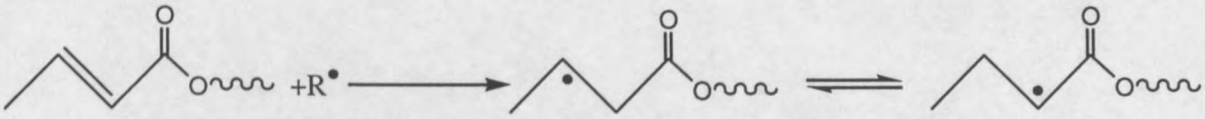

Figure 5.1. Possible resonance structures for CRO (2).

5.3.1. Co-polymerization

Sherrington [21] observed that the polymerization of a range of amphiphilic methacrylic quaternary ammonium salts, below their CMC, is very inefficient and conversions are very low. The concentration of the amphiphilic component, MET (**1**) to be co-polymerized with styrene and methyl methacrylate, was well above its CMC in all cases.

The co-polymerization products, MET-PS and MET-PMMA, were characterized by FTIR and ^{1}H and ^{13}C NMR. All samples showed a high conversion from monomer to polymer with residual amounts of monomer left in the co-polymer. This can be identified by the presence of a very small vibration band for the carbon-carbon double bond around 1650cm^{-1} in the FTIR-spectrum. A typical infrared spectrum that is representative for MET-polystyrene is seen in Figure 5.2. Figure 5.3 is a typical spectrum obtained for MET-poly(methyl methacrylate). A summary of the assignment of bands representative for the poly(styrene-co-MET) and poly(methyl methacrylate-co-MET) is given in Table 5.1.

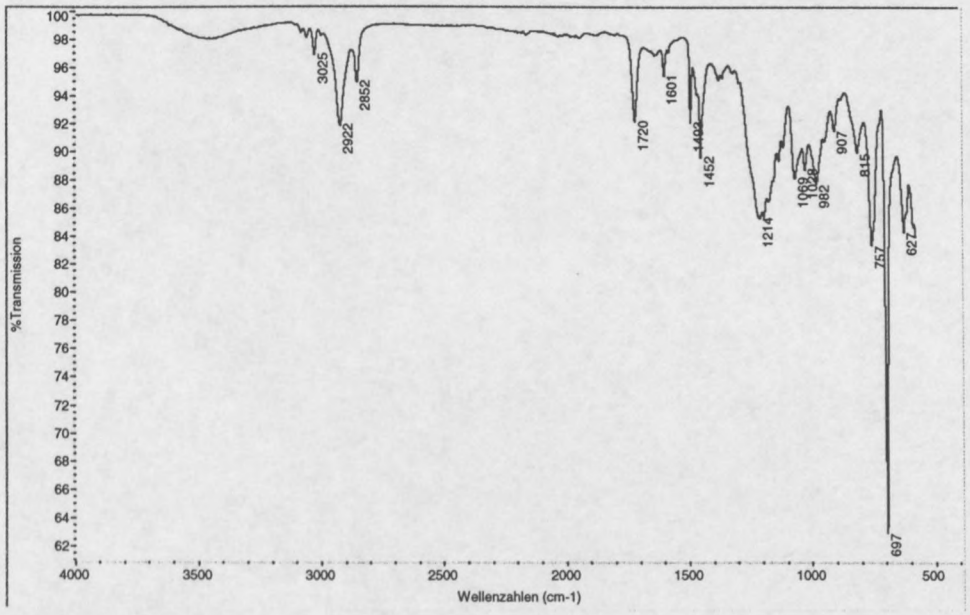

Figure 5.2. Representative infrared spectrum of MET-styrene co-polymers.

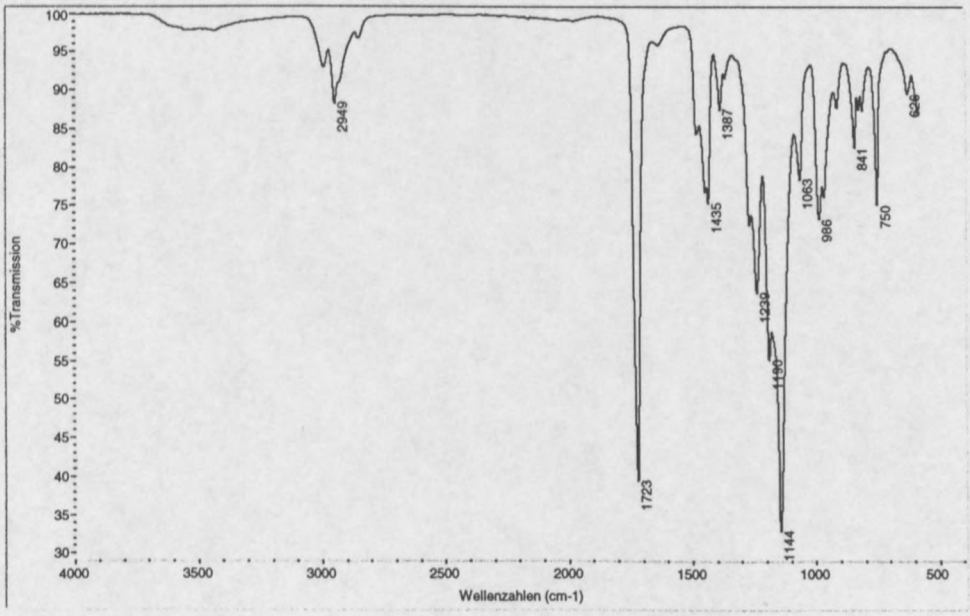

Figure 5.3. Representative infrared spectrum of MET-MMA co-polymers.

Table 5.1. IR band assignment for co-polymers MET-PS and MET-PMMA.

	Poly(styrene-co-MET)	Poly(methyl methacrylate-co-MET)
Assigned groups	Wavelength (cm^{-1})	Wavelength (cm^{-1})
$-CH_2-$	3026, 2923, 2853	2994, 2949, 2857
-O-C=O	1720	1723
Aromatic ring	1601	-
Aromatic ring	1493	-
$-CH_2-$	1452	1435
$-CH_3$	1387	1387
-C-O-	1213	1239, 1144
$-SO_2O-$	1069	1063
Aromatic ring	757, 697, 627	-
$-CH_2-$	815	841, 750

The amount of incorporated MET (**1**) was quantified by the ratio between the integrated areas of the carbonyl band centered around 1720 cm^{-1} and the –C-O- band around 1144 cm^{-1} (for copolymers with PMMA) or the aromatic band at 697 cm^{-1} (for copolymers containing PS) after an ATR correction was done to the spectra. The co-polymers displayed an increase in the ratio of integrated areas as the amount of MET (**1**) in each co-polymer was increased (see Table 5.2). Though a trend can be observed, it is not possible to calculate the exact amount incorporated.

Due to solubility problems, the NMR spectra were recorded using a mixture of DMF and deuterated chloroform ($CDCl_3$) (9:1 v/v). In both ^1H NMR and ^{13}C NMR a small residual amount of monomer is still present, visible at δ = 5,63 and 6,12 ppm in ^1H NMR and at δ = 151and 173 ppm in ^{13}C NMR. A broadening of peaks was observed in all cases which made precise quantification of monomer conversion and MET (**1**) inclusion in the co-polymer as well as individual peak identification, very difficult.

Table 5.2. Values of ratios of integrated areas in FTIR used to determine amount of MET (1) incorporated into co-polymer.

Co-polymer	FTIR band ratios
MET-5-PS	0,665
MET-10-PS	0,671
MET-20-PS	1,438
MET-5-PMMA	0,922
MET-10-PMMA	0,949
MET-20-PMMA	1,041

5.3.1.1. Solubility of co-polymers

The products remained in solution after the polymerization reaction, although after isolation and drying they would not re-dissolve in chloroform. This behavior has been reported before [21, 100, 101], even in the case of polymers which appear to be initially fully soluble. It seems that in the dry state the ionic groups are tightly bound within a hydrophobic network; indeed they may form microphase-separated domains [21].

The products have trouble dissolving after precipitation and drying, even after a prolonged dissolution time. Co-polymers of mixed polarity are known for their solubility problems as one of the co-monomers is very polar and the other is very non-polar [101]. MET (**1**) is soluble in polar solvents such as water or chloroform and PMMA and PS are soluble in non-polar solvents such as toluene. Both series of co-polymers were insoluble in the following solvents: water, 1,2-dichlorobenzene, 1,2,4-trichlorobenzene, tetrahydrofuran, methanol, dichloromethane, chloroform, acetone, 1-methyl-2-pyrrolidone and hexafluoro-2-propanol. Toluene, *m*-cresol, and chlorobenzene swelled the samples. The samples were soluble in N,N-dimethylformamide (DMF) after being heated to 80 °C and stirred for 24 hours.

5.3.2. Analysis of polymers

5.3.2.1. Molecular weight determination

Molecular weight was determined by GPC. In order to obtain reference points for the measurements, the elution time of a range of polystyrene standards was determined using DMF as solvent. Generally a trimodal distribution of molecular weights were found for each

co-polymer (see Figure 5.4 for typical examples). The molecular weights were apparent. Table 5.3 lists all the molecular weight found for the different co- polymers.

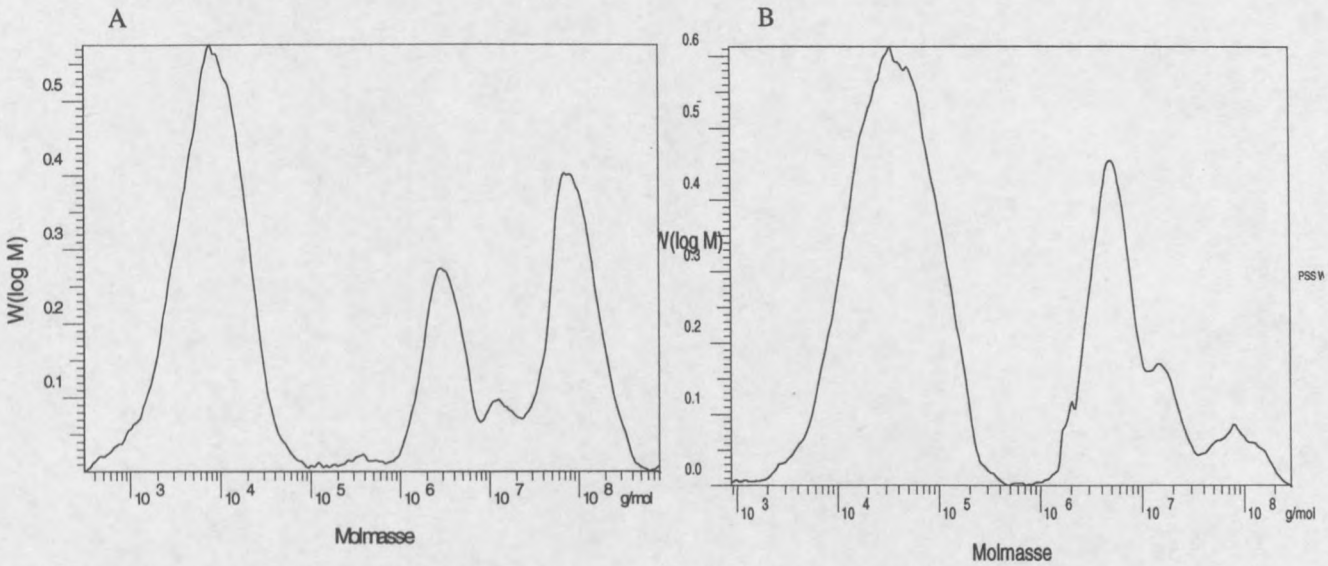

Figure 5.4. Typical molecular weight distribution for (A) MET-10-PS and (B) MET-10-PMMA.

Table 5.3. Molecular weight values of co-polymers determined by GPC, using a polystyrene calibration curve.

Sample	M_n (g/mol)	M_w (g/mol)	D
MET-5-PMMA	3,83e7	5,43e7	1,42
	2,15e6	3,68e6	1,71
	1,60e4	5,28ee4	3,29
MET-10-PMMA	7,58e7	9,50e7	1,25
	4,81e6	7,93e6	1,65
	2,03e4	5,15e4	2,53
MET-20-PMMA	5,74e6	2,04e7	3,56
	1,32e4	4,03e4	3,05
MET-5-PS	4,07e7	6,89e7	1,69
	8,93e5	2,05e6	2,30
	3,32e3	1,08e4	3,24
MET-10-PS	6,12e7	1,04e8	1,71
	2,44e6	3,81e6	1,56
	4,73e3	1,33e4	2,82
MET-20-PS	6,78e7	9,65e7	1,42
	1,02e6	2,94e6	2,89
	3,94e3	9,19e3	2,33

It was observed that the very high molecular weight fraction has a narrow molecular weight distribution (D) while the fraction with medium molecular weight had a broad molecular weight distribution. This narrow molecular weight distribution is because the column has a exclusion limit above 10 000 000 g/mol after which the material is not separated anymore and pass as they are. A broad molecular weight distribution is expected for polymers that have been made by a free-radical mechanism. It can be speculated that the last two extremely high molecular weights indicate the formation of either aggregates or micelles when the co-polymer is in solution. To determine whether aggregation or micelle formation takes place at these extremely high molecular weights, fractions were taken at the different peak elution times to investigate the chemical composition of each fraction. The different fractions were deposited drop-wise at three different places on a germanium disk and the solvent was evaporated before each fraction was investigated by FTIR. Figure 5.5 shows the FTIR spectra of the different MET-20-PMMA fractions.

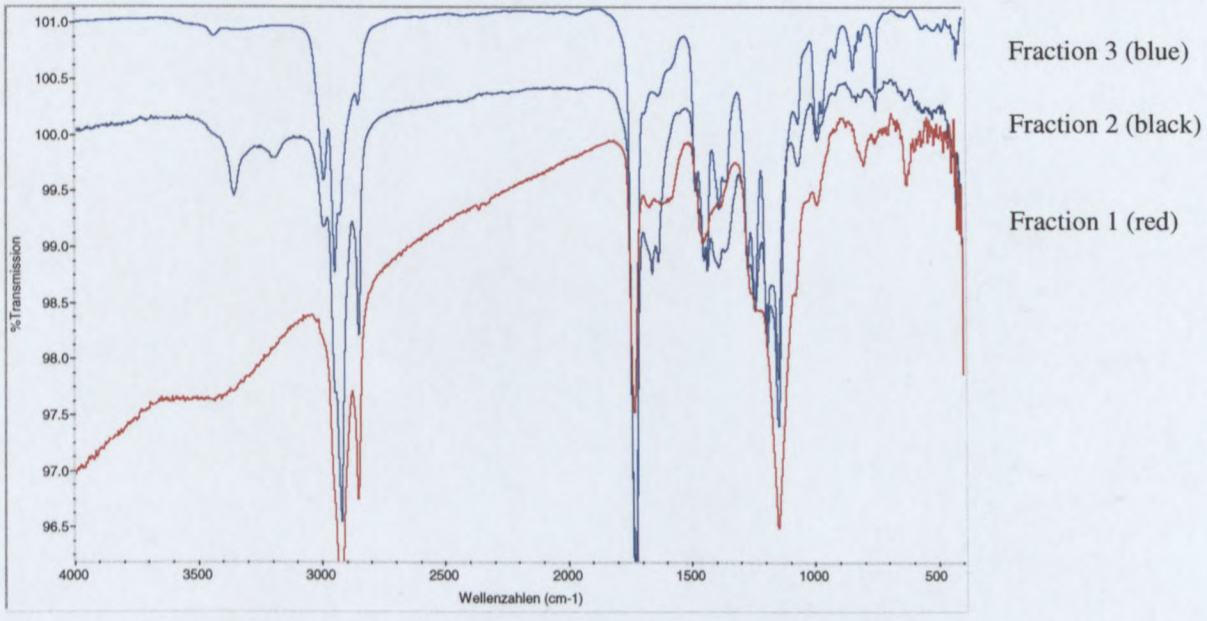

Figure 5.5. Overlay of infrared spectra of different fractions MET-20-PMMA to determine chemical composition of fraction 1, 2 and 3.

The investigation showed that the fraction of medium molecular weight (fraction 3) has a FTIR spectrum which is identical to that of the dry co-polymer, just with different peak intensities. Fraction 2, which has a molecular weight of around 5 000 000 g/mol, was also similar to the dry sample, but with broadened peaks and different peak intensities. It was surprising to find in fraction 2 the presence of an absorption band at 1659 cm^{-1}. This indicates the presence of a carbon-carbon double bond. It can be speculated that the residual amount of

monomer left after polymerization (see section 5.3.1.1) forms micelles or aggregates with the co-polymer to give rise to the high molecular weight. Fraction 1, that has the highest molecular weight, showed a broadening of all absorption bands. The most prominent features of the sample MET-20-PMMA is the -CH_2-, and -CO- absorption bands (refer to Table 5.1). These were all present in the spectrum, but very broadened. Fraction 1 also showed a very broad, less defined peak in the region of 1650 cm^{-1}, that indicates the presence of monomer. It can be concluded from these FTIR spectra that all the fractions have similar chemical composition and that only the fractions with extremely high molecular weight appear to have residual monomer in the co-polymer that possibly either forms aggregates with the co-polymers when it is in solution.

5.3.2.2. Thermal stability

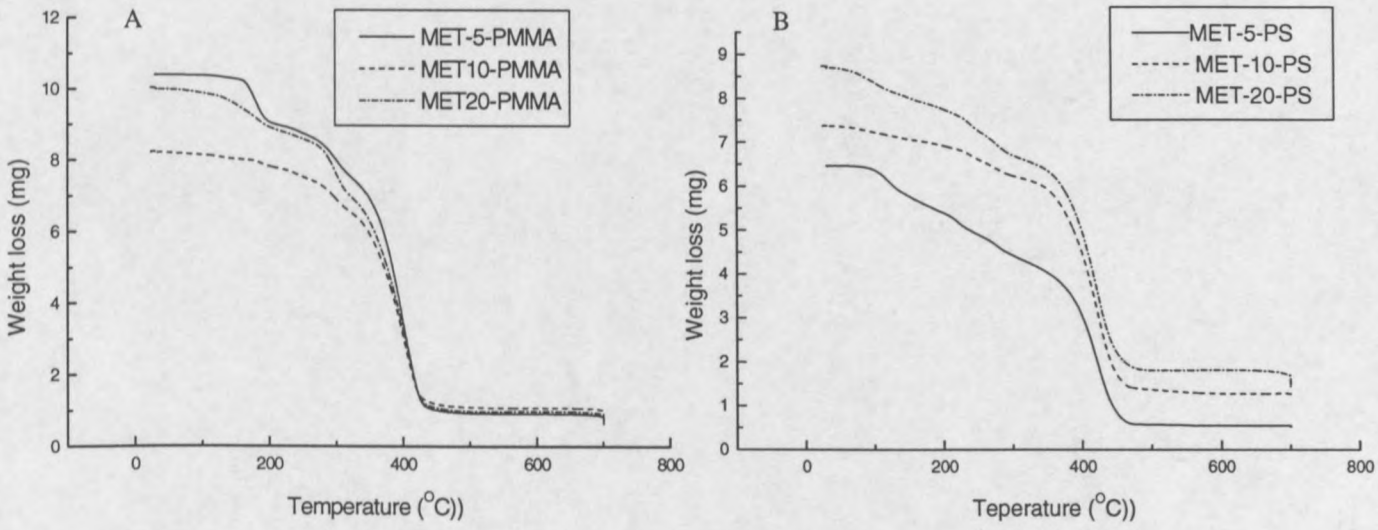

Figure 5.6. TGA thermograms of co-polymers (A: MET-PMMA series, B: MET-PS series).

The thermal stability of the co-polymers was determined by thermal gravimetric analysis. All the co-polymers showed a multi-step degradation pattern (Figure 5.6). Specific onset temperatures and the total percentage of weight loss are tabulated in Table 5.4. The first weight loss step was gradual with an onset at around 100 °C. This weight loss step is probably due to bound water to the MET (**1**) side chains in the sample. The onset of the second degradation step was around 330 °C. This step is probably caused by the degradation of the polystyrene or poly(methyl methacrylate) in the sample. It can clearly be seen that the

polymers are thermally stable up to about 300 °C, after which they degrade rapidly and completely (for accurate temperatures to which the different samples are stable, see Table 5.3).

Table 5.4. Degradation onset temperatures measured by TGA of co-polymers

Sample	Onset (°C)	Mid point (°C)	% Weight loss
MET-5-PS	336,2	385,7	91,67
MET-10-PS	360,8	403,7	82,37
MET-20-PS	349,3	398,6	83,09
MET-5-PMMA	328,6	376,7	91,88
MET-10-PMMA	331,1	379,1	85,95
MET-20-PMMA	315,4	369,0	90,32

Theoretically, the amount of polymer left after being heated to 700 °C should give information of the composition of the sample. The higher portion of MET (**1**) that is incorporated into the polymer should correlate to a lower total percentage weight loss as it contains the most sulphur. The latter degrades at much higher temperatures and should leave the most residue. This trend is not reflected in the measurements and thus no comment can be made about the composition of the samples.

5.3.2.3. Differential Scanning Calorimetry (DSC)

The DSC curves for all the samples display the same trend (see Figure 5.7 for typical examples). Details regarding the temperatures for the different peaks found in the different co-polymers are listed in Table 5.5.

Table 5.5. Specific melting and crystallization temperatures for the different co-polymers.

Co-polymer	Crystallization temperature (°C)	Melting temperature (°C)
MET-5-PS	125,6	174,0
MET-10-PS	119,6	141,9
MET-20-PS	118,7	144,7
MET-5-MMA	122,5	148,3
MET-10-MMA	125,4	144,9
MET-20-MMA	102,5	138,3

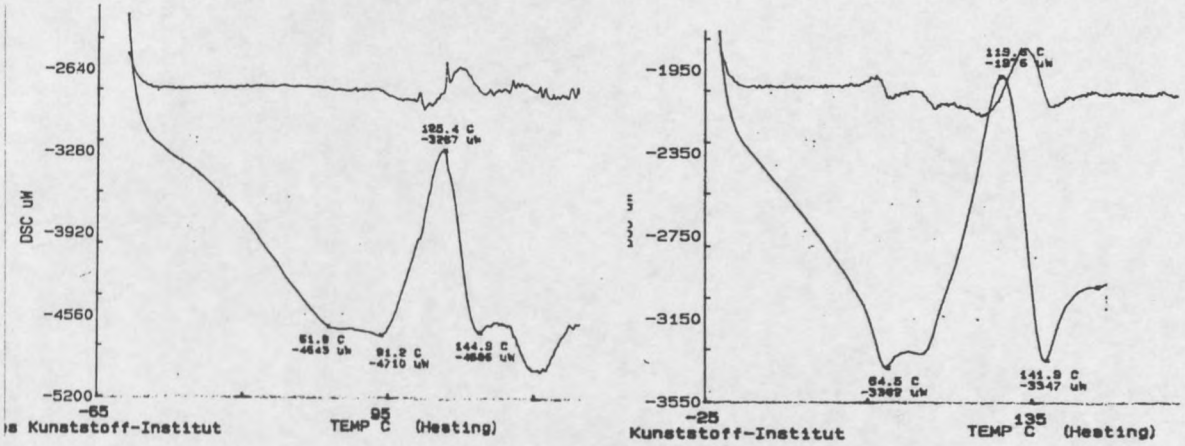

Figure 5.7. Typical DSC heating curve for (left) MET-10-PMMA and (right) MET-10-PS.

A crystallization peak is observed at around 120 °C. This is caused by to the possible side-chain crystallization of the 11 hydrocarbon chain. Side-chain crystallization will take place when the hydrocarbon chains align and the sodium ions form intermolecular bridges. This behavior is reported in literature for similar co-polymers [102, 103] (see in Figure 5.8).

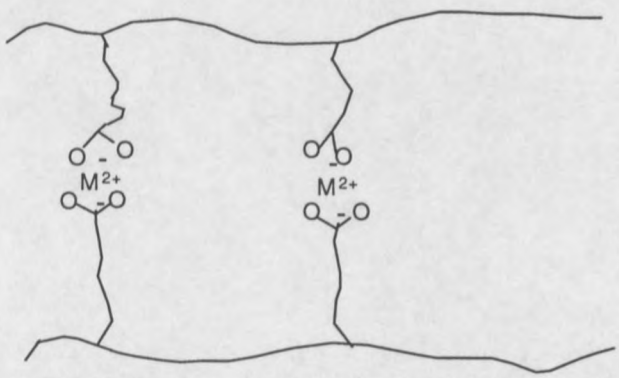

Figure 5.8. Formation of intermolecular bridges in ionic co-polymer [103].

Overlapping with the crystallization peak in the curves, is the melting peak at around 140 °C. It is possible that only that portion of the sample that has side-chain crystallinity melts as no physical melting transition could be detected under a polarized light microscope with a heating stage up to 200 °C.

No T_g could be detected for any of the samples as it might lie within the endothermic melting peak.

Transmission electron microscopy (TEM) of a 50 nm microtomed sample of MET-20-PS showed that a micro-structure formed in the co-polymer. Figure 5.9 shows that lamellar nano-structures were formed. The dark regions in Figure 5.9 represent polystyrene and the light areas MET agglomerates. This agglomeration of the surfactant repeat units can be seen to consist of bead-like structures so that the order is not perfectly lamellar but incorporates micellular structures as well. This would account for the mixed order found in the polyelectrolyte-surfactant complexes (section 4.3.1.4).

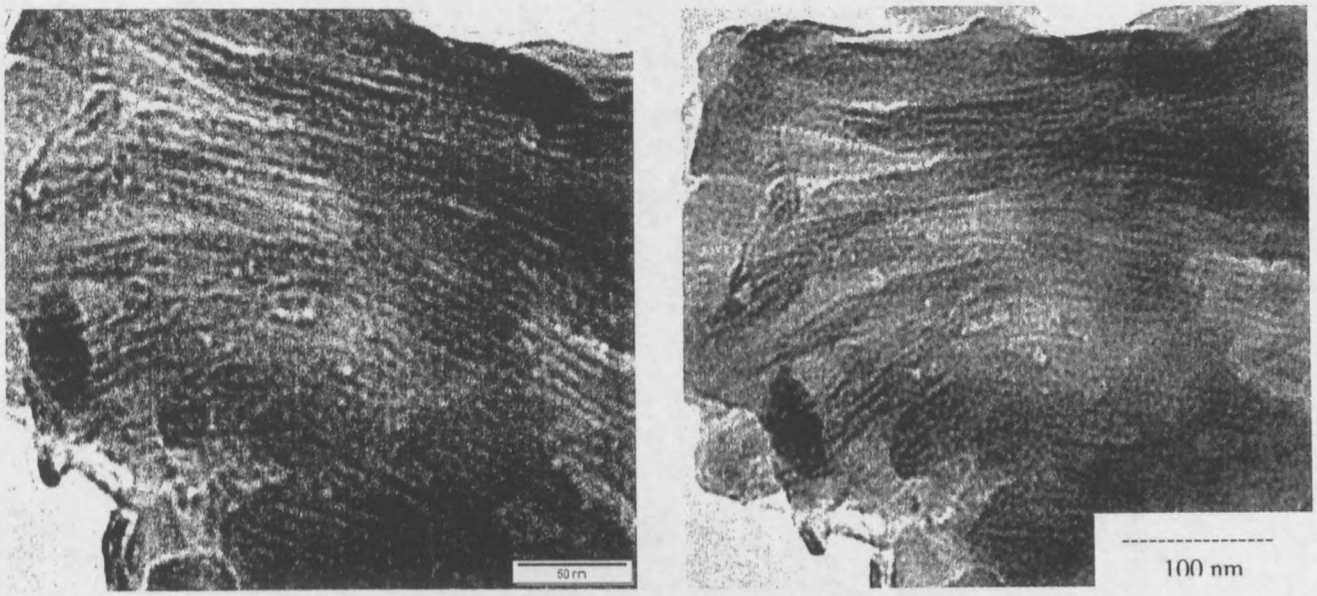

Figure 5.9. TEM photos of MET-20-PS (at different magnifications) showing a lamellar micro-structure.

These lamellar nano-structures are hard to quantify exactly and lie in the region of 3 nm broad and 25 nm long. The expected nano-structure thickness is around 3,8 to 4 nm.

The TEM photograph adds evidence to the structure in the side-chain crystallinity seen in the DSC heating curve. It can be said that MET self-assembles via the formation of intermolecular bridges (Figure 5.8) to form very fine nano-structures within the polystyrene matrix.

Chapter 6
Conclusions

6.1. Conclusions

- The surfmers MET (**1**) and CRO (**2**), both with sulfate and polar acrylic ester end groups and connected by a hydrocarbon spacer chain, were successfully synthesized and purified. Attempts to synthesize PSA-MA (**3**) were unsuccessful. **1** and **2** were characterized by means of ^{1}H and ^{13}C NMR spectroscopy, elemental analysis, CMC, TGA, DSC, melting point determination and microscopy. NMR and elemental analysis proved that the surfactants were more than 95 % pure. Lower CMC values were obtained for **1** and **2** than those reported in the literature. This is because of their higher purity and less inorganic salts present as a second impurity in the prepared samples. TGA showed that CRO (**2**) is thermally more stable than MET (**1**). DSC and microscopy indicated that **1** and **2** behave in a liquid crystalline manner. This behavior was indicated by the observation of two melting points in the DSC. Microscopy indicated two changes in the behavior of **1** and **2** before the melting occurred. Crystals were formed during the cooling cycle.

- A 2 % solution of the purified MET (**1**) or CRO (**2**) were slowly added to a 2 % pDADMAC (**4**) solution to form polyelectolyte-surfactant complexes by common precipitation.

- Both complexes were analyzed by SAXS to investigate their suitability as a stable host with well defined phase morphology. Complexes with both surfactants showed no known nor well defined phase morphology. This mean that the complexes are not suitable hosts for templating. Two possible reasons for the low order are: (1) the destabilization of the lyotropic phase by the polar acrylic ester group and (2) the formation of a 'loop' structure.

- 5, 10 and 20 % MET (**1**) were successfully co-polymerized with styrene and methyl methacrylate by means of a free radical mechanism. A glassy type of material was obtained in all cases. ^{1}H NMR, ^{13}C NMR and FTIR spectroscopy were used to characterize the different co-polymers. GPC indicated a trimodal molecular weight

distribution of medium and very high molecular weight. FTIR spectroscopy of each peak indicated the chemical compositions to be the same. Aggregates or micelles formed when the co-polymers were in solution which results in the very high molecular weight. TGA showed that the co-polymers lose mass in two basic steps: bound water to MET first and polystyrene or poly(methyl methacrylate) later. DSC indicated side-chain crystallinity, which would form molecular bridges. TEM indicates the formation of mixed lamellar nano-structures

6.2. Recommendations for future work

Future work should focus on the investigation into the copolymers of MET (**1**) with styrene and methyl methacrylate, including:

- Investigation into the behavior when the co-polymers are in solution and the formation of aggregates or micelles.
- Investigation into the side-chain crystallinity and formation of molecular bridges.
- Investigation into the micro-structures formation with microscopy and SAXS.
- Investigation into the formation of poly-liquid crystalline behavior by SAXS and TEM.

Chapter 7

References

[1] M. Antonietti, C. Göltner *Angew. Chem. Int. Ed. Engl.* **1997**, *36*, 910.

[2] J.W. McBain *Trans. Faraday Soc.* **1913**, *9*, 99.

[3] www.nas.edu/bpa/reports/bmm/bmm.html.

[4] www.nanogram.com.

[5] www.nanoslurry.com.

[6] www.rutgers.edu/~mjohnm/nanomat.html.

[7] C. Faul, PhD thesis, Stellenbosch University, **2000.**

[8] J. Unzue, H.A.S. Schoonbrood, J.M. Asua, A. Montoya Goni, D.C. Sherrington, K. Stähler, K.-H. Goebel, K. Tauer, M. Sjöberg, K. Holmberg *J. Appl. Polym. Sci.* **1997**, *66*, 1803.

[9] R.J. Spontak, P. Alexandridis *Curr. Opin. Colloid Sci.* **1999,** *4,* 140.

[10] H. Hasegawa *Curr. Opin. Colloid Interface Sci.* **1998**, *3*, 264.

[11] Y.L. Yang, F. Qui, H.D. Zhang, J.W. Zhang *Prog. Nat. Sci.* **1998**, *95*, 513.

[12] Peter A. Lovell and Mohamed S. El-Asser (ed.) *Emulsion Polymerization and Emulsion Polymers*, John Wiley and Sons, New York, **1999.**

[13] W.C. Griffin *J. Soc. Cosmet. Chem.* **1949**, *1*, 311.

[14] www.cop.ufl.edu, **2001.**

[15] www.asnt.org/publications, American Society for Nondestructive Testing, Inc. **2001.**

[16] www.netsci-journal.com/97v4/97014/vitc.html.

[17] F.M. Menger, S. Wrenn *J. Phys. Chem.* **1974**, *78*, 1387.

[18] C.M. Paleos *Polymerization in Organized Media* Gordon & Breach Science Publishers, Philadelphia, **1994.**

[19] A. Montoya-Goni, D.C. Sherrington *Polymer* **1999**, *40*, 1067.

[20] Jacob N. Israelachivili *Intermolecular and surface forces*, 2nd ed. Academic Press, London **1992.**

[21] S.M. Hamid, D.C. Sherrington *Polymer* **1987**, *28*, 325.

[22] D.F. Evans, H. Wennerström *The Colloidal Domain*, Wiley-VCH New York, **1994.**

[23] www.abalone.cwru.edu, Case Western Reserve University, **2001.**

[24] Y. Chevalier, C. Chachaty *J. Phys.Chem.* **1985**, *89*, 880.

[25] C. Tanford *The hydrophobic effect,* Wiley, New York, **1980.**

[26] J.N. Israelachivili, D.J. Mitchell, B.W. Ninham *J. Chem.Soc. Faraday Trans I* **1976**, *72*, 1525.

[27] T. Shimizu, M. Kogiso, M. Masuda *J. Am. Chem. Soc.* **1997**, *119*, 6209.

[28] T. Shimizu, M. Kogiso, M. Masuda *Nature* **1996**, *383*, 487.

[29] T. Shimizu, M. Masuda *J. Am. Chem. Soc.* **1997**, *119*, 2821.

[30] F. Reinitzer *Liq. Cryst.* **1989**, *5*, 7 (English translation of original paper: F. Reinitzer *Monatsh. Chem.* **1888**, *9*, 421).

[31] O. Lehmann *Verhandl. d. Deutchen Phys. Ges., Sitzung v.* **1900**, *16.3*, 1.

[32] T. Svedberg *Kolloid-Z.* **1916**, *18*, 54.

[33] T. Svedberg *Kolloid-Z.* **1916**, *18*,101.

[34] T. Svedberg *Kolloid-Z.* **1917**, *20*, 73.

[35] T. Svedberg *Kolloid-Z.* **1917**, *21*, 19.

[36] J.M. Seddon *Biochimica et Biophysica Acta* **1990**, *131*, 1.

[37] M.E. Cates, S.A. Safran *Curr. Opin. Colloid Interface Sci.* **1996**, *1*, 327.

[38] P. Kekicheff, C. Grabielle-Madelmont *J. Phys. (France)* **1987**, *48*, 1571.

[39] P. Kekicheff, C. Grabielle-Madelmont, M. Ollivon *J. Coll. & Interf. Sc.* **1989**, *131*, 112.

[40] P. Kekicheff *J. Colloid Interface Sci.* **1989**, *131*, 133.

[41] K.M. McGrath, P. Kekicheff, M. Kleman *J. Phys. II (France)* **1993**, *3*, 903.

[42] A. Blumstein (Ed.) *Liquid Crystalline Order in Polymers,* Academic Press, New York, **1978.**

[43] S. Förster, M. Antonietti *Adv. Mater.* **1998**, *10*, 195.

[44] Y. Bouligand *Liquid Crystals* **1999**, *26*, 501.

[45] H.B. Bull, H.J. Neurath *J. Biol. Chem.* **1937**, *118*, 163.

[46] M.L. Anson *Science* **1939**, *90*, 256.

[47] H. Arai, M. Murata, K. Shinoda *J. Colloid Interface Sci.* **1971**, *37*, 223.

[48] E.D. Goddard in *Interactions of Surfactants with Polymers and Proteins* (Ed. E.D. Goddard & K.P. Ananthapadmanabhan) CRC Press, Boca Raton, **1994.**

[49] K. Hayagawa, J.C. Kwak *J. Phys. Chem.* **1982**, *86*, 3866.

[50] K. Hayagawa, A.L. Ayub, J.C. Kwak *J. Colloids Surfaces* **1982**, *4*, 389.

[51] K. Hayagawa, J.P. Santerre, J.C. Kwak *Macromolecules* **1983**, *16*, 1642.

[52] K. Hayagawa, J.C. Kwak *J. Phys. Chem.* **1983**, *87*, 506.

[53] M.N. Jones *J. Colloid Interface Sci.* **1967**, *23*, 36.

[54] M.N. Jones *J. Colloid Interface Sci.* **1968**, *26*, 532.

[55] E.D. Goddard *Colloids Surf.* **1986**, *19*, 301.

[56] K. Shirahama, K. Tsujii, T. Takagi *J. Biochem.* **1974**, *75*, 309.

[57] Y. Li, P.L. Dublin in Structure and flow in surfactant solutions (Ed. C.A. Herb & R.K. Prud'homme) *ACS Symposium Series 578,* American Chemical Sociey, Washington DC, **1994.**

[58] J. Lui, N. Shirhahma, H. Abe, K. Sakomoto *J. Phys. Chem. B* **1997**, *101*, 7520.

[59] K. Thalberg, B. Lindman in *Surfactants in Solution, Vol 11* (Ed.K.L. Mittal, D. Shah), Plenum Press, New York, **1991.**

[60] W.J. MacKnight, E.A. Ponomarenko, D.A. Tirrel *Acc. Chem. Res.* **1998**, *31*, 781.

[61] A. Ciferri *Macromol. Chem. Phys.* **1994**, *195*, 457.

[62] M. Shimomura, T. Kunitake P*olymer J.* **1984**, *16*, 187.

[63] Y. Ishuawa, T. Kunitake *J. Am. Chem. Soc.* **1991**, *113*, 621.

[64] Y. Okahata, K. Taguchi *J. Am. Chem. Soc.* **1985**, *107*, 5300.

[65] Y. Okahata, G. Enna *J. Phys. Chem.* **1992**, *92*, 4546.

[66] E.D. Goddard, K.P. Ananthapadmanabhan Applications in Polymer-Surfactant Systems in *Surfactant Science Series, Vol 77: Polymer-surfactant System* (Ed. J.C. Kwak) Marcel Dekker Inc., New York, **1998.**

[67] M. Uchida, T. Kunitake, T. Kajiyama *New Polymeric Materials* **1994**, *4*, 199.

[68] F. Caruso, D. Trau, H. Möhwald, R. Renneberg *Langmuir* **2000**, *16*, 1584.

[69] A. Harada, S. Nozukara *Polym. Bull.* **1984**, *11*, 175.

[70] S. Ujiie, K. Iimura *Macromolecules* **1992**, *25*, 3175.

[71] M. Antonietti, J. Conrad *Angew. Chem.* **1994**, *106*, 1927.

[72] M. Antonietti, J. Conrad *Angew. Chem. Int. Ed. Eng.* **1994**, *33*, 1869.

[73] A.Thünemann *Polym. Int.* **2000**, *49*, 636.

[74] M. Antonietti, M. Maskos *Macromolecules* **1996**, *29*, 4199.

[75] M. Antonietti, D. Radloff, U Wiesner, H.W. Spiess *Macromol. Chem. Phys.* **1996**, *197*, 2713.

[76] M. Antonietti, A. Wentzel *Colloids Surf. A: Phys. Eng. Asp.* **1998**, *134*, 141.

[77] M. Antonietti, M. Neese, G. Blum, F. Kremer *Langmuir* **1996**, *12*, 4436.

[78] M. Antonietti, M. Maskos, F. Kremer, G. Blum *Acta Polym.* **1996**, *47*, 460.

[79] M. Antonietti, C. Burger *J. Adv. Mater.* **1995**, *7*, 751.

[80] M. Antonietti, A. Wentzel, A. Thünemann *Macromolecules* **1996**, *12*, 2111.

[81] C. Faul, M. Antonietti, R. Sanderson, H.-P. Hentze *Langmuir* **2001**, *17*, 2031.

[82] http://www.ukc.ac.uk/physical-sciences/main/external_services/CHN.html.

[83] H. Utschick *Methods of Thermal Analysis*, Ecomed Verlagsgesellschaft AG, Landsberg, **1999**.

[84] D. Cambell, J.R. White *Polymer Characterization – physical techniques*, Chapman & Hall, London, **1989**.

[85] J. Chiu (Ed.) *Polymer Characterization by Thermal Anayisis,* Marcel Dekker Inc., New York, **1974**.

[86] www.gom.mse.iastate.edu/Complete/NonFrames/htm.

[87] F.B. Rosevear *J. Am. Oil. Chem. Soc.* **1954**, *31*, 628.

[88] P.A. Winsor *Chem. Rev.* **1968**, *68*, 1.

[89] M. Spencer *Fundamentals of Light Microscopy,* Cambridge University Press, Cambridge, **1982.**

[90] Mark, Bikales, Overberger, Menges *Encyclopedia of Polymer Science and Enginering, Vol. 17* Wiley, New York, **1989**.

[91] A. Laschewesky *Advances in Polymer Science, Vol. 125*, Springer Verlag, Berlin, **1995.**

[92] *Organikum, Organisch-chemische Grundpraktikum* VEB Deutscher Verlag der Wissenschafen, Berlin, **1986**.

[93] K. Urushido, A. Matsumoto, M. Oiwa *J. Polym. Sci., Polym. Chem. Ed.* **1981**, *19*, 59.

[94] M. Antonietti, Personal communications, **2001**.

[95] M. Dreja, W. Lennartz *Macromolecules* **1999**, *32*, 3528.

[96] http://www.shef.ac.uk/space/Pages/xrayscatt.htm.

[97] S. Zhou, H. Hu, C. Burger, B. Chu *Macromolecules* **2001**, *34*, 1772.

[98] www.otl.berkley.edu/UCB99068.html.

[99] C.M. Paleos, C.I. Stassinpoulou, A. Malliaris *J. Phys. Chem.* **1983**, *87*, 251.

[100] H.H. Freedman, J.P. Mason, A.I. Medalia *J. Org. Chem.* **1958**, *23*, 76.

[101] S.K. Sinha, A.I. Medalia *J. Am. Chem. Soc.* **1957**, *79*, 281.

[102] G.P. Hellmanns Personal communications, **2002**.

[103] R. Sauerwein PhD thesis, Technische Hochschule, Darmstadt, **1997**.

Addendum

1. CMC **88**

Figure 1. CMC of MET 88

Figure 2. CMC of CRO 88

2. TGA spectra **89**

Figure 3. TGA of MET 89

Figure 4. TGA of CRO 89

5. DSC spectra **90**

Figure 5. DSC thermogram of first heating cycle for MET 90

Figure 6. DSC thermogram of cooling cycle for MET 90

Figure 7. DSC thermogram of second first heating cycle for MET 91

Figure 8. DSC thermogram of first heating cycle for CRO 91

Figure 9. DSC thermogram of cooling cycle for CRO 92

Figure 10. DSC thermogram of second heating cycle for CRO 92

1. CMC determination

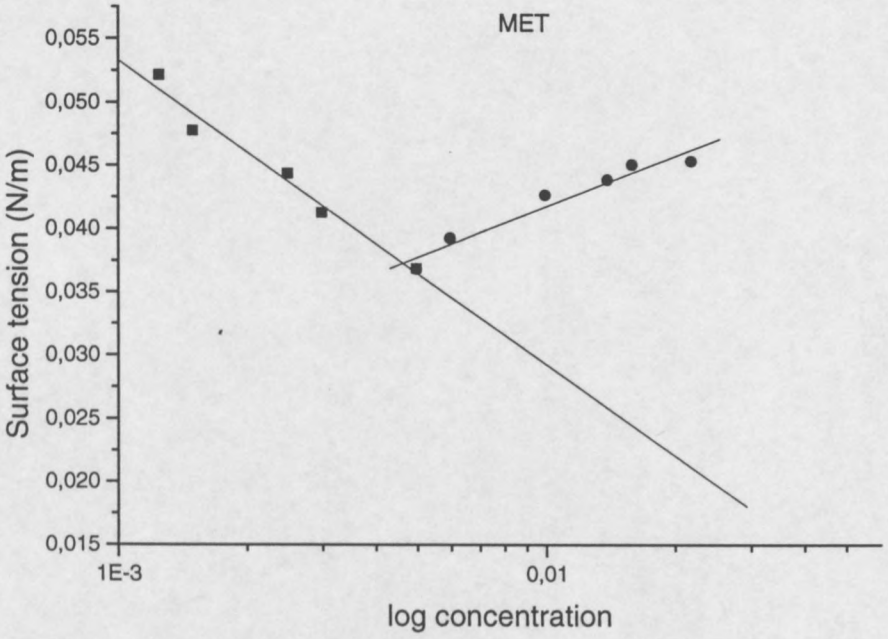

Figure 1. CMC determination of MET (1).

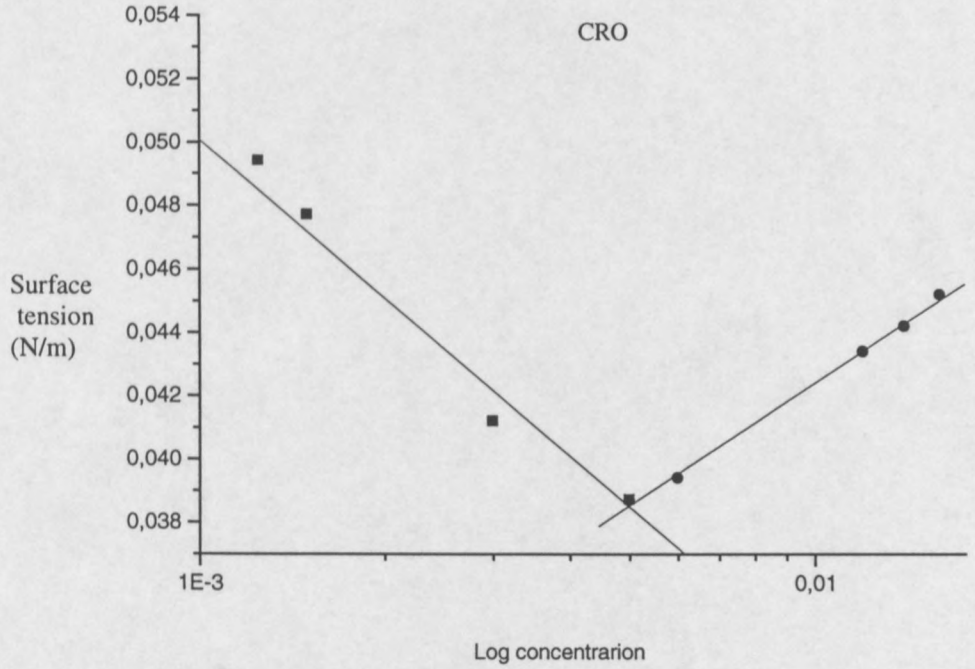

Figure 2. CMC determination of CRO(2).

2. Thermal Gravimetric Analysis (TGA)

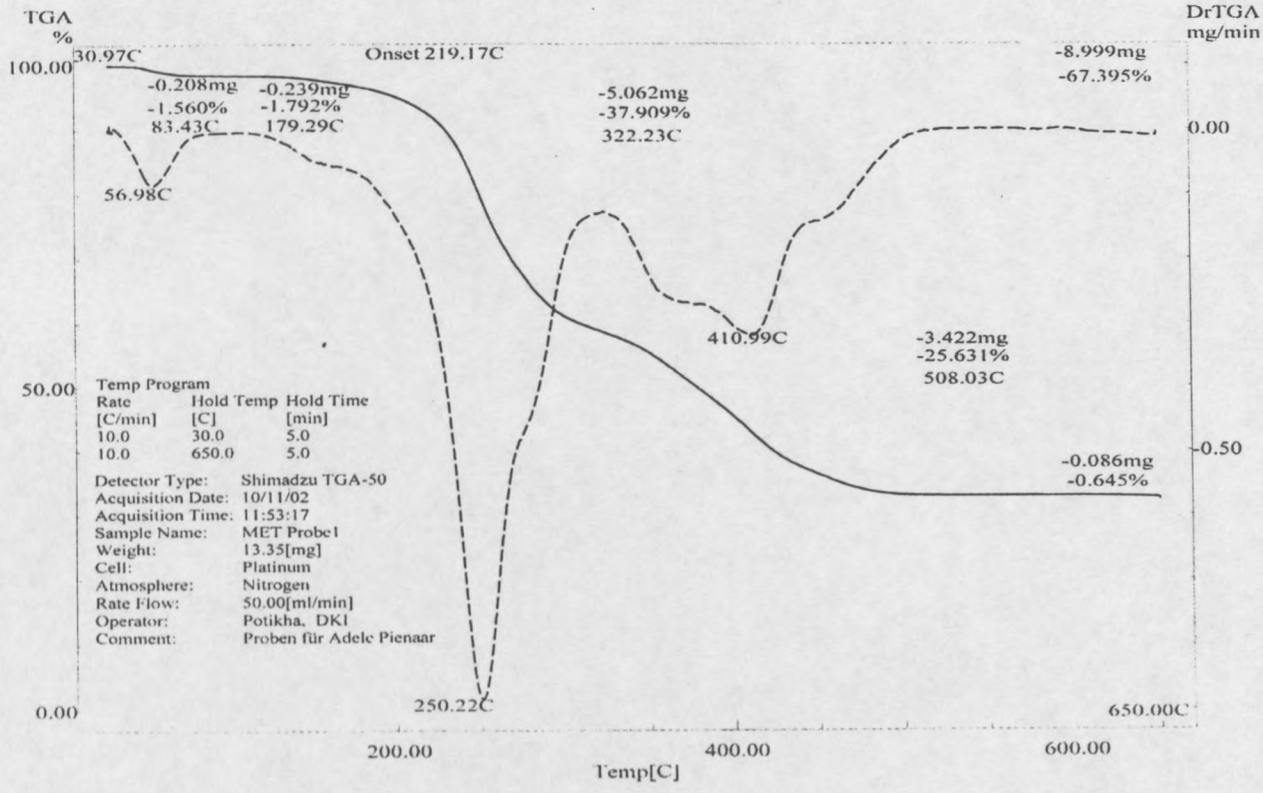

Figure 3. TGA of MET (1).

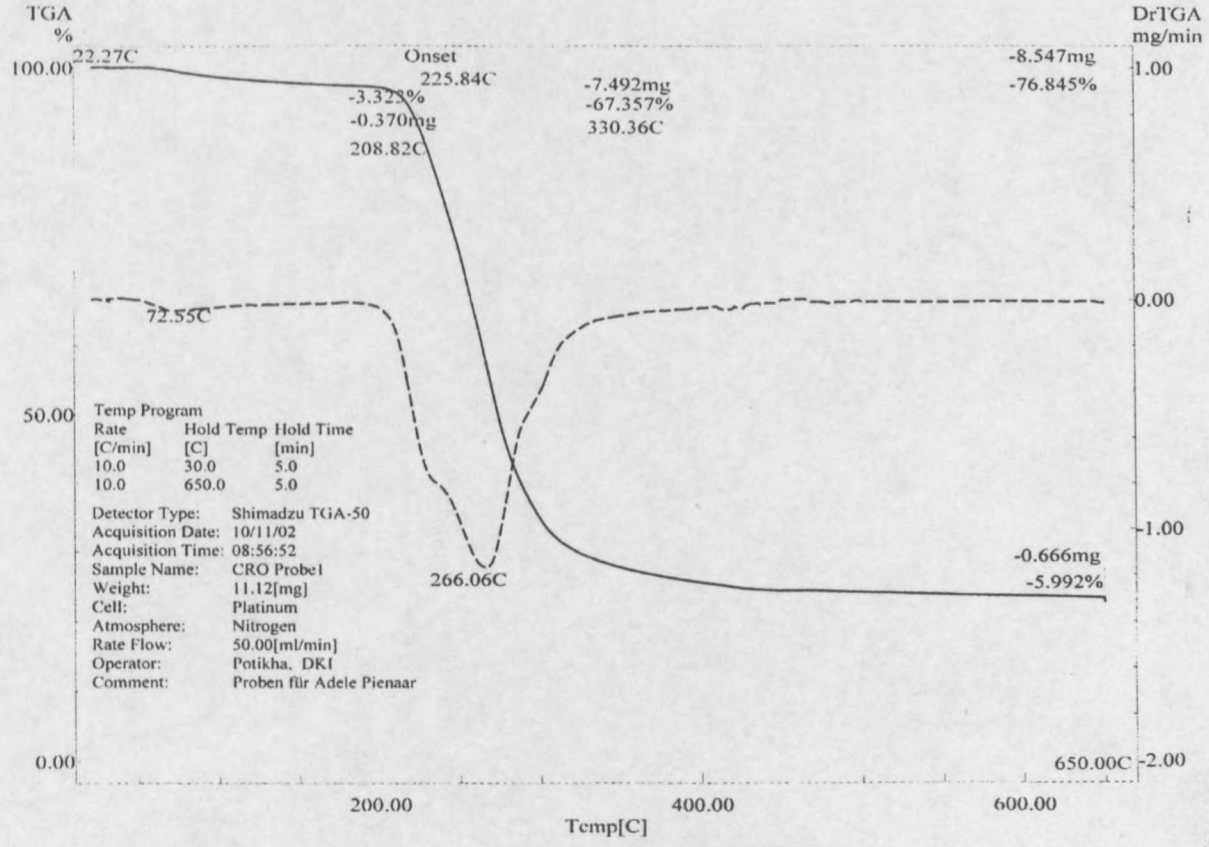

Figure 4. TGA of CRO (2).

3. Differential Scanning calorimetry (DSC)

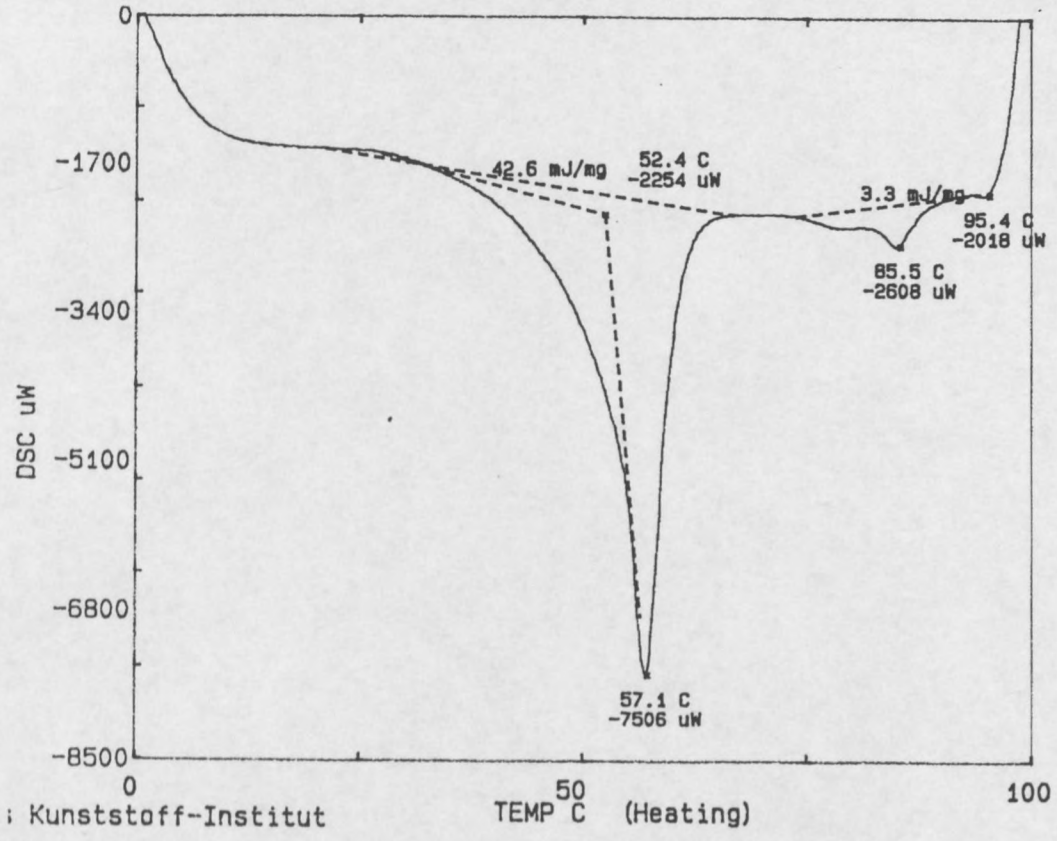

Figure 5. MET (1) first heating cycle.

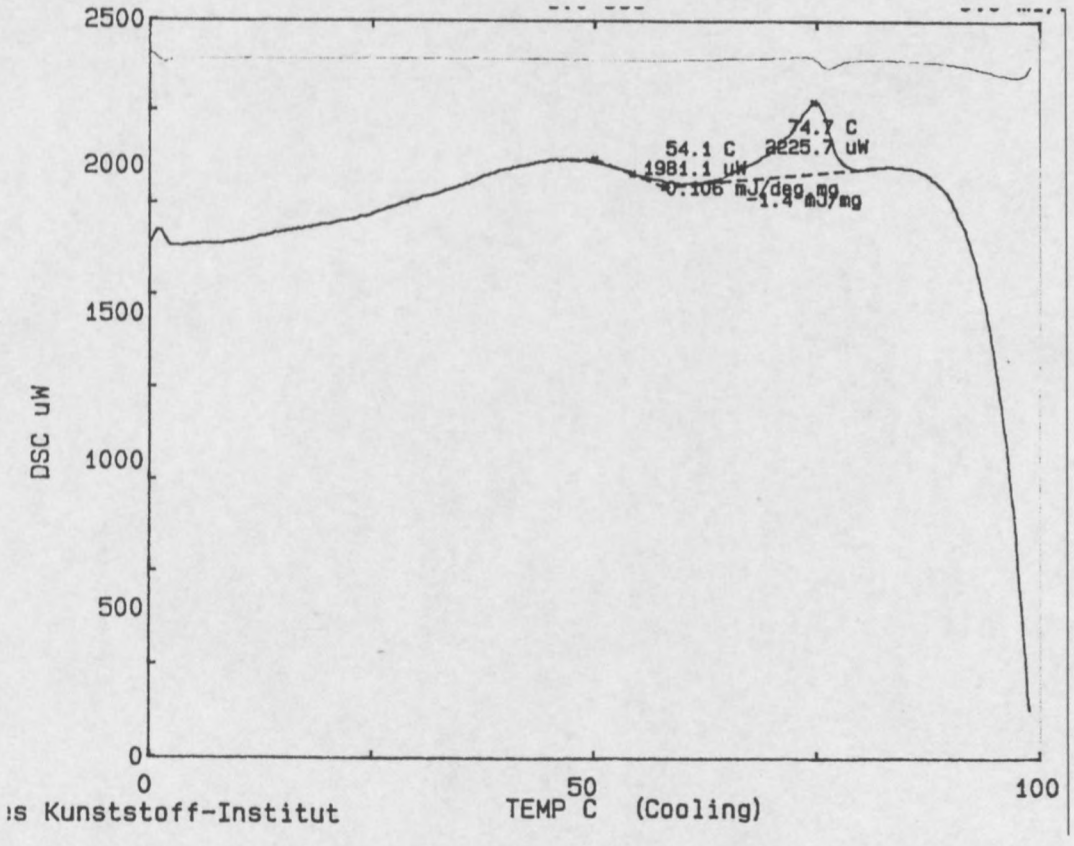

Figure 6. MET (1) cooling cycle.

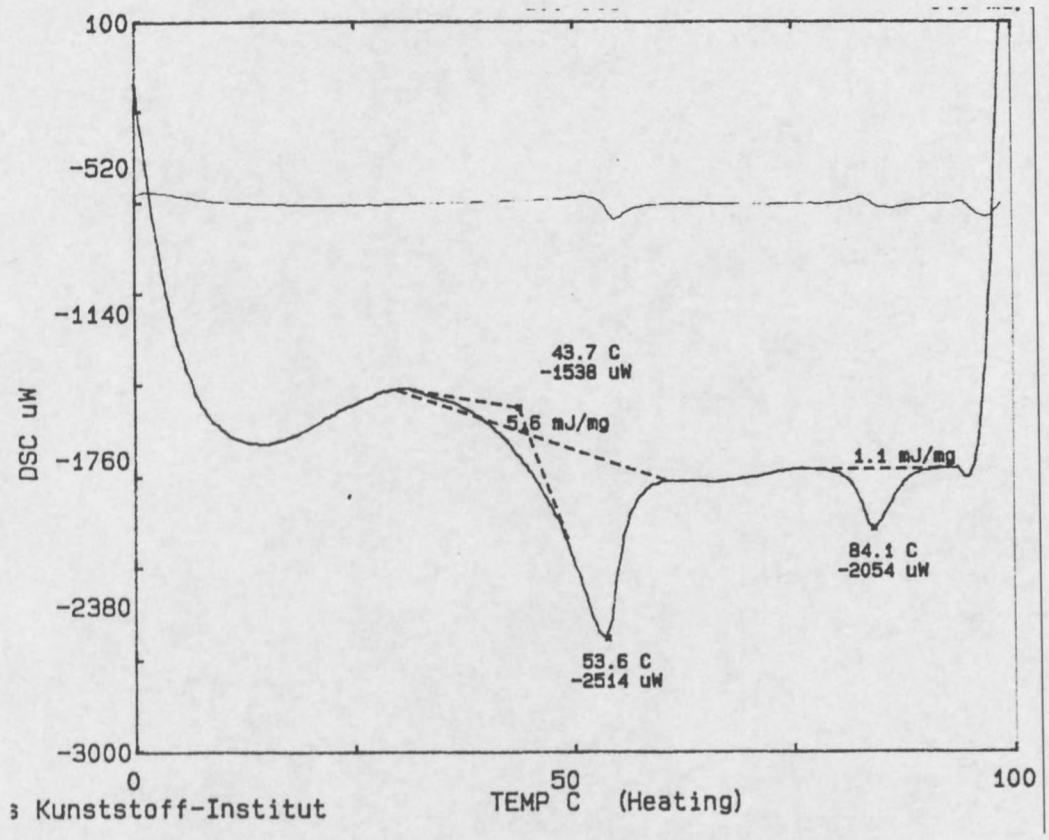

Figure 7. MET (1) second heating cycle.

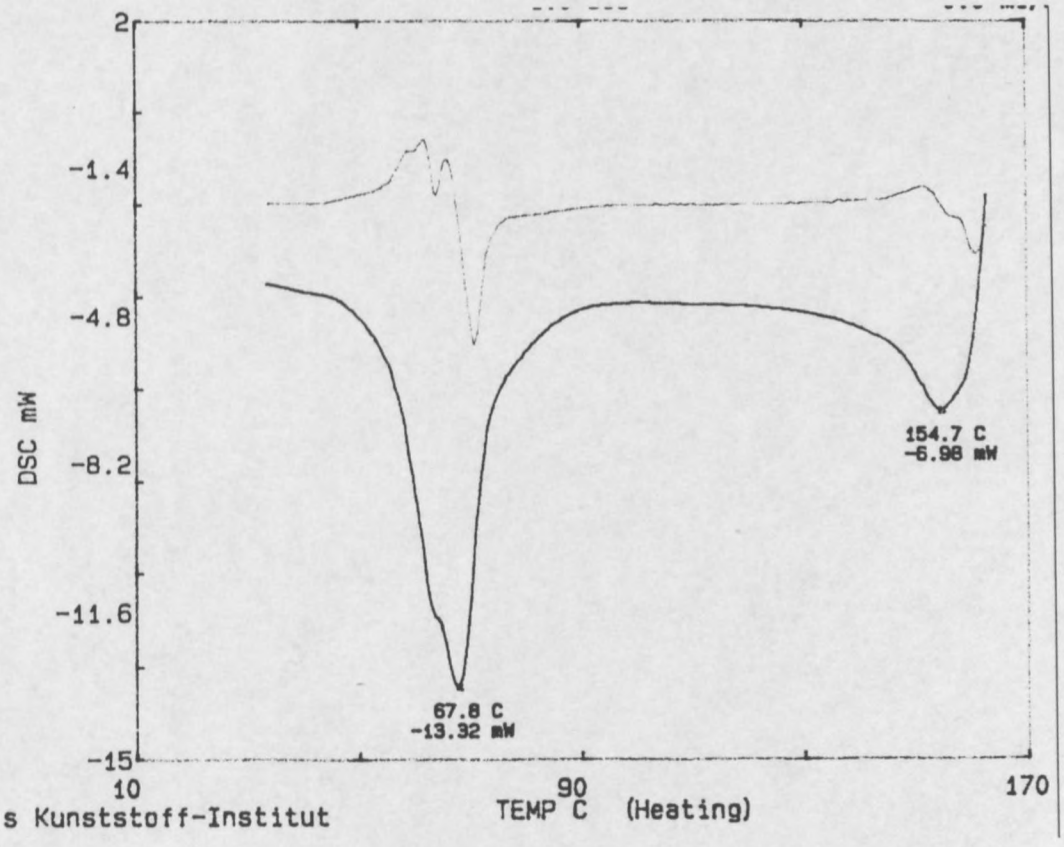

Figure 8. CRO (2) first heating cycle.

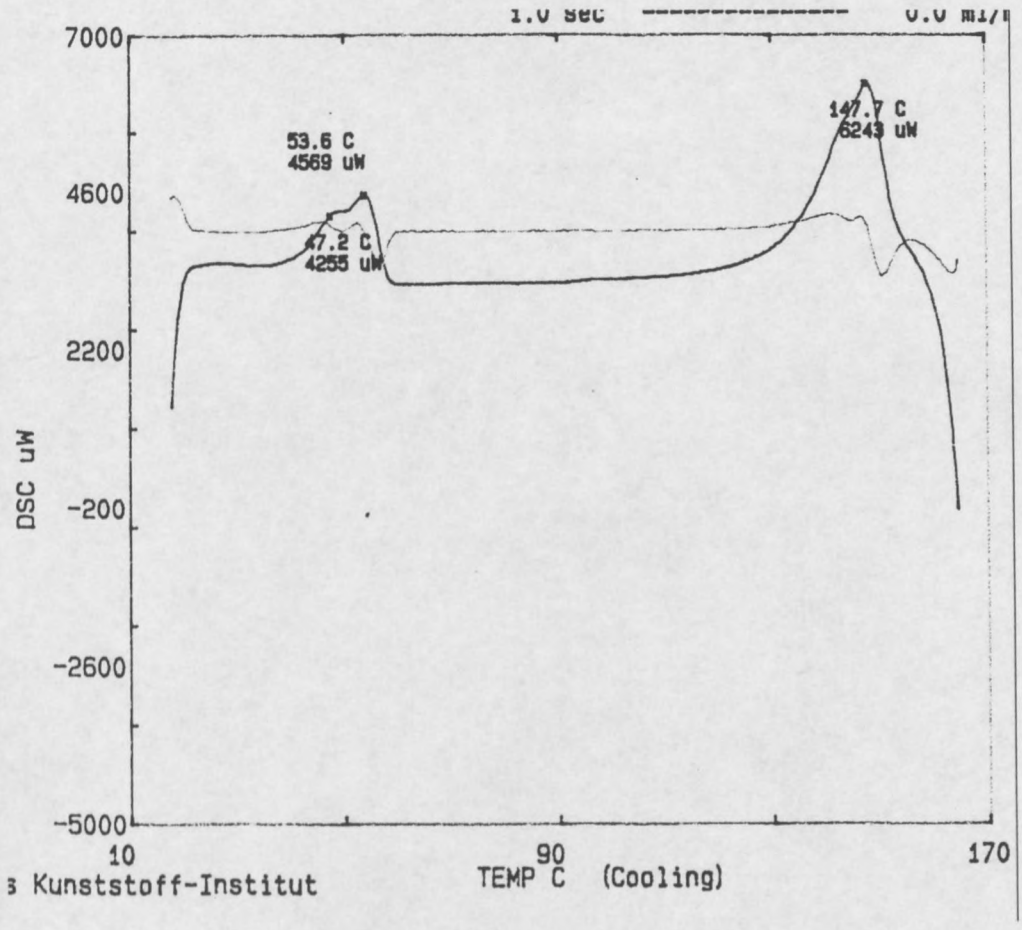

Figure 9. CRO (2) cooling cycle.

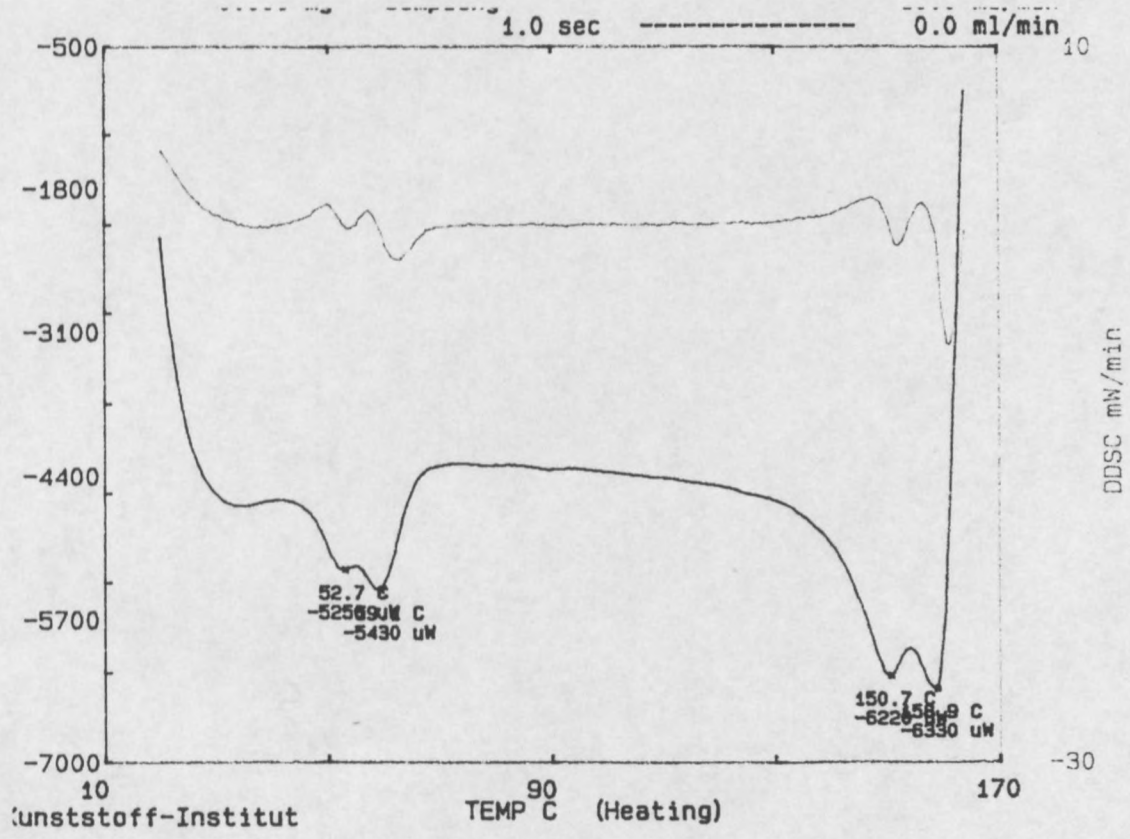

Figure 10. CRO (2) second heating cycle.